

UNIVERSITY OF HAWAII LIBRARY

**MULTI-GRATING DEMULTIPLXER UTILIZING  
CHIRPED GRATING**

**A THESIS SUBMITTED TO THE GRADUATED DIVISION OF THE  
UNIVERSITY OF HAWAI'I IN PARTIAL FULFILLMENT  
OF THE REQUIREMENTS FOR THE DEGREE OF**

**MASTER OF SCIENCE**

**IN**

**ELECTRICAL ENGINEERING**

**MAY 2005**

**By  
Ray J. Park**

**Thesis Committee:**

**Audra Bullock, Chairperson  
Victor M. Lubecke  
Vinod Malhotra**

## **Acknowledgement**

I would like to thank Dr. Bullock for her support throughout the project.

I would also like to thank Dr. Malhotra and Dr. Lubecke for being on thesis member.

## **Abstract**

In today's optical communication systems, the demultiplexer limits the number of channels that can be transmitted through the optical fiber, since its wavelength channels demultiplexing limit is typically larger than 0.5 nm. To increase this limitation of the demultiplexer, this thesis discusses the research and development of a demultiplexer constructed with cascading diffraction gratings.

To achieve larger channel separation, a multi-grating demultiplexer was developed using diffraction gratings with different profile in different configurations. With different configuration utilizing different grating, an improvement of 50% to 1700% in separation of wavelength channels was achieved compared to the single grating system. In addition routing properties of the chirped grating were researched.

Over all, the research presented here demonstrates that it is possible to increase the wavelength channel spacing and route the channels using multi-grating system.

## TABLE OF CONTENT

Acknowledgement	iii
Abstract	iv
List of Tables	viii
List of Figures	vi
Chapter 1: Communication Network	1
Introduction	1
1.1 Communication technologies	2
1.2 Fiber optic communication setup	3
1.3 Components of fiber optic communication system	4
1.3.1 Light source	4
1.3.2 Channel	5
1.3.2.1 Multimode fiber	5
1.3.2.2 Single-mode fiber	6
1.3.3 Amplifier	6
1.3.4 Multiplexing of Optical signal	7
1.3.4.1 Multiplexing scheme in hybrid communication system	7
1.3.4.2 Multiplexing scheme in all optical system	8
1.3.5 Multiplexer and Demultiplexer	8
1.3.6 Router/Switch	9
1.3.7 Receiver	9
1.4 Wavelength add/drop multiplexer (WADM)	9
Chapter 2: Different Grating Technologies	11
2.1 Bragg grating (FBG)	11
2.2 AWG (Arrayed Waveguide Grating)	13
2.3 Diffraction grating	16
2.4 Improvements made in the diffraction grating	18
Chapter 3: Theory and Calculation	19
3.1 Theory	19
3.1.1 Chirped grating	20
3.2 Calculations	21
3.2.1 Initial testing of the Theory	22
3.2.2 Final setup calculation	25
Chapter 4: Setup and Procedures, Setups and Measurement	28
4.1 Testing of the theory	28
4.1.1 Layout of the measurement setup	29
4.1.2 Reference setup	30
4.1.2.1 Actual dimensions for first setup	31



4.1.2.2 Measurement technique in first setup.....	32
4.1.2.3 Reference setup results (Single grating).....	33
4.1.3 Dual grating setup.....	34
4.1.3.1 Results for the two 600 grooves/mm gratings in series.....	36
4.2 First experiment with continuous chirped grating (Lateral measurement setup).....	36
4.2.1 Reference setup results (Single grating).....	38
4.2.2 Results for the two 600 grooves/mm gratings in series.....	39
4.2.3 Results for the 600 grooves/mm grating and the 1st chirped grating in series.....	40
4.2.3.1 Results at region I of the 1st chirped grating.....	41
4.2.3.2 Results at region II of the 1st chirped grating.....	42
4.2.3.3 Results at region III of the 1st chirped grating.....	43
4.2.4 Results for the 600 grooves/mm grating and the 2nd chirped grating in series.....	44
4.2.4.1 Results at region I of the 2nd chirped grating.....	44
4.2.4.2 Results at region II of the 2nd chirped grating.....	45
4.2.4.3 Results at region III of the 2nd chirped grating.....	46
4.3 Final setup with continuous chirped grating (Circular measurement setup).....	47
4.3.1 Reference Setup (Single grating).....	48
4.3.1.1 Actual setup dimensions for final setup.....	49
4.3.1.2 Measurement technique final setup.....	50
4.3.2 Dual grating setup.....	51
4.3.2.1 Results for the two 600 grooves/mm gratings in series.....	52
4.3.3 Results for the 600 grooves/mm grating and the 1st chirped grating in series.....	53
4.3.3.1 Results at region I of the 1st chirped grating.....	54
4.3.3.2 Results at region II of the 1st chirped grating.....	55
4.3.3.3 Results at region III of the 1st chirped grating.....	56
4.3.4 Results for the 600 grooves/mm grating and the 2nd chirped grating in series.....	56
4.3.4.1 Results at region I of the 2nd chirped grating.....	56
4.3.4.2 Results at region II area of the 2nd chirped grating.....	57
4.3.4.3 Results at region III of the 2nd chirped grating.....	58
4.4 Wavelength routing properties of the dual grating system.....	59
4.4.1 Results from lateral setup results.....	60
4.4.1.1 Position shifting of 1st grating.....	61
4.4.1.2 Position shifting of 2nd grating.....	61
4.4.2 Final setup results.....	62
4.4.2.1 Position shifting of 1st grating.....	62
4.4.2.2 Position shifting of 2nd grating.....	62
Chapter 5: Discussion of Results.....	63

5.1 Wavelength channel's peak power separations.....	63
5.1.1 Single grating (Reference measurement).....	63
5.1.2 Dual grating measured results.....	65
5.1.2.1 Two 600 groove/mm in series.....	65
5.1.2.2 Dual grating (1st Chirp grating).....	66
5.1.2.2.1 Testing Setup.....	67
5.1.2.2.2 Final setup.....	67
5.1.2.3 Dual grating (2nd Chirp grating).....	68
5.1.2.3.1 Testing Setup.....	68
5.1.2.3.2 Final Setup.....	68
5.1.3 Dual grating measured results vs. calculated results.....	70
5.2 Power fluctuation.....	72
5.2.1 Initial setup.....	72
5.2.2 Testing setup.....	73
5.2.3 Final setup.....	73
5.3 Wavelength routing properties.....	75
5.3.1 Routing of wavelength channel in testing setup.....	75
5.3.1.1 1st Chirp grating.....	75
5.3.1.2 2nd Chirp grating.....	76
5.3.2 Routing of wavelength channel in final setup.....	77
5.3.2.1 1st Chirp grating.....	77
5.3.2.2 2nd Chirp grating.....	78
5.4 Beam Broadening.....	79
Chapter 6: Conclusion.....	81
6.1 Testing of grating system.....	82
6.2 Testing of dual grating system.....	82
6.2.1 First Stage.....	82
6.2.2 Testing Setup.....	83
6.3 Final setup.....	84
6.4 Dual grating measured results vs. calculated results.....	85
6.5 Routing Property.....	85
6.7 Unwanted Effects of Chirped grating.....	85
Closing.....	86
Reference.....	87

## LIST OF TABLES

<u>Table</u>	<u>Page</u>
1. Average separation between the channels' peak power.....	64
2. Wavelength channels separation improvement.....	66
3. Average power fluctuation between the wavelength channels' peak power.....	69
4. The wavelength channels' peak power position shift as change in the 1 <sup>st</sup> chirped grating density for the testing setup.....	75
5. The wavelength channels' peak power position shift as change in the 2 <sup>nd</sup> chirped grating density for the testing setup.....	76
6. The wavelength channels' peak power position shift as change in the 1 <sup>st</sup> chirped grating density for the final setup.....	77
7. The wavelength channels' peak power position shift as change in the 2 <sup>nd</sup> chirped grating density for the final setup.....	78

## LIST OF FIGURES

<u>Figure</u>	<u>Page</u>
1. Arrayed Waveguide Grating (AWG).....	13
2. Diffraction grating.....	16
3. Diffraction behavior of wavelength.....	20
4. Geometry of initial dual grating setup.....	22
5. Geometry of final dual grating setup.....	25
6. Schematic of the measurement setup.....	28
7. Dimensions of the setup.....	29
8. Measurement.....	30
9a. Reference measurement setup.....	32
9b. Dual standard ruled grating (DS configuration), both grating with 600 grooves/mm .....	32
9c. Standard/chirped ruled grating (SC configuration), initial grating with 600 grooves/mm and groove-spacing varying grating for second grating.....	32
10. Actual measurement for each wavelength for single 600 grooves/mm (Reference measurement).....	33
11. Peak power position of each wavelength for single 600 grooves/mm. (Reference measurement) .....	31
12. Peak power position of each wavelength for dual grating. Two 600 grooves/mm grating in series.....	33
13. Actual measurement for each wavelength for dual grating. Two 600 grooves/mm in series.....	33
14. Peak power position of each wavelength for single 600 grooves/mm. For the testing setup measurement (Reference measurement).....	37
15. Actual measurement for each wavelength for single 600 grooves/mm. For the testing setup measurement (Reference measurement).....	38
16. Peak power position of each wavelength for dual grating. Two 600 grooves/mm grating in series for the testing setup measurement.....	39
17. Actual power measurement for each wavelength for the two 600 grooves/mm in series. For the testing setup measurement.....	39
18. Peak power position of each wavelength for dual grating. 600 grooves/mm and 1 <sup>st</sup> chirp grating in series for the testing setup measurement. (at region I of chirped grating).....	40

19. Actual power measurement for each wavelength for the 600 grooves/mm and 1 <sup>st</sup> chirped grating in series for the testing setup measurement. (at region I of chirped grating)	40
20. Peak power position of each wavelength for dual grating. 600 grooves/mm and 1 <sup>st</sup> chirped grating in series for the testing setup measurement. (at region II of chirped grating)	41
21. Actual power measurement for each wavelength for the 600 grooves/mm and 1 <sup>st</sup> chirped grating in series for the testing setup measurement. (at region II of chirped grating)	41
22. Peak power position of each wavelength for dual grating. 600 grooves/mm and 1 <sup>st</sup> chirped grating in series for the testing setup measurement. (at region III of chirped grating)	42
23. Actual power measurement for each wavelength for the 600 grooves/mm and 1 <sup>st</sup> chirped grating in series for the testing setup measurement. (at region III of chirped grating)	42
24. Peak power position of each wavelength for dual grating. 600 grooves/mm and 2 <sup>nd</sup> chirped grating in series for the testing setup measurement. (at region I of chirped grating)	43
25. Actual power measurement for each wavelength for the 600 grooves/mm and 2 <sup>nd</sup> chirped grating in series for the testing setup measurement. (at region I of chirped grating)	43
26. Peak power position of each wavelength for dual grating. 600 grooves/mm and 2 <sup>nd</sup> chirped grating in series for the testing setup measurement. (at region II of chirped grating)	45
27. Actual power measurement for each wavelength for the 600 grooves/mm and 2 <sup>nd</sup> chirped grating in series for the testing setup measurement. (at region II of chirped grating)	45
28. Peak power position of each wavelength for dual grating. 600 grooves/mm and 2 <sup>nd</sup> chirped grating in series for the testing setup measurement. (at region III of chirped grating)	46
29. Actual power measurement for each wavelength for the 600 grooves/mm and 2 <sup>nd</sup> chirped grating in series for the testing setup measurement. (at region III of chirped grating)	46
30. Final measurement setup	47
31. The dimension for the final setup	48
32. Final setup measurement technique	49
33. Peak power positions of each wavelength for the two 600 grooves/mm grating in series for the final setup measurement	52
34. Peak power measurement for each wavelength for the two 600 grooves/mm grating in series for the final setup measurement	52
35. Peak power position of each wavelength for dual grating. 600 grooves/mm and 1 <sup>st</sup> chirped grating in series for the testing setup measurement. (at region I of chirped grating)	53

36. Actual peak power measurement for each wavelength for the 600 grooves/mm and 1 <sup>st</sup> chirped grating in series for the testing setup measurement. (at region I of chirped grating).....	53
37. Peak power position of each wavelength for dual grating. 600 grooves/mm and 1 <sup>st</sup> chirped grating in series for the testing setup measurement. (at region II of chirped grating).....	54
38. Actual peak power measurement for each wavelength for the 600 grooves/mm and 1 <sup>st</sup> chirped grating in series for the testing setup measurement. (at region II of chirped grating).....	54
39. Peak power position of each wavelength for dual grating. 600 grooves/mm and 1 <sup>st</sup> chirped grating in series for the testing setup measurement. (at region III area of chirped grating).....	55
40. Actual peak power measurement for each wavelength for the 600 grooves/mm and 1 <sup>st</sup> chirped grating in series for the testing setup measurement. (at region III area of chirped grating).....	55
41. Peak power position of each wavelength for dual grating. 600 grooves/mm and 2 <sup>nd</sup> chirped grating in series for the testing setup measurement. (at region I area of chirped grating).....	57
42. Actual peak power measurement for each wavelength for the 600 grooves/mm and 2 <sup>nd</sup> chirped grating in series for the testing setup measurement. (at region I area of chirped grating).....	57
43. Peak power position of each wavelength for dual grating. 600 grooves/mm and 2 <sup>nd</sup> chirped grating in series for the testing setup measurement. (at region II of chirped grating).....	58
44. Actual peak power measurement for each wavelength for the 600 grooves/mm and 2 <sup>nd</sup> chirped grating in series for the testing setup measurement. (at region II area of chirped grating).....	58
45. Peak power position of each wavelength for dual grating. 600 grooves/mm and 2 <sup>nd</sup> chirped grating in series for the testing setup measurement. (at region III area of chirped grating).....	59
46. Actual peak power measurement for each wavelength for the 600 grooves/mm and 2 <sup>nd</sup> chirped grating in series for the testing setup measurement. (at region III area of chirped grating).....	59
47. Channel's peak power position shifting as the groove density of 1 <sup>st</sup> chirped grating varies from region I to region II and region II to region III.....	60
48. Channel's peak power position shifting as the groove density of 1 <sup>st</sup> chirped grating varies from region I to region II and region II to region III.....	60
49. Channel's peak power position shifting as the groove density of 2 <sup>nd</sup> chirped grating varies from region I to region II and region II to region III.....	61
50. Channel's peak power position shifting as the groove density of 2 <sup>nd</sup> chirped grating varies from region I to region II and region II to region III.....	61

51. Calculated Position of wavelength channel for 1 <sup>st</sup> and 2 <sup>nd</sup> chirped grating.....	70
52. Calculated angular position of wavelength channel for 1 <sup>st</sup> and 2 <sup>nd</sup> chirped grating.....	70
53. Calculated position of wavelength channel for 1 <sup>st</sup> and 2 <sup>nd</sup> chirped grating for the different region .....	71
54. Calculated position of each wavelength channel as the groove density varies for testing setup.....	74
55. Calculated angular position of each wavelength channel as the groove density varies for the final set.....	74
56. Calculated position of wavelength channel for the case when the wavelength channel interacted over the range of the chirped grating without overlapping the same groove density area.....	79
57. Calculated position of wavelength channel for the case when the wavelength channel interacted over the range of the chirped grating with overlapping the same groove density area.....	79

## **Chapter 1**

### **Introductions and Communication Network**

#### **Introduction**

Fast paced increase in the need for the higher bandwidth in communication systems has led to the development optical networks. While moving to an optical network topology has increased the available bandwidth, today's communication technologies still do not fully utilize the potential of optic communication systems, due to limiting constraints in the optical system components. All optical network systems have the potential to dramatically increase the efficiency of communication networks however, due to high cost and power loss today's communication networks still rely on optical-to-electrical and electrical-to-optical conversion network elements. The difficult task in creating all optic networks is the development cost effective, flexible, and reliable Wavelength Add Drop Multiplex (WADM) components capable of demultiplexing/multiplex a highly dense signal efficiently.

Even with the advancement in optical components within the optical communication systems, the available wavelength channel ranges are limited. These limitations arise from the optical fiber, which has narrow wavelength ranges with low loss centered at wavelength, 0.8  $\mu\text{m}$ , 1.3  $\mu\text{m}$  and 1.5  $\mu\text{m}$ . In addition to the limitations of the optical fiber,



the optical amplifiers, such as the erbium dope fiber amplifier (EDFA), currently in used also limit the minimum channel spacing due to the limited range of wavelengths it can amplify uniformly, typically about 35-40 nm [23]. Therefore, in order to increase the efficiency of optical communication systems, the number of channels within the available wavelength ranges needs to be increased. However, in today's optical communication systems, the demultiplexer is one of the factors which limits the number of channels that can be transmitted through the optical fiber, since it can only demultiplex wavelength channels with wavelength separations larger than 0.5 nm. Therefore, to increase the number of the wavelength channels, there is a need for a demultiplexer that is capable of separating closely packed wavelength channels. To meet this need, this thesis discuss the research and development of a demultiplexer constructed with cascading diffraction gratings to achieve a demultiplexer that is capable of separating the closely packed, less than 0.5 nm, wavelength channels.

## **1 Communication Network**

### **1.1 Communication Technologies**

Current communication systems consist of two types of technologies, wireless and wired. For the wireless technology, microwaves or radiowaves are used to transmit information over the air. For wired technology, we use metal-based transmission media or fiber optic-based media to transmit information over the land. When comparing the two wired technologies, fiber optic-based technology offers many advantages over metal base technology. Compared to metal-based technology, fiber optic-based technology

offers larger bandwidth, lower loss, no electromagnetic interference, smaller cross-talk, and higher security. Also, optical fiber is smaller and lighter than the metallic counter part, and consequently, it is much easier to install than metallic-based connections.

## **1.2 Fiber Optic Communication Setup**

The basic communication system setup consists of a signal transmitter, channel, and receiver. First, the signal is modulated on a carrier frequency using one of many different modulation methods. Second, the modulated signal is transmitted over the channel. Finally, the modulated signal is received at the receiver and demodulated.

Currently, most of the communication system setups are a mixture of metallic-based connections and fiber optic based connections. Typically in short-haul communications, metallic-based channel media are used and for the long haul, some metallic and fiber optic channels are used to transmit signals. In long-haul transmission using fiber optics, the information source is converted into electrical signals then converted into optical signals and transmitted over the fiber optic cables.

Even with introduction and development of many different technologies in optical communication systems, full capabilities of the optic networks are not utilized due to limitations of the individual components within the optical systems. These limitations include: dispersion of wavelengths while traveling in the optical fiber, lack of stable and narrow spectral widths, and incapability of separating closely packed wavelengths.

Still with the limitations of the optical system components, current communication systems do not fully utilizes the potential of fiber optic technologies that are available. The biggest cause of these limitations is the mixture of metallic (electrical) and optic

(light) based components. With all the improvements and developments, current communication systems still depends on the electrical signals within the networks (e.g. at routers, regenerator, and repeater), which limits the bandwidth and speed. This limitation arises mostly at the nodes within the communication-network. As the signal reaches the nodes of the network, each signal is distributed (routed) through the network. Current communication systems still depend on an electrical means to distribute (route) the communication signal to a designated point instead of routing the light signal directly to the intended path or channel. This means that the optical signal must be transformed into an electrical signal each time it reaches a node of the communication network and then routed to its designated node or receiver.

In order to use the full bandwidth of optical technologies available, an all optical approach in such networks is desirable. To realize the all optical network, some of the key optical system components within the system are in need of improvement.

### **1.3. Components of Fiber Optic Communication System**

In the fiber optic communication system there are many different components that are essential, including, light source, optical fiber, multiplexer, demultiplexer, optical amplifier, router/switch, and receiver [14].

#### **1.3.1 Light Source**

In order to send a signal over the fiber optic system, the signal needs to be converted from an electrical signal to an optical signal before launching it into the fiber. To convert the electrical signal to an optical signal, some type of light source is required. The light

sources currently used with fiber optics are semiconductor light source; either a light emitting diode (LED) or a semiconductor laser. Using either LED or laser, the signal is modulated with different modulation schemes, either internally or externally depending on the required bandwidth, and then the signal is transmitted over the channels (transmission media).

Of the two light sources available, laser-based sources are more widely used due to their high power and narrow spectral width, even though they are more costly than the LEDs. Still some systems requiring low to moderate data rates use LED base light sources, since LEDs offer relatively low cost and are less sensitive to temperature [14].

### **1.3.2 Channel**

To deliver a light signal, fiber optic cable is used to guide the optical signal through the systems. In fiber optic systems, there are two general classifications of fiber optic cable, multimode and single mode fiber. Multimode fibers are still used for some applications calling for moderated distances and/or data rates. But, due to the limitations of the multimode transmission, single mode fiber currently dominates the market, even though single mode fibers are more costly, more difficult to fabricate within certain tolerances requirement, and more difficult to couple light into from the source [11].

#### **1.3.2.1 Multimode Fiber**

In the early stages of optical communication systems, the multimode fibers were used. Typically, the multimode has core size of 50  $\mu\text{m}$  and cladding size of 125  $\mu\text{m}$ . This large core size allows many modes of propagation to exist within the fiber, which gives rises to

the modal dispersion, a condition where different propagation modes of the light pulse (signal) travel different paths resulting in temporal spreading of the pulse. This type of modal dispersion limits the data rate of multimode fiber to less than 100 Mb/s.

#### **1.3.2.2 Single-mode Fiber**

To reduce the effect of modal dispersion in fiber, single mode fibers were developed. Typically, single-mode fiber has core size of 9  $\mu\text{m}$  and cladding size of 125  $\mu\text{m}$ . Theoretically, this core size allows only one mode of propagation to exist within the fiber at a given wavelength that minimizes dispersion [29]. However, even the single propagation mode still suffers from chromatic dispersion [24], a condition arising from the spectral spread in the light and the spectral dependence of the refractive index of the material. In chromatic dispersion the different frequency components travel at different phase velocities within the waveguide medium, the fiber core. Nevertheless, single mode fiber allows at much higher data rate, 10 to 40 Gb/s, than the multimode. Further, single mode fiber can be designed not to have net dispersion at a given wavelength (or over a narrow wavelength range). These qualities make single mode fiber the transmission medium of choice for high bandwidth applications.

#### **1.3.3 Amplifier**

Most times in long-haul communications, the signal needs to be amplified between connections. Prior to the advent of optical amplifiers, amplification of an optical signal required that it be converted to an electrical signal, reconditioned and amplified electrically, and converted back to an optical signal to be launched in the network again.

However, since the introduction of the erbium doped fiber amplifier (EDFA), which allows optical amplification of the signal, it has been possible to transmit optical signals over long haul without having to introduce electrical nodes that slow the data rate [9]. Still, for extremely long-haul networks, optical signals need to be reshaped (regenerated), due to distortion caused by the optical amplifiers and fiber, including amplified spontaneous emission (ASE) and dispersion.

### **1.3.4 Multiplexing of Optical Signals**

To efficiently use the available bandwidth, typically, different channels are multiplexed into a single channel. Electronically, signals are multiplexed in the time or frequency domain, known as TDM (time division multiplexing) for time domain and FDM (frequency division multiplexing) for frequency domain. Also CDM (code division multiplexing) is used in many of today's communication systems. Each of these multiplexing schemes lends themselves best to certain modulation approaches. Optically, signals are multiplexed in the wavelength domain, known as WDM (wavelength division multiplexing), which is complimentary to the other multiplexing schemes. In addition to WDM, all optical multiplexing scheme utilizing TDM and CDM are currently implemented [13].

#### **1.3.4.1 Multiplexing Scheme in Hybrid Communication System**

In hybrid communication networks, where electrical and optical systems are used together, WDM alone cannot satisfy the all the needs of a large network, especially when a single carrier wavelength is used for single channel. Therefore, signals in current

communication network are multiplexed electronically into either TDM or CDM signals and further multiplexed with WDM as the electrical signal are converted into an optical signal.

#### **1.3.4.2 Multiplexing Scheme in All Optical System**

Based on electrical multiplexing schemes, optical signals are also being multiplexed using TDM, CDM, and WDM [10]. In OTDM (optical time division multiplexing), unlike electrical TDM, where signals are divided in time slots, electrical pulses are converted into optical pulses and then optical pulses are compressed using special fiber [10]. In WDM, each wavelength is used as a carrier for a signal. Finally, in OCDM (optical code division multiplexing), a signal is coded and decoded using similar technique as the electrical counter part [11].

#### **1.3.5 Multiplexer and Demultiplexer**

In optical systems, ability to combine (multiplex) and separate (demultiplex) the closely spaced carriers into each wavelength channel is crucial. As the capability of separating closely spaced wavelength channels increases, the capacity for sending more information over the fiber increases. However, there is a limit to bit rate which can be transmitted, as the bit rate increases the channel spacing has to increase, but current technology has not yet reached the maximum channel spacing for available bit rates.

There are many different methods in which the light signals are separated according to wavelengths. The technologies most often used to demultiplex/multiplex optical signals in current optic systems, employing DWDM (dense wavelength division multiplexing) re

methods base on reflective/refractive gratings, array waveguide gratings, and fiber Bragg gratings (FBG) [2].

### **1.3.6 Router/Switch**

Once the optical signals have been delivered to a node of the network and the mixed signals have been demultiplexed, each signal is routed to its designated destination. To route the optic signals, there are several different methods utilized, which depend on the number of channels and channel spacing. For a low number of channels, FBG based routers or simple mirror-based routers are used to direct the signals. Currently, for moderate to high density channels spacing, MEMS (microelectronic mechanical systems) are being implemented.

Routers and switches are the main cause of delay in the optical network, especially when mechanical-based routers are used (e.g. routers using motors to rotate the mirrors).

### **1.3.7 Receiver**

Once the optical signal reaches the destination, it is detected, demodulated, and decoded in electrical form by the receiver. To the convert optical signal to an electrical signal, semiconductor-based photo detectors are used. The electrical signal is amplified and passed along for equalization and discriminated by electrical circuitry [14].

## **1.4 Wavelength add/drop multiplexer (WADM)**

One of the key components in the optical network system is WADM (wavelength add/drop multiplexer), also known as OADM (optical add/drop multiplexer). WADM



allows the signals to be dropped or added at the nodes of the system network, allowing efficient use of the optical fiber network. Without an OADM, it would be necessary to place additional optical cable for each path between the nodes in the optical network.

In next chapter, Chapter 2, more detail about the gratings used in today optical communication technologies will be discuss along with their use in this project.

## **Chapter 2**

### **Different Grating Technologies**

There are three primary types of gratings used to develop multiplexer and demultiplexer systems: Bragg gratings, arrayed waveguide gratings, and diffraction gratings. Each grating type offers unique properties, which can be used to develop diverse multiplexer/demultiplexer characteristics for different requirements within optical systems. The following sections will describe each of these.

#### **2.1 Bragg grating**

For simple or less dense WDM systems, a multiplexer/demultiplexer is constructed using a Fiber Bragg Grating (FBG). The FBG offers both narrow and broad wavelength demultiplexing/multiplexing capabilities. Typical FBG multiplexer/demultiplexer structures consists of a Bragg grating and a 3-dB coupler.

The fiber Bragg grating is a periodic (or near periodic) distribution of alternating regions of higher and lower refractive index. The effect of the alternating refractive index produces a narrowband mirror, which reflects a narrow range of wavelengths around the Bragg wavelength (given in Eq.1) and allows all other wavelengths to pass through. At the interface between the alternating refractive index a portion of the forward going signal is reflected and the rest is passed. At each successive junction, another portion of the forward going signal gets reflected back. At or near the grating's matched

wavelength, known as the Bragg wavelength or Bragg frequency, all of the reflected waves add in phase and as a result the signal is nearly completely reflected [15].

The Bragg wavelength is given in Eq. 1,

$$\lambda_B = 2n_0\Lambda \quad (1)$$

where  $n_0$  is the average refractive index of the propagation modes and  $\Lambda$  is the period of index modulation.

Currently the most common method of producing fiber Bragg gratings is through the use of a silica phase mask and ultraviolet light (UV). First, the proper grating size is etched onto the phase mask and the fiber is exposed to UV light. Due to the UV sensitivity of the fiber core, when the core is exposed to UV light, the index of refraction of the core changes. This change in refractive index creates a periodic structure of varying index of refraction, which acts as the Bragg grating. Another method of fabrication without the use of a phase mask is through the use of two UV sources. In this method, two UV sources are shone across the optical fiber and the fringes produced by the interference of the two sources cause the change in refractive index.

Normally a FBG is able to reflect a narrow range of the wavelengths near or at Bragg wavelength. However, through used of a chirped Bragg grating, where the periodic structure of the altering refractive index changes from low to high with distance through the grating, broad wavelength ranges can be reflected.

Even though the FBG-based demultiplexer is capable of demultiplexing a narrow range of wavelengths, the FBG is only capable of demultiplexing a single wavelength

range at a time. Therefore, in order to demultiplex a multi-channel system, multiple FBG demultiplexers are needed in series. For example, in order to demultiplex a 16 channel signal, a minimum of 8 FBG demultiplexers are required in a cascade configuration, with each FBG having a different Bragg wavelength. Because of this characteristic, FBG-based demultiplexers are typically used for less dense WDM systems.

Since a demultiplexer using FBG is capable of demultiplexing a single wavelength range at a time, there have not been many improvements made to FBG-based demultiplexers recently. Most of the improvements to the FBG technologies have been in development of efficient and cost effective ways of creating accurate periodic structures for FBGs.

## 2.2 AWG (Arrayed Waveguide Grating)

One of the most widely used multiplexer/demultiplexer technologies is the AWG multiplexer/demultiplexer. The AWG consists of input and output waveguides, typically star couplers, with the arrayed waveguide between them, having a constant path-length difference between neighboring waveguides, see Figure 1.

As the multi-channel signal enters the input section of the AWG, it is distributed evenly throughout the input waveguides, due to the power distribution characteristic of the star

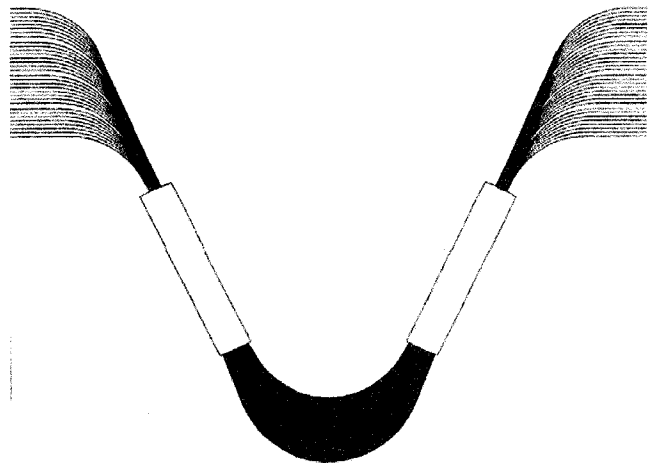


Figure 1: Arrayed Waveguide Grating (AWG)

coupler [12]. As the redistributed light beams enter the arrayed waveguide section of the AWG, each light beam travels a slight different path length, where the difference is given in Eq. 2.

$$\Delta L = \frac{n_s d D \lambda_0}{N_c f(\Delta \lambda)} \quad (2)$$

Here,  $D$  is the lateral separation of the input waveguides,  $d$  is the arrayed waveguide separation,  $f$  is the radius of curvature of the star coupler,  $N_c$  is the group index of the effective core index  $n_c$ ,  $n_s$  is the effective index of slab region,  $\lambda_0$  is the center wavelength of the WDM system, and  $\Delta \lambda$  is the channel spacing of the WDM system. As the light travels through the arrayed waveguide, it experiences a phase shift due to the different path lengths traveled. This relative phase shift between each channel at the exit of arrayed waveguide is given by Eq. 3.

$$\Delta \phi = \frac{\Delta L}{\lambda} \quad (3)$$

As the light exits the arrayed waveguide section of the AWG, each of the light beams constructively interfere into single focal points on the second slab. The location of the focal point for each channel depends on its carrier wavelength. The physical length separation of the wavelengths for the AWG is given by Eq. 4.

$$\frac{\Delta x}{\Delta \lambda} = \frac{N_c f(\Delta L)}{n_s d \lambda_0} \quad (4)$$

In the AWG, the number of array waveguides is increased in order to minimize the loss. Also, the number of the array waveguides is increased as the number of channel increases.

In an attempt to increase the demultiplexing-abilities of AWGs, Takada et al [4][5], used two AWGs, one as the primary and the other as the secondary in tandem. In an improved version [5], a 1 X 5 multiplexer/demultiplexer with flat-top interference filter and five 1 X 288 AWGs with a 10 GHz channel spacing as second filters were used.

The primary AWG separated the signals into 5 channels in succession according to the wavelength. Then the 5 channels were demultiplexed using the secondary 1 X 288 AWG for each channel.

Even though Takada et al. [5] were able to develop a lower transmission loss demultiplexer/multiplexer, capable of separating signals with channel spacing of 10 GHz, the method of using two-stage AWG had its down falls. In order to demultiplex the 288 channels in the secondary AWGs, a 5-inch wafer was required to make a single secondary AWG due to the large number of arrayed waveguides and long focal length. The secondary AWG needed more than 1000 arrayed waveguides and more than 4 cm of spacing for focal area.

To optimize the performances of the tandem AWG demultiplexer/multiplexer, additional processes were implemented on secondary AWG. The temperature of the secondary AWG's substrate had to be controlled in order to obtain all the channels from the output of the secondary AWG. In addition, UV irradiation was used to sharpen the pass band of AWG to compensate for the phase error. Even with the phase error compensation with UV irradiation, larger side lobes were present on the higher bands, which led to higher phase error.

In further development of cascading AWGs in tandem, Takada et al. were able to increase the number of channels separated using 3-stages [6], without sacrificing much in transmission loss. In the 3-stage configuration, Takada was able to reduce the size of the biggest AWG, but a number of different parameter AWGs had to be fabricated individually.

## 2.3 Diffraction Grating

Another common method used in multiplexer and demultiplexer technology is the use of diffraction gratings. The diffraction grating is simply a reflective or transmitting surface with periodic grooves, see Figure 2. There are two types of diffractive gratings commonly used in today's multiplexer and demultiplexer scheme, ruled and holographic. Even though both types of gratings consist of closely spaced, straight-line grooves in parallel on the substrates, there are differences between the two. The differences between the ruled and holographic grating arise from not only the way each grating is manufactured but also by the physical profile of each groove [23]. The ruled gratings have a saw tooth-shaped groove profiles tilted at a specific angle (the blaze angle) that is designed to have maximum efficiency at a specific (blaze) wavelength. The holographic grating has a sinusoidal groove profile. Because the holographic grating has a sinusoidal pattern groove, holographic gratings cannot be blazed easily and the

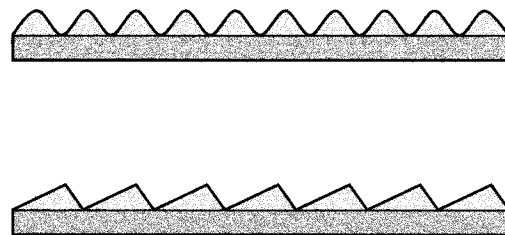


Figure 2: Diffraction grating, holographic grating profile on top and ruled grating on the bottom

efficiency is usually less than a comparable ruled grating. However, when the groove spacing-to-wavelength ratio is nearly one, holographic gratings have virtually the same efficiency as ruled gratings and they can be fabricated with much higher groove densities.

Both ruled and holographic diffraction gratings separate a multi-wavelength source into its component wavelengths by diffraction, a process in which light incident on a surface with dimensions similar in size to its wavelength is dispersed at certain angles. As the multiple wavelengths hit the grating, each wavelength is diffracted into a different angle. It is this difference in diffraction angle that separates light into each spectral component.

In a transmission grating the diffracted light is passed through at an angle equal to the diffraction angle. For reflective gratings, the light is first diffracted as it is reflected by the coating on the surface of the grooves at an angle equal to the diffraction angle.

The relationship between the incident angle, wavelength, and groove density to the diffraction angle is given by grating the equation in Eq. 5.

$$n\lambda = \Lambda(\sin(\theta_i) \pm \sin(\theta_d)) \quad (5)$$

Here,  $n$  is the integer diffraction mode-order for the light,  $\Lambda$  is the spatial period of the groove on the grating,  $\theta_i$  is the incident angle,  $\theta_d$  is the diffracted angle, and  $\lambda$  is the wavelength of the light. This grating equation is the same for both the ruled and the holographic grooves in reflective and transmission gratings. The grating equation can be rewritten in the form given by Eq. 6 to show the relationship between the incident angle and diffracted angle. Equation 6 shows that, the diffracted angle depends on the



wavelength, groove period, and incident angle. As wavelength increases and or the groove period decreases, the diffracted angle increases.

$$\theta_d = \sin^{-1}(\frac{n\lambda}{\Lambda} - \sin(\theta_i)) \quad (6)$$

Currently, not much attention has been given to the diffraction grating scheme since the diffraction of light is well studied and diffraction by a single grating is limited by the grating Equation. Therefore, there has not been much room to improve the diffraction grating. Most of the efforts associated with diffraction gratings have been in manufacturing process, to increase the consistency of groove profile and groove spacing. Other improvements in diffractive grating technology have been in shaping of gratings to focus light without using lenses or to line up the light to couple into fiber.

## **2.4 Improvement of Diffraction Grating Demultiplexer**

Of the three types of gratings, the diffraction grating was chosen for this thesis to construct a tunable demultiplexer. In the Chapter 3, the theory and calculations supporting the design will be discussed to show the feasibility of the demultiplexer developed through this research. The system presented here, which is capable of demultiplexing wavelength channels that are separated by less than 0.5 nm, was engineered by cascading two diffraction gratings, one normal ruled grating and a chirped grating. In later chapters, Chapter 4 and Chapter 5, the experiment setup and measured data will be presented. Finally, in Chapter 6, the results of the data will be discussed.

## Chapter 3

### Theory and Calculation

#### 3.1 Theory

Most diffraction based multiplexers and demultiplexers schemes use a single grating to separate the WDM signals. Yet, a single grating system with limited space, however it is configured, can only resolve limited wavelength channel spacing. In order to increase the demultiplexing capability of a single grating system, the physical space between the grating and the output fiber has to be increased, since angular separation between the wavelengths is limited by the diffraction equation (see Eqs. 5 and 6).

As can be seen from Eq. 6, for a single grating system, only two factors can be controlled to increase the separation between the wavelengths, incident angle and groove density. However, the values of incident angle and groove density are limited by the Eq. 7, given below that expresses the range of angles over which diffraction is possible. If Eq. 7 is not satisfied, the values of the all the diffraction angles becomes imaginary, which signifies that only the mirror reflection or total internal reflection/refraction exist.

$$\frac{n\lambda}{\Lambda} - \sin(\theta_i) \leq 1 \quad (7)$$

In addition, the groove density of the grating is limited by the wavelength since as the grating's groove period gets smaller than the wavelength, the grating does not diffracts

the light, but reflects it as mirror would. Therefore, once this limitation is reached, the separation can only be increased by increasing the distance between the output fiber and grating. Doing so is not ideal since prevailing demand is for smaller, more reliable, and cost effective systems.

To increase the separation between the wavelengths for a given device size using the grating system, multiple gratings in series are used. By having a series of gratings, the incident angle and/or the groove density for each of the individual wavelength channel changes at the second grating, giving rise to an increase in separation, as shown in Figure 3. As Figure 3 shows, the wavelengths are initially separated by the first grating, then the separated wavelengths travel different paths to the second grating, where the shorter wavelengths travel to a second grating with smaller diffracted angles than the longer wavelengths. This wavelength-dependent change in incident angle for the second grating gives rise to larger diffraction angle changes in the second grating, and hence, larger angular separation of the wavelengths. The drawback to using such a configuration is the loss that is encountered by using two gratings in series. This issue will be addressed in later chapters. For now, we proceed with the derivation of the resolution performance for dual grating demultiplexers.

### 3.1.1 Chirped Grating

In order to increase the effectiveness of the dual grating system, the chirped grating

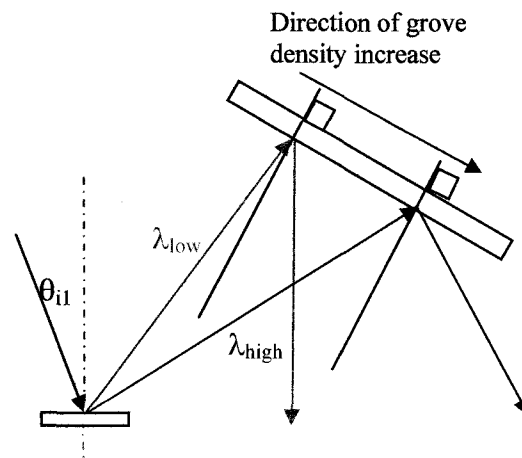


Figure 3: Diffraction behavior of wavelength

is introduced in this research. The idea of the chirped grating, a grating fabricated such that groove density varies from one position to another position within the same grating, arose from grating equation. This equation shows that diffraction angle is greatly influenced by the groove density of the grating, and thus, by changing the groove density as a function of the wavelength one can control the diffraction angle. By controlling the diffraction angle, the channels can be routed to a desired location. In order to accomplish this routing, a dual grating system must be implemented. By placing the chirped grating at the position of first (master) grating would not make much sense, since at the first grating, all channel would interact within the same area, since each channels travels as a single beam. However, once the multi-channel beam diffracts from the first grating, each wavelength is spatially separated. Therefore, by introducing a chirped grating at the second (slave) grating position, where each wavelength interact with a different location on the second grating, it would be possible to diffract each channel with a different groove density. Thus by changing the location of incidence for each channel on the chirped grating, either by rotation of the master grating or translation of the slave grating, one can route a particular channel to desired location. Further, the additional diffraction of the channels form the second grating can effectively introduce additional separation of the channel, which will be shown in the calculation in this chapter.

### **3.2 Calculations**

Using the grating equation (see Eqs. 5 and 6), two different setup calculations were made to predict the position of each WDM channel as travels through the series of diffraction grating.

### 3.2.1 Initial testing setup calculation

To test the theory before the chirped grating could be fabricated, a dual-grating setup, as shown in Figure 4, was setup and tested. For the initial setup, the following calculations were done to predict the position of the each wavelength.

The experiment was setup such that for given angle at the second grating, the diffracted angle would be in the increasing x-axis direction.

Recall that Eq. 6 is, given as:

$$\theta_{d1} = \sin^{-1}\left(\frac{\lambda_t}{\Lambda_1} - \sin(\theta_{i1})\right) \quad (6)$$

where  $\lambda_t$  is the wavelengths,  $\theta_{i1}$  is the incident angle on first grating, and  $\Lambda_1$  is the groove density of the first grating. Using this diffracted angle as the incident angle for a second grating, the second diffracted angle  $\theta_{i2}$  is given by Eq. 8:

$$\theta_{d21} = \sin^{-1}\left(\frac{\lambda_t}{\Lambda_2} - \sin(\theta_{d1} - \theta_g)\right) \quad (8)$$

Here  $\theta_{i2}$  (labeled as angle b in Figure 4) is the incident angle of the light on the second grating, and  $\Lambda_2$  is the groove density of the second grating.

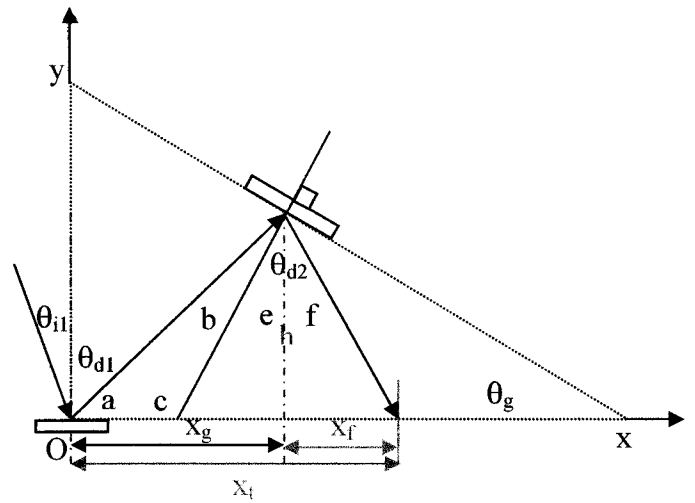


Figure 4: Geometry of initial dual grating setup

Given the angle of second grating ( $\theta_{d2}$ ) and the height of the grating  $h_{y0}$ , which is the vertical distance between the x-axis and the position of the reference wavelength  $\lambda_0$  at second grating, the line equation of the second grating position is written as:

$$y = (-m_g \cdot x) + h_{y0} - (x_{x0} \cdot m_g) \quad (9)$$

Then the line equation of the light path between the first grating and second grating can be written as:

$$y = m_a \cdot x \quad (10)$$

Here  $m_g$  is slope of second grating path equation,  $m_a$  is the slope of the light path between the first and second gratings,  $h_{y0}$  is the y position of the reference wavelength at the second grating,  $\lambda_0$  is the reference wavelength, and  $x_{x0}$  is the x position of reference wavelength.

Combining the two equations above results in:

$$y = \frac{m_g \cdot x_{g0} + h_{y0}}{1 + \frac{m_g}{m_a}} \quad (11)$$

where the slopes can be written as:

$$m_a = \tan(\theta_a) \quad (12)$$

$$m_g = \tan(\theta_g) \quad (13)$$

Then by using trigonometric relations, the x position of second grating is given as

$$x_g = \frac{\tan(\theta_g) \cdot x_{g0} + h_{y0}}{1 + \frac{\tan(\theta_g)}{\tan(\theta_a)}} \cdot \tan(\theta_{d1}) \quad (14)$$

and the horizontal distance between each wavelength from the grating to the final position on the x-axis where the output fiber is positioned is given as:

$$x_f = y \cdot \tan(\theta_{d2} - \theta_g) \quad (15)$$

Thus, the final x position of the each wavelength is the sum of the  $x_g$  and  $x_f$ , which is written as:

$$x_t = y \cdot (\tan(\theta_{d1}) + \tan(\theta_{d2} - \theta_g)) \quad (16)$$

Substituting for y gives the final equation:

$$x_t = \left[ \frac{\tan(\theta_g) \cdot x_{g0} + h_{y0}}{1 + \frac{\tan(\theta_g)}{\tan(\theta_a)}} \right] [\tan(\theta_{d1}) + \tan(\theta_{d2} - \theta_g)] \quad (17)$$

This final position  $x_f$  gives location of each wavelength relative to the position of initial light incident area of the first grating, which is defined as the origin.

### 3.2.2 Final Setup Calculation

The final dual-grating setup is set as shown in Figure 5. Unlike the initial measurement, the output fiber was placed in the  $y$ -axis. For the final setup, the following calculations were done to predict the output position of each wavelength.

The experiment was setup such that for a given angle at the second grating, the diffracted angle would be in the increasing  $y$ -axis direction, see Figure 5. Since the diffracted angle of second grating is in the increasing  $y$ -direction, the diffracted angle of second grating is different from the initial setup, where diffracted angle of second grating is now written as:

$$\theta_{d23} = \sin^{-1}\left(\frac{\lambda_t}{\Lambda_2} - \sin(\theta_g - \theta_{d1})\right) \quad (18)$$

Using the same method as the initial calculations with the line equation of the wavelength path and grating path position, and combining the two equations gives:

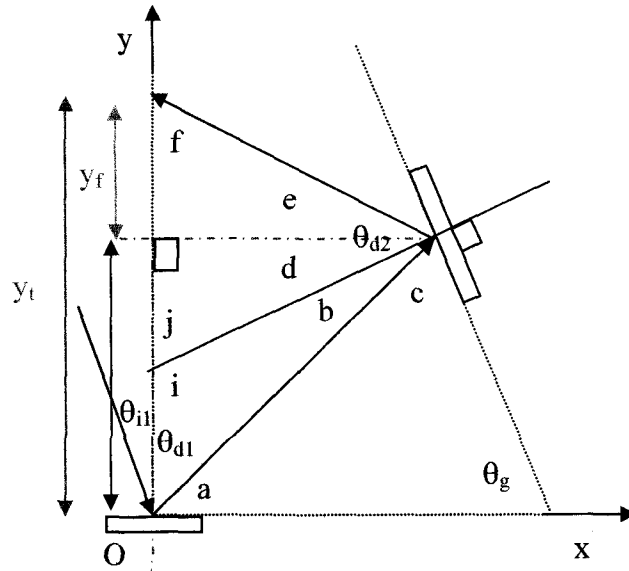


Figure 5: Geometry of final dual grating setup



$$x = \frac{m_g \cdot h_{x0} + y_{g0}}{m_g + m_a} \quad (19)$$

Again using trigonometric relations the y-position of second grating is given as;

$$y_g = x \frac{\sin(b+d)}{\sin(\theta_{d1})} \quad (20)$$

or

$$y_g = x \frac{\cos(\theta_{d1})}{\sin(\theta_{d1})} = x \cdot \cot(\theta_{d1}) \quad (21)$$

The vertical distance between the each wavelength from the grating to the final position on the y-axis, where the output fiber is positioned is given as:

$$y_f = x \frac{\sin(e)}{\sin(f)} \quad (22)$$

or

$$y_f = x \cdot \cot(\theta_{d2} + \theta_g) \quad (23)$$

Thus, the final y-axis position of each wavelength is the sum of  $y_g$  and  $y_f$ , which is written as

$$y_t = x \cdot (\cot(\theta_{d1}) + \cot(\theta_{d1} + \theta_g)) \quad (24)$$

Substituting x into the about equation gives:

$$y_t = \left[ \frac{\tan(\theta_g) \cdot h_{x0} + y_{g0}}{\tan(\theta_g) + \tan(\theta_a)} \right] \left[ \cot(\theta_{d1}) + \cot(\theta_{d2} + \theta_g) \right] \quad (25)$$

From the equations 17 and 25 both gives calculated position of the each channel for each configuration. As it can be seen by the equations, the relationship between the channel's wavelength and position is not linear, which is undesirable. However, by controlling the grating density variation of second grating (chirped), the position of each channel could be come more linear.

In next chapter, Chapter 4, where all the data will be presented that show the non-linearity of dual grating system.

## Chapter 4

### Experiment Procedures, Setups and Measurement

To test the theory of the dual grating system, multiple experiments were set up using two gratings in series. The following sections detail the various setups, experimental procedures, and results.

#### 4.1 Testing of the Theory

To test the efficacy of the multiplexer/demultiplexer scheme, various measurements were made with different components in one of two basic measurement configurations.

For the first measurement configuration, a single grating system, consisting of

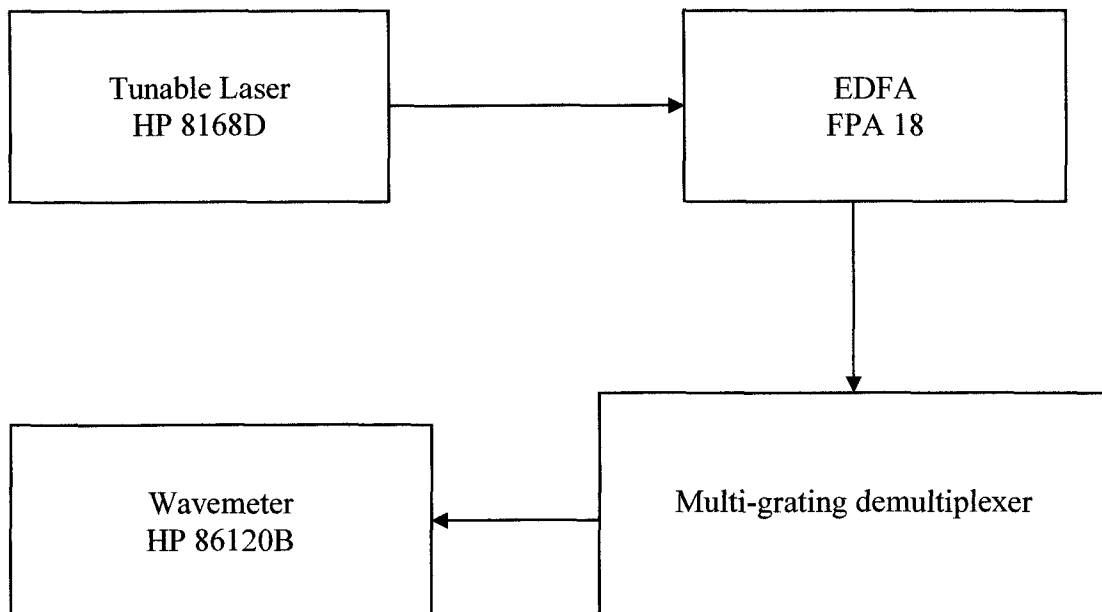


Figure 6: Schematic of the measurement setup

collimating optics and a uniform ruled grating (600 grooves/mm), was set up and tested as a reference. Then a second configuration using a dual grating system was set up and tested. In this second configuration, the original ruled grating was used along with one of the following gratings to increase the physical separation between the wavelengths:

1. Uniform 600 grooves/mm
2. Chirped grating

Groove spacing varied from 300 grooves/mm to 600 grooves/mm for the chirped grating (using segmented grating, which is described in a later section of this chapter)

#### 4.1.1 Layout of the Measurement Setup

A schematic of the experimental setup is shown in Figure 6, and the physical dimensions of this

setup are shown in

Figure 7. For the

laser source, a

tunable laser HP

8168D was used.

Since the maximum

output power from

the tunable laser

was 350  $\mu$ W (-4.6

dBm), an EDFA,

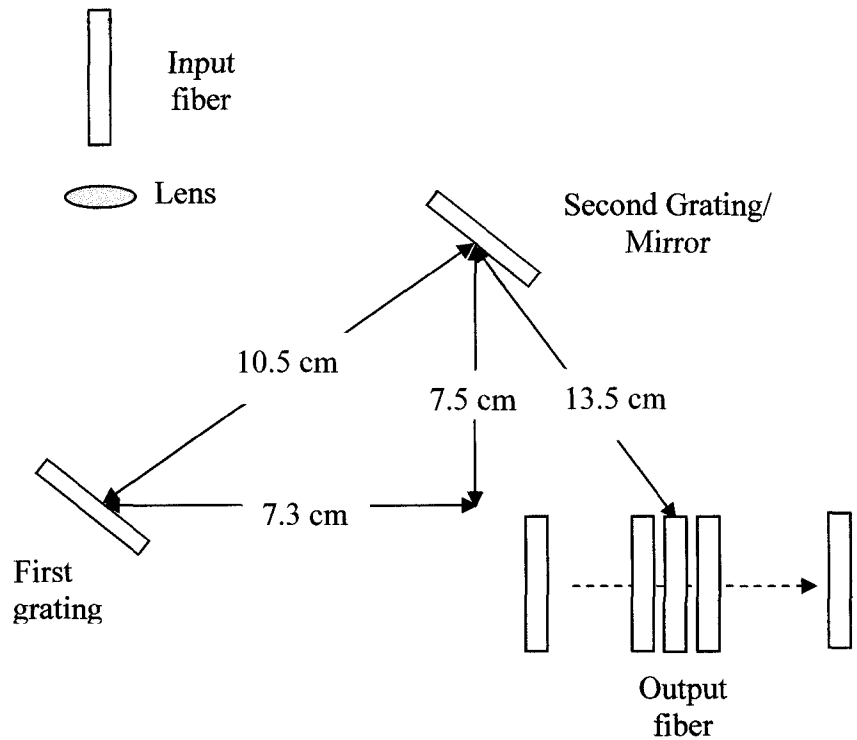


Figure 7: Dimensions of the setup

Newport FPA18, was used to amplify the tunable laser to 18 dBm. However, this caused the unwanted effect of spectral spreading of the laser due to ASE (amplified spontaneous emission), which could not be compensated for with the available equipment and shows up in the experimental results as broadened channel width. The experimental setup is shown in Figure 8. The amplified light was focused through the lens and transmitted through the multi-grating system. After the incoming signal was separated by the demultiplexing systems, the diffracted wavelengths were collected into single-mode fiber, designated in Figure 8 as the Output fiber. The output power was measured with a wavemeter, HP 86120B

#### 4.1.2 Reference Setup

First, to compare the results between the single and dual grating configurations, measurements using a single grating were performed (see Figure 9a). In this

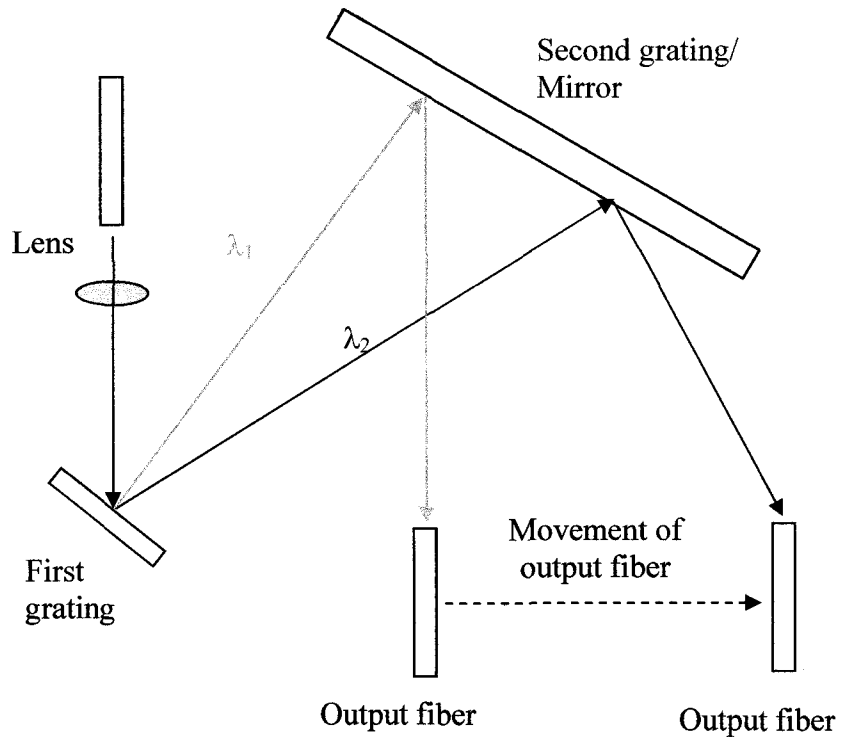


Figure 8: Measurement

setup, the input signal containing multiple wavelengths was diffracted via a gold-coated ruled grating with 600 grooves/mm (Edmund Optics). Since the separation of the channels increased as the distance between the grating and collection fiber increased, from the angular spreading of light from the first grating, the distance between the initial grating and output fiber needed to be held constant for all the setups. Therefore, in order to minimize the affect of the variation of the distance between the first grating and the output fiber, a mirror was placed between the first grating and the output fiber. This insured that all setups, both single and dual grating, had the same overall physical length.

#### **4.1.2.1 Actual Dimensions for First Setup**

In the setup, the components were placed such that they would minimize the distance between the each other. The dimension of the setup is as follows (also shown in Figure 7). The horizontal distance between the first grating and the second grating was 7.3 cm, which is labeled  $x_g$  in Figure 4. The vertical distance between the first grating and the second grating was 7.5 cm, which is labeled  $h$  in Figure 4. The distance between center of the first grating and center of the second grating was 10.5 cm. The distance between center of the second grating and the position of the output fiber where the middle wavelength's peak power was measure was 13.5 cm.

The system was constructed this way for following reasons. First, it was desirable to reduce the total size of the demultiplexer scheme. Second, in order to transmit the light over the total path length of the demultiplexer the light needed to be collimated. However, collimating the light required a second lens to be placed at the output fiber to refocus the light into the fiber. The placement of an additional lens (ball lens) in front of the output

fiber was difficult, though, and ultimately ineffective due to the lack of a stable lens holder that would fit within the allotted space and allow adjustment of the ball lens position to focus the light into the output fiber. Therefore, an additional lens in front of the output fiber was not used. Further, the minimization of the demultiplexer size in turn caused a constraint in the working area, which allowed only one lens to be used in front of the input fiber of the system to focus the light into output fiber after it had been transmitted through the demultiplexer scheme.

#### 4.1.2.2 Measurement Technique in First Setup

Using a tunable laser in series with an EDFA, a single wavelength, starting at the lowest laser wavelength (1545 nm), was transmitted through the multi-grating system. The actual power was measured using the

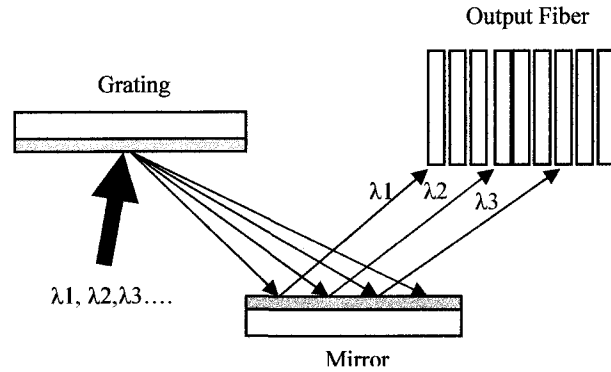


Figure 9a: Reference measurement setup.

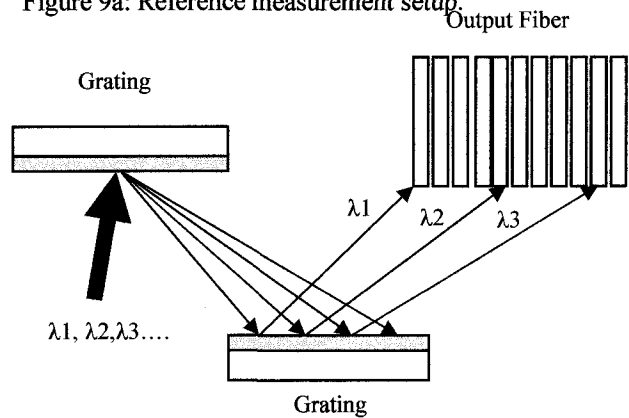


Figure 9b: Dual standard ruled grating (DS configuration), both grating with 600 grooves/mm

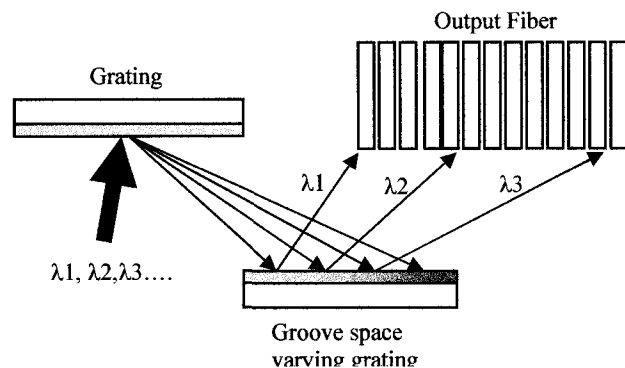


Figure 9c: Standard/chirped ruled grating (SC configuration), initial grating with 600 grooves/mm and groove-spacing varying grating for second grating

wavemeter by sweeping the output fiber in small intervals (0.05 mm) horizontally. Then, the power at each position was recorded with the HP wavemeter. Once the full beam width of the wavelength was measured, the individual channel wavelength was increased by 1 nm and this procedure was repeated until the wavelength reached 1555 nm.

#### 4.1.2.3 Reference Setup Results (Single Grating)

The following sections present the results of the experiments. The data for each of the setups are shown in Figures 10, 11, 12, and 13.

In the single 600 grooves/mm grating measurement, the spatial separation between each wavelength channel was small. The average spatial separation between each channel's peak power position was  $\Delta x / \Delta \lambda \approx$

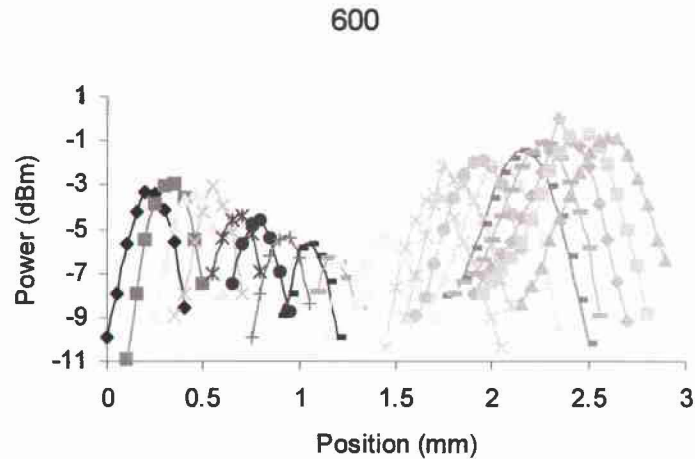


Figure 10: Actual measurement for each wavelength for single 600 grooves/mm. (Reference measurement)

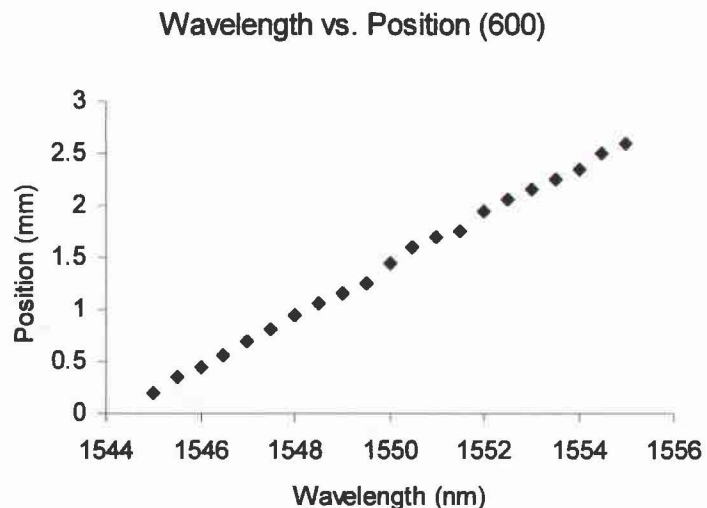


Figure 11: Peak power position of each wavelength for single 600 grooves/mm. (Reference measurement)



0.24 mm/nm. The optical channels ranged in wavelength from 1545 nm (at the initial position on x-axis) to 1555 nm in increments of 0.5 nm, see Figure 10.

The actual power measurement for each channel with the single 600 grooves/mm grating is shown in Figure 11. In the measurements, the power fluctuated between neighboring channels. On average, the peak power of each channel fluctuated  $\Delta P/\Delta\lambda \approx 0.67$  dBm/nm from the neighboring channels. The power difference between the highest power channel and the lowest power channel was 2.8 dBm. This power fluctuation in the measurements, which occurred in all the measurements, was partially due to the ineffective coupling into the output single-mode fiber, due to the small numerical aperture. More on this will be discussed in Chapter 5.

#### **4.1.3 Dual Grating Setup**

For the first dual grating measurement, the mirror was replaced with a second gold-coated ruled grating with 600-grooves/mm (see Figure 9b). An increase in the separation of the channels was expected in this case due to the change of incident angle of light on the second grating as well as from the additional diffraction resulting from the grating itself.

For the second dual grating measurement, the mirror was replaced with a segmented chirped grating with groove spacing varying from 300 to 600 grooves/mm, see Figure 9c. In this setup, a continuous chirped grating was not available, so the chirped grating was constructed by placing different groove spaced gratings next to each other. This in turn created a defect area at the joining of gratings. Because of this defect, measuring small wavelength spacing was not possible; however, a demonstration of the concept was

achievable.

The measurements were taken by moving a single fiber laterally from one end of the output to other. The measurement started from the position closest to the second grating, where the shortest wavelength was measured, and continued to the farthest output position, where the longest wavelength was measured. Measurements for all setups were conducted in same manner

to minimize the measurement variation. Also, the position of shortest wavelength was kept constant to avoid additional separation due to differences in path length.

For all measurements, the power transmitted to first grating was set at 5 dBm and the first-order diffraction mode was chosen to separate the signals.

Physical wavelength position, starting from the

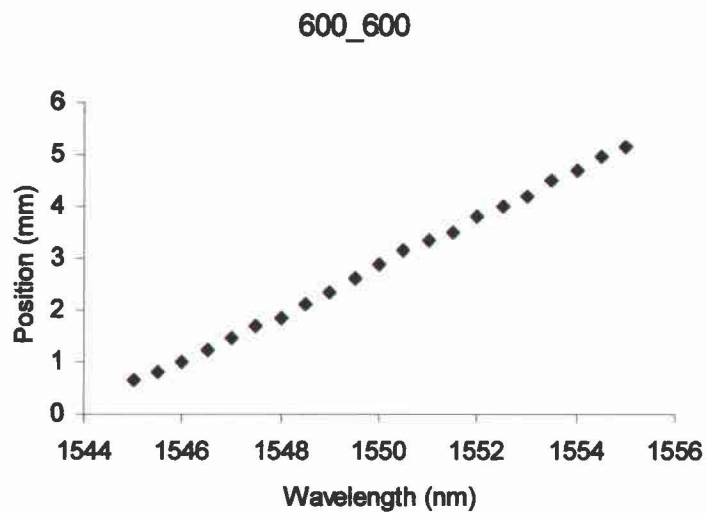


Figure 12: Peak power position of each wavelength for dual grating. Two 600 grooves/mm grating in series

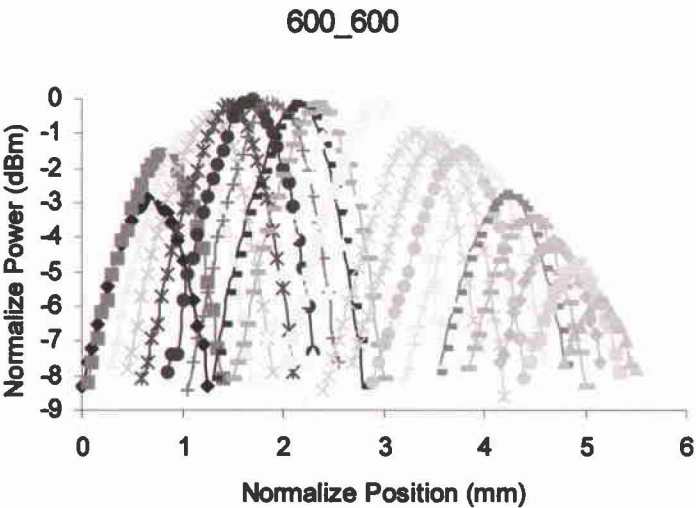


Figure 13: Actual measurement for each wavelength for dual grating. Two 600 grooves/mm in series.

shortest wavelength and continuing to the longest wavelength, is shown in Figures 9a, 9b, and 9c for both the dual standard-ruled grating (DS) and standard/chirped-ruled grating (SC) configurations, respectively. The position of shortest wavelength measured using the single grating and mirror configuration was set as a reference point for all other measurements. The channel wavelength separations were kept at  $\Delta\lambda = 0.5$  nm for the single grating and dual grating setups due to the minimum resolution of the wavemeter used in the experiment. For the segmented chirped grating configuration, the maximum channel separation was 1545 nm at the low end and 1555 nm at the high end. This large wavelength separation was selected in order to avoid the defects that occurred at the edges of the gratings, as well as to control groove density encountered by each of the wavelengths.

#### **4.1.3.1 Results for the Two 600 grooves/mm Gratings in Series**

The normalized position of the peak powers for each channel from the two gratings in series with 600 grooves/mm is shown in Figure 12. The average spatial separation between each channel's peak power position was  $\Delta x/\Delta\lambda \approx 0.44$  mm/nm.

The actual power measurements from the two grating in series are shown in Figure 13. On average, the peak power of each channel fluctuated  $\Delta P/\Delta\lambda \approx 0.67$  dBm/nm from the neighboring channels. The power difference between the highest power channel and the lowest power channel was 2.8 dBm.

## **4.2 First Experiment with Continuous Chirped Grating (Lateral Measurement Setup)**

After testing the dual grating system, two chirped gratings were fabricated, one grating with groove density varying from 300 grooves/mm to 600 grooves/mm and a second grating with groove density varying from 100 grooves/mm to 600 grooves/mm. Both gratings' groove density increased continuously over a 5 mm length. However, since the initial separation from the first grating (600 grooves/mm) did not separate the channels wide enough to cover the

full length of the chirped grating, each chirped grating was divided into three sections. The chirped grating with groove density varying from 300 grooves/mm to 600

grooves/mm was divided into sections consisting of groove density varying from 300 grooves/mm to 400 grooves/mm, 400 grooves/mm to 500 grooves/mm, and 500 grooves/mm to 600 grooves/mm. The chirped

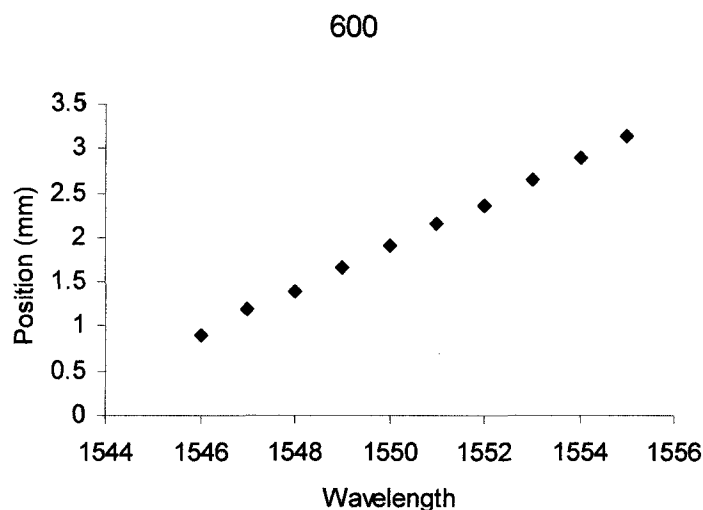


Figure 14: Peak power position of each wavelength for single 600 grooves/mm. For the testing setup measurement (Reference measurement)

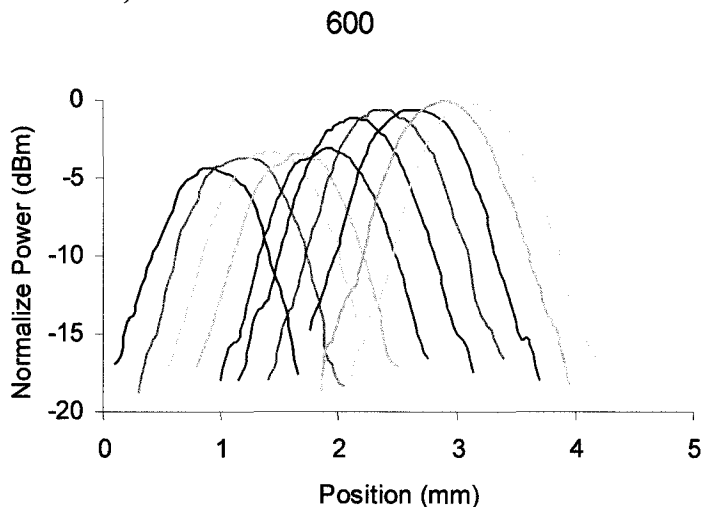


Figure 15: Actual measurement for each wavelength for single 600 grooves/mm. For the testing setup measurement (Reference measurement)

grating with groove density varying from 100 grooves/mm to 600 grooves/mm was divided into sections consisting of groove density varying from 100 grooves/mm to 275 grooves/mm, 275 grooves/mm to 450 grooves/mm, and 450 grooves/mm to 600 grooves/mm.

With these new chirped gratings, the previous experimental procedures were repeated. All the measurement including the single grating (reference measurement) and two 600 grooves/mm gratings in series were repeated to insure that any in advertent changes to the variables within the setup were accounted for in all tests. For example, in this second testing series, the position between the gratings were reduced to increase the power delivered to the collection fiber. However, this resulted in limited range in the incident angle for the first grating due to the geometry of the setup and the physical size of the grating.

#### 4.2.1 Reference Setup Results (Single Grating)

The normalized position of each channel for the single 600 grooves/mm grating is shown in Figure 14. The average spatial separation between each channel's peak power position was  $\Delta x/\Delta\lambda \approx$

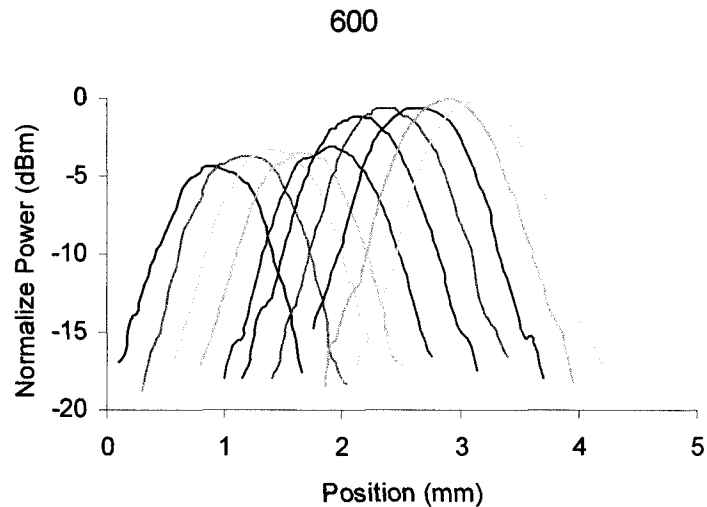


Figure 15: Actual measurement for each wavelength for single 600 grooves/mm. For the testing setup measurement (Reference measurement)

0.25mm/nm from the neighboring channels. The results of this reference measurement differed from the previous measurement due to slight difference in distance between the input and output (or collection) fiber.

The actual power measurements from the single 600 grooves/mm as the reference measurement for this setup is shown in Figure 15. On average, the peak power of each channel fluctuated  $\Delta P/\Delta\lambda \approx$

0.55 dBm/nm from the neighboring channels. The power difference between the highest power channel and the lowest power channel was 4.4 dBm.

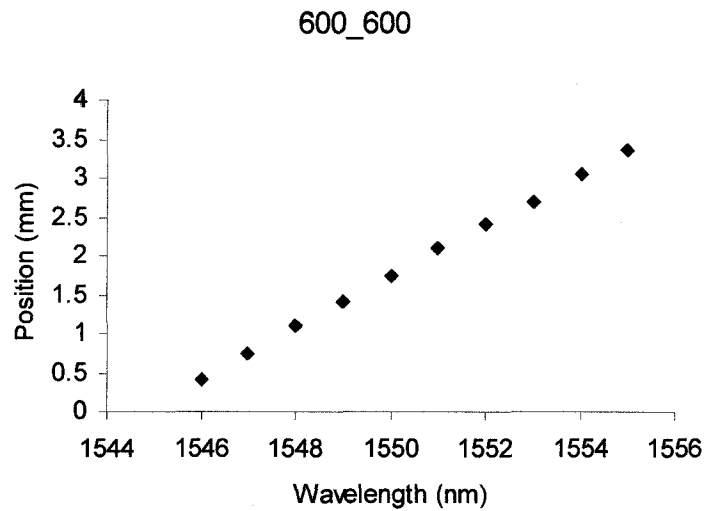


Figure 16: Peak power position of each wavelength for dual grating. Two 600 grooves/mm grating in series for the testing setup measurement.

#### 4.2.2 Results for the Two 600 grooves/mm Gratings in Series

The normalized position of each channel for the two 600 grooves/mm grating in series is shown in Figure 16. The average spatial separation between each

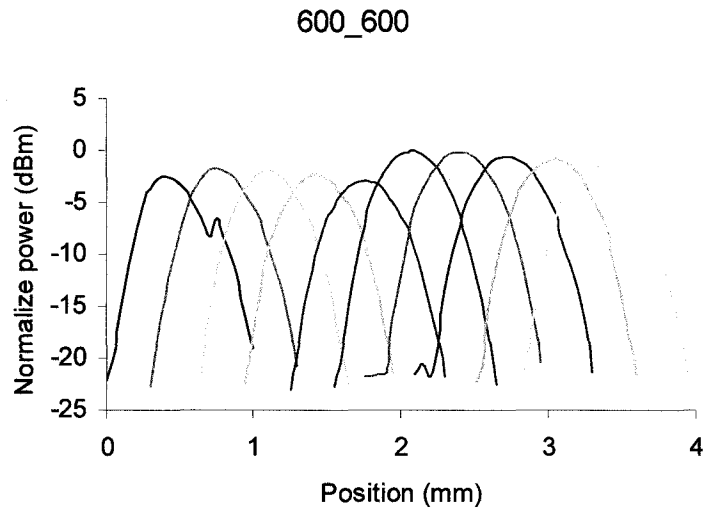


Figure 17: Actual power measurement for each wavelength for the two 600 grooves/mm in series. For the testing setup measurement.

channel's peak power position was  $\Delta x/\Delta\lambda \approx 0.33$  mm/nm.

The actual power measurements from the two 600 grooves/mm gratings in series are shown in Figure 17. On average, the peak power of each channel fluctuated  $\Delta P/\Delta\lambda \approx 0.67$  dBm/nm from the neighboring channels.

The power difference between the highest power channel and the lowest power channel was 2.8 dBm.

#### 4.2.3 Results for the 600 grooves/mm Grating and the 1st Chirped Grating in Series

The measurements from the 600 grooves/mm grating in series with the 1st chirped grating, having a grooves density that

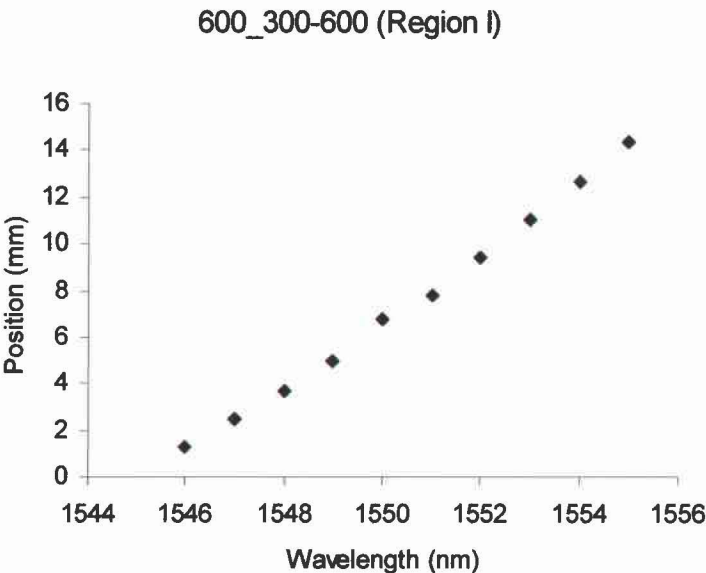


Figure 18: Peak power position of each wavelength for dual grating. 600 grooves/mm and 1<sup>st</sup> chirp grating in series for the testing setup measurement. (at region I area of chirped grating)

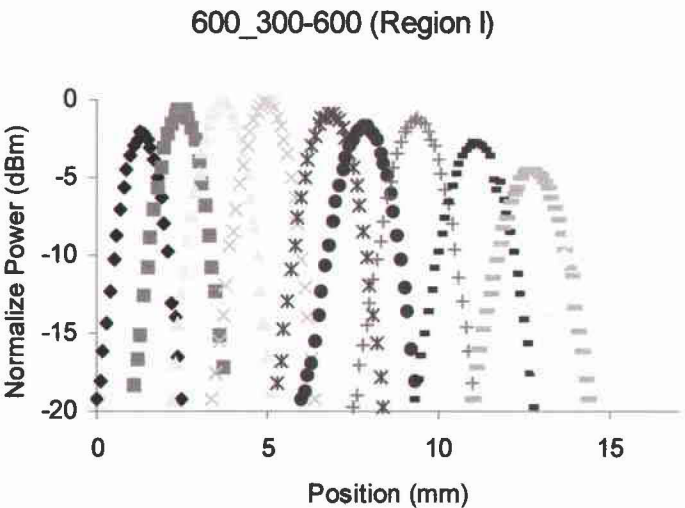


Figure 19: Actual power measurement for each wavelength for the 600 grooves/mm and 1<sup>st</sup> chirped grating in series for the testing setup measurement. (at region I area of chirped grating).

varying from 300 grooves/mm to 600 grooves/mm, are shown in Figures 18, 19, 20, 21, 22 and 23. Due to the small separation of the channels from the first grating (600 grooves/mm), the chirped grating was divided into three sections, region I (RI: 300 grooves/mm to 400 grooves/mm), region II (RII: 400 grooves/mm to 500 grooves/mm), and region III (RIII:

500 grooves/mm to 600 grooves/mm), each with different groove densities. The division of the groove density on the grating was an approximation base on the fact that each grating's density varied constantly from one end to other. This was done for all of the following chirped grating measurements for same reason.

#### 4.2.3.1 Results at

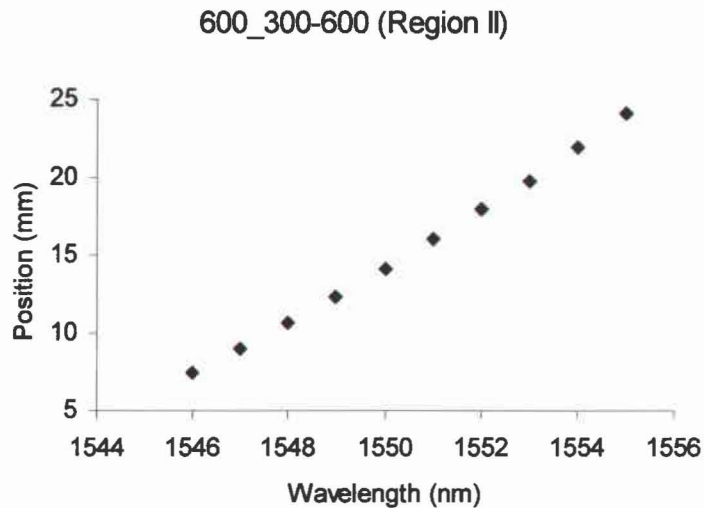


Figure 20: Peak power position of each wavelength for dual grating. 600 grooves/mm and 1<sup>st</sup> chirped grating in series for the testing setup measurement. (at region II of chirped grating)

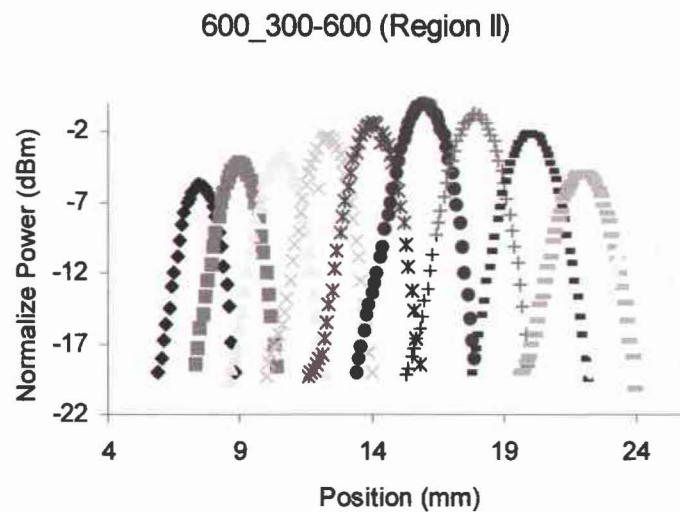


Figure 21: Actual power measurement for each wavelength for the 600 grooves/mm and 1<sup>st</sup> chirped grating in series for the testing setup measurement. (at region II of chirped grating).



### Region I of the 1st Chirped Grating

The normalized position of each channel for the 600 grooves/mm grating in series with region I of the 1st chirped grating is shown in Figure 18. The average spatial separation between each channel's peak power position was  $\Delta x/\Delta\lambda \approx 1.46$  mm/nm.

The actual power measurements from the 600 grooves/mm grating and region II of 1st chirped grating in series are shown in Figure 19. On average, the peak power of each channel fluctuated  $\Delta P/\Delta\lambda \approx 1.13$  dBm/nm from the neighboring channels. The power difference between the highest power channel and the lowest power channel was 7.1 dBm.

#### 4.2.3.2 Results at the

600\_300-600 (Region III)

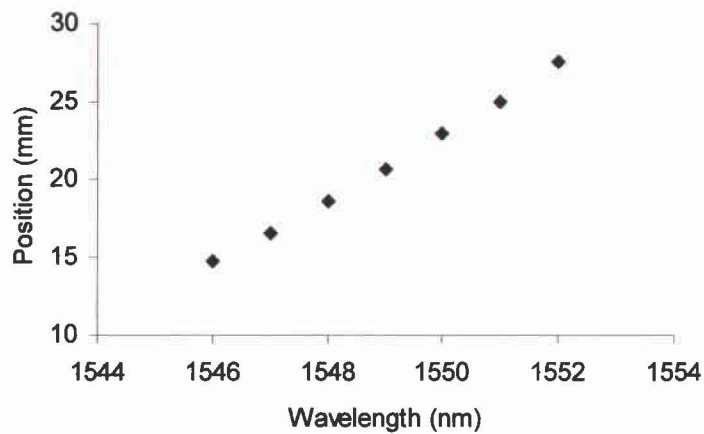


Figure 22: Peak power position of each wavelength for dual grating. 600 grooves/mm and 1<sup>st</sup> chirped grating in series for the testing setup measurement. (at region III of chirped grating)

600\_300-600 (Region III)

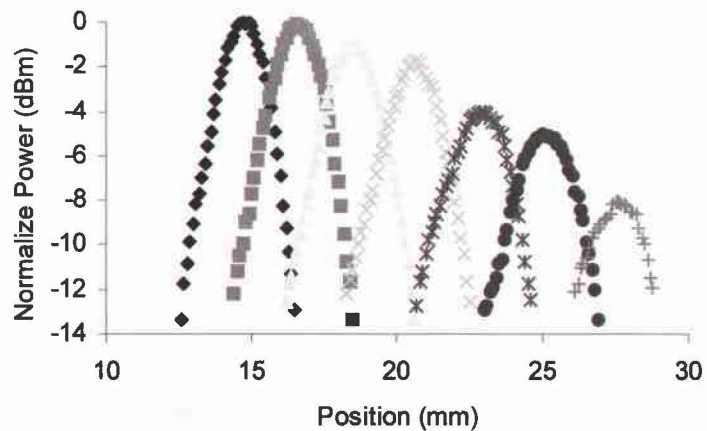


Figure 23: Actual power measurement for each wavelength for the 600 grooves/mm and 1<sup>st</sup> chirped grating in series for the testing setup measurement. (at region III of chirped grating).

## Region II of 1st Chirped Grating

The normalized position of each wavelength for the 600 grooves/mm grating in series with region II of the 1st chirped grating are shown in Figure 20. The average spatial separation between each channel's peak power position was  $\Delta x/\Delta\lambda \approx 1.86$  mm/nm.

The actual power measurements from the 600 grooves/mm grating and region II of the 1st chirped grating is shown in Figure 21. On average, the peak power of each channel fluctuated  $\Delta P/\Delta\lambda \approx 1.6$  dBm/nm from the neighboring channels. The power difference between the highest power channel and the lowest power channel was 8.6 dBm.

### 4.2.3.3 Results at

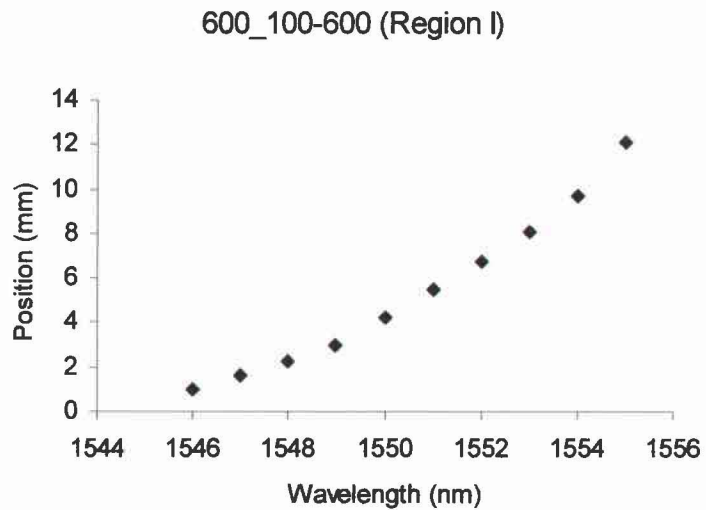


Figure 24: Peak power position of each wavelength for dual grating. 600 grooves/mm and 2<sup>nd</sup> chirped grating in series for the testing setup measurement. (at region I of chirped grating)

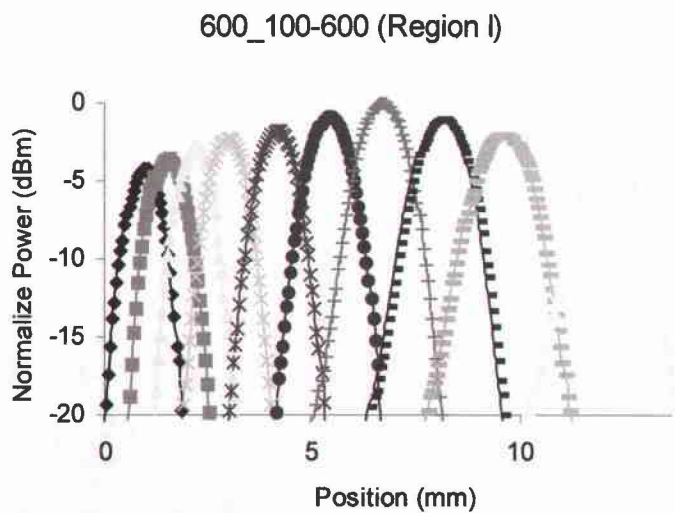


Figure 25: Actual power measurement for each wavelength for the 600 grooves/mm and 2<sup>nd</sup> chirped grating in series for the testing setup measurement. (at region I of chirped grating).

### **Region III of the 1st Chirped Grating**

The normalized position of each channel for the 600 grooves/mm grating series with region III of the 1st chirped grating is shown in Figure 22. The average spatial separation between each channel's peak power position was  $\Delta x/\Delta\lambda \approx 2.15$  mm/nm.

The actual power measurements from the 600 grooves/mm grating and region III of the 1st chirped grating are shown in Figure 23. On average, the peak power of each channel fluctuated  $\Delta P/\Delta\lambda \approx 1.35$  dBm/nm from the neighboring channels. Due to the large power fluctuations, some of the channels could not be measured. The power difference between the highest power channel and the lowest power channel in 1546 nm to 1552 nm ranges was 8.1 dBm.

#### **4.2.4 Results for the 600 grooves/mm Grating and the 2nd Chirped Grating in Series**

The measurements from 600 grooves/mm grating series with the 2nd chirped grating having groove density varying from 100 grooves/mm to 600 grooves/mm is shown in Figures 24, 25, 26, 27, 28, and 29.

##### **4.2.4.1 Results at Region I of the 2nd Chirped Grating**

The normalized position of each channel for the 600 grooves/mm grating in series with region I of the 2nd chirped grating is shown in Figure 24. The average spatial separation between each channel's peak power position was  $\Delta x/\Delta\lambda \approx 1.24$  mm/nm.

The actual power measurements from the 600 grooves/mm grating and region I of the 2nd chirped grating are shown in Figure 25. On average, the peak power of each channel fluctuated  $\Delta P/\Delta\lambda \approx 0.86$  dBm/nm from the neighboring channels. The power difference

between the highest power channel and the lowest power channel in 1546 nm to 1554 nm range was 4.2 dBm.

#### 4.2.4.2 Results at Region II of the 2nd Chirped Grating

The normalized position of each channel for the 600 grooves/mm grating series with region II of the second chirped grating is shown in Figure 26. The average spatial separation between each channel's peak power position was  $\Delta x/\Delta\lambda \approx 1.81$  mm/nm.

The actual power measurements from the 600 grooves/mm grating and the region II of 2nd chirped grating are shown in Figure 27. On average, the peak power

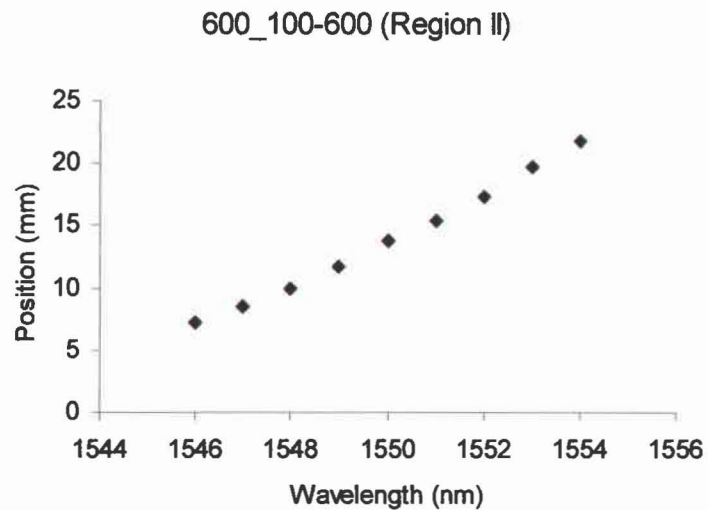


Figure 26: Peak power position of each wavelength for dual grating. 600 grooves/mm and 2<sup>nd</sup> chirped grating in series for the testing setup measurement. (at region II of chirped grating)

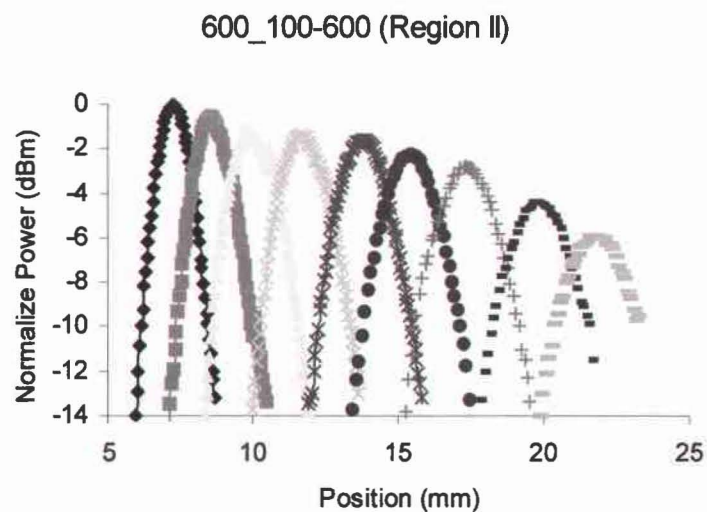


Figure 27: Actual power measurement for each wavelength for the 600 grooves/mm and 2<sup>nd</sup> chirped grating in series for the testing setup measurement. (at region II of chirped grating).

of each channel fluctuated  $\Delta P/\Delta\lambda \approx 0.74$  dBm/nm from the neighboring channels. As was the in region III measurements of the 1st chirped grating, the full range of the channels could not be measured because the power dropped too low to be measured by the wavemeter for some of them. The power difference between the highest power channel and the lowest measured power in the 1546 nm to 1554 nm range was 5.9 dBm.

#### 4.2.4.3 Results at Region III of the 2nd Chirped Grating

The normalized position of each channel for the 600 grooves/mm grating series with the region III of the second chirped grating is shown in Figure 28.

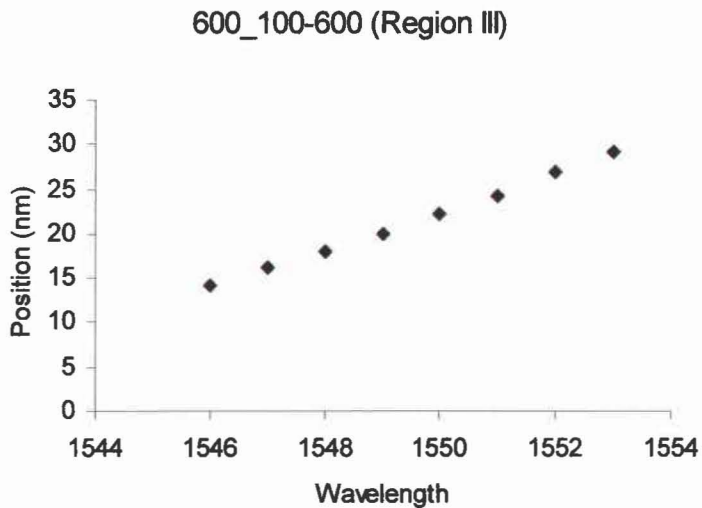


Figure 28: Peak power position of each wavelength for dual grating. 600 grooves/mm and 2<sup>nd</sup> chirped grating in series for the testing setup measurement. (at region III of chirped grating)

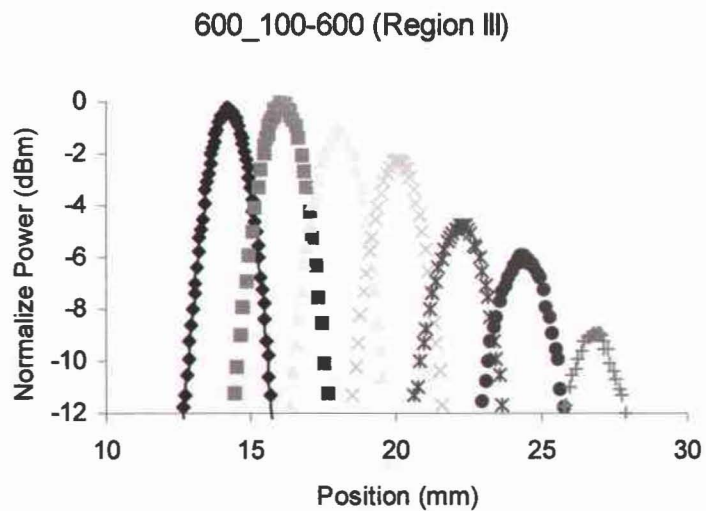


Figure 29: Actual power measurement for each wavelength for the 600 grooves/mm and 2<sup>nd</sup> chirped grating in series for the testing setup measurement. (at region III of chirped grating).



The average spatial separation between each channel's peak power position was  $\Delta x/\Delta\lambda \approx 2.15 \text{ mm/nm}$ .

The actual power measurements from the 600 grooves/mm grating and the region III of 2nd chirped grating are shown in Figure 29. On average, the peak power of each channel fluctuated  $\Delta P/\Delta\lambda \approx 1.76 \text{ dBm/nm}$  from the neighboring channels. As in the previous measurements, the full range of channels could not be measured. The power difference between the highest power channel and the lowest measured power channel in 1546 nm to 1553 nm ranges was 12.1 dBm. This large power fluctuation arises from the incident angle of the light entering the output fiber that is caused by the large spectral separation. More will be discussed in a later chapter.

#### 4.3 Final Setup with Continuous Chirped Grating (Circular Measurement Setup)

To reduce the variation of the power collected by the output fiber caused by the increase in entrance angle as this output fiber was moved laterally, the set up for the output fiber was changed as shown in Figure 30. As was done for all the previous measurements, the

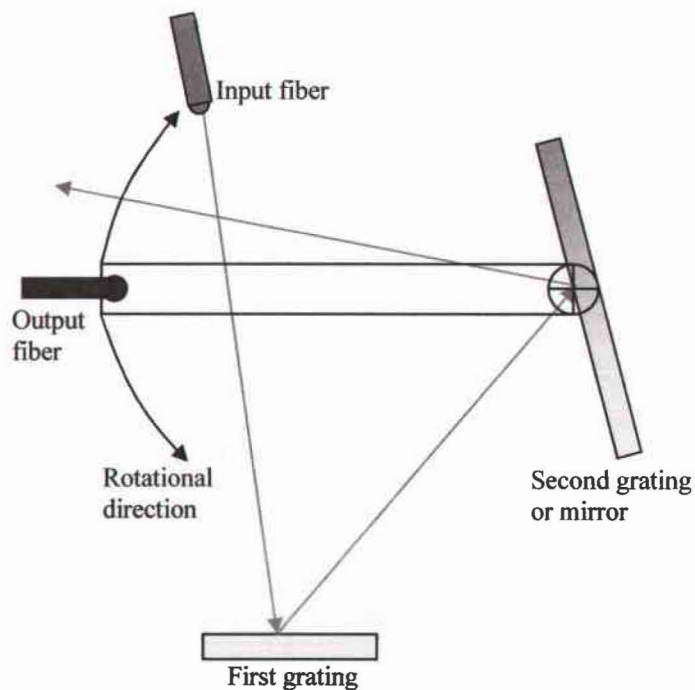


Figure 30: Final measurement setup

single grating system was set up and tested to be used as a reference measurement. Then the second configuration using the dual grating system was setup and measured as well. In the second setup, the following gratings were used as the second grating to increase the physical separation between the wavelengths:

1. Uniform 600 grooves/mm
2. Chirped grating

Groove density varied from 300 grooves/mm to 600 grooves/mm for the first chirped grating and from 100 grooves/mm to 600 grooves/mm for the second, which was divided into three

sections as it was in previous configuration.

#### 4.3.1 Reference Setup (Single Grating)

First, measurements using a single grating were repeated, as was done in all of the

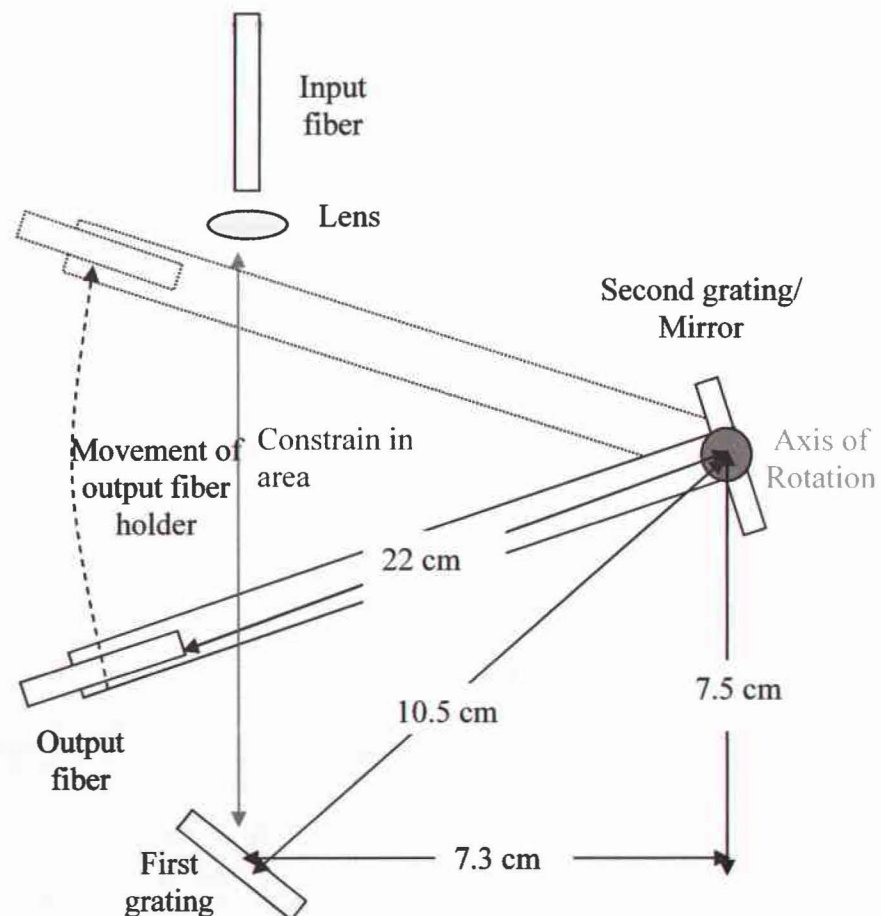


Figure 31: The dimensions for final setup

previous measurements, for consistency.

In the final setup, reference measurements in steps of 1nm could not be done accurately due to the small angular changes between the wavelengths. Thus measurements were taken at the two end wavelengths, 1545 nm and 1555 nm, and the result was  $\Delta\theta \approx 0.8$  degrees separated the wavelengths.

Due to lack of fine control over the angular movement of the output fiber, actual power measurement of each could not be measured accurately, therefore the actual power measurement done in this testing stage was not conducted. Only the peak powers and the positions of the peak power were measured.

#### 4.3.1.1 Actual Setup

##### Dimensions for Final Setup

For the same reason given in the previous setup, only one lens in front of the input fiber was used to focus the light into output fiber. As many of the dimensions as

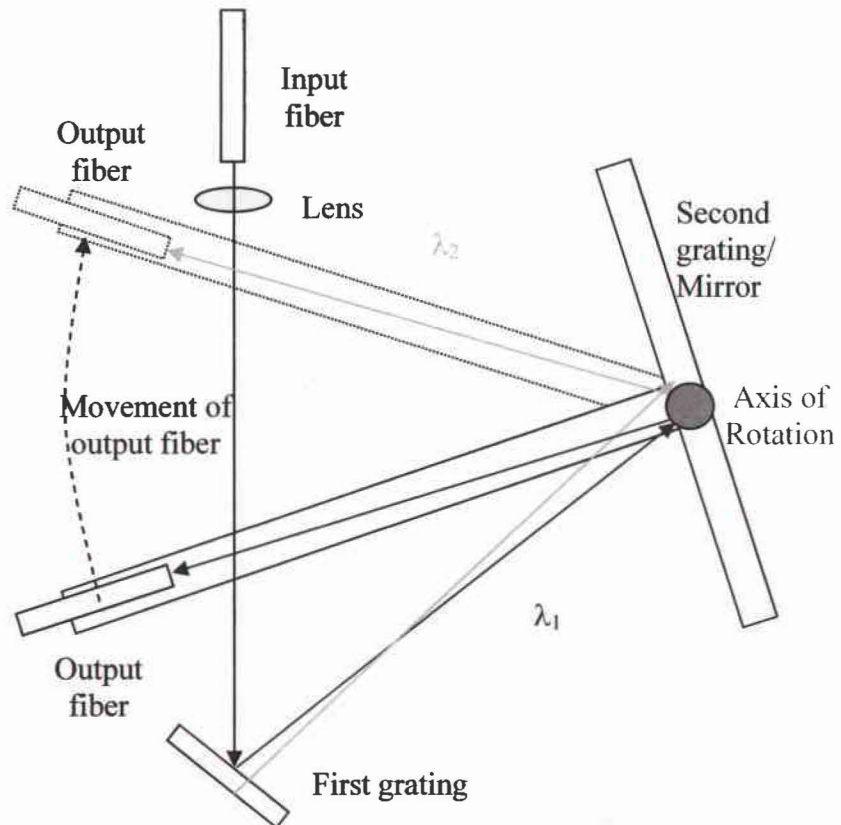


Figure 32: Final setup measurement technique



possible in this final setup were kept the same as before. The difference between the previous setup and this final setup was that the output fiber was placed on the rotation stage and the distance between center of the second grating and the output fiber was increased from 13.5 cm to 22 cm from the axis of rotation. The increase in the distance between the center of the second grating and output fiber in the final setup was due to the additional space introduced by the rotational stage. Also, there was a change in the position of the output fiber holder (now in y-axis position instead of x-axis as it was in previous setup), which did not allow the bulky output fiber holder to be placed closer to the output fiber due to area constraints induced by the first grating and the input fiber holders, shown in Figure 31. However, because angular measurements were determined for both systems, dimensional differences could be removed from the experimental results. This left only the coupling efficiencies as the primary difference.

#### **4.3.1.2 Measurement Technique Final Setup**

Again in the final setup, using a tunable laser in series with EDFA, a single wavelength channel, starting with the lowest wavelength (1545 nm), was transmitted through the multi-grating system. However, in the final setup, precise control over the rotation stage, where the output fiber was placed, was not achievable since the available equipment only allowed unidirectional movement of the rotator (the rotator was only able to be pushed by the micro-meter in one direction). For this reason only the position of the peak power was measured using the wavemeter, unlike the previous measurement, where the whole beam profiles were collected. The peak power for the given wavelength was detected by moving the output fiber in one direction. Since the movement of the rotator

on which the output fiber was placed moved in circular path the position for each wavelength's peak power was recorded in degrees. The wavelength was increased by 1 nm and the rotator was rotated from the position where the previous wavelength was measured to determine the shift in the position. This procedure was repeated until the wavelength reached 1555 nm.

#### **4.3.2 Dual Grating Setup**

For the first dual grating measurement, the mirror was replaced with a second gold-coated 600-grooves/mm ruled grating. Then for the second dual grating measurement, the mirror was replaced with a first chirped ruled grating (groove spacing varying from 300 to 600 grooves/mm). Finally, the mirror was again replaced with a second chirped ruled grating (groove spacing varying from 100 to 600 grooves/mm).

The measurements were taken by rotating on a single fiber from Position I, located at the shortest wavelength to Position II, located at the longest wavelength. All measurements were conducted in same manner to minimize the measurement variation and the first-order diffraction mode was chosen to separate the signals.

Physical wavelength position, starting from the shortest to longest wavelength, is shown in Figures 33 and 35 for both the dual standard grating setup and the standard-chirped grating configurations, respectively. The position of shortest wavelength measured using the single grating with mirror configuration was set as a reference point for all other measurements. In this measurements, the channel wavelength separations were kept at  $\Delta\lambda = 1$  nm, which is larger than the previous measurement ( $\Delta\lambda = 0.5$  nm) for the single grating and dual grating setups due to the limitations with the fine control

of the rotator used to translated the collection fiber. For the chirped grating configuration, the channel separation was 1545 nm at the low end and 1555 nm at the high end. This large wavelength separation was selected in order to avoid the defects that occur at the edges of the gratings, as well as to control groove density encountered by each of the wavelengths.

#### 4.3.2.1 Results for

**the Two 600**

**grooves/mm**

**Gratings in Series**

The normalized

position of each

channel for the

series of two 600

grooves/mm is

shown in Figure 33.

The average angular

separation between

each channel's peak

power position was

$\Delta\theta/\Delta\lambda \approx 0.12$  deg/nm.

The result of the

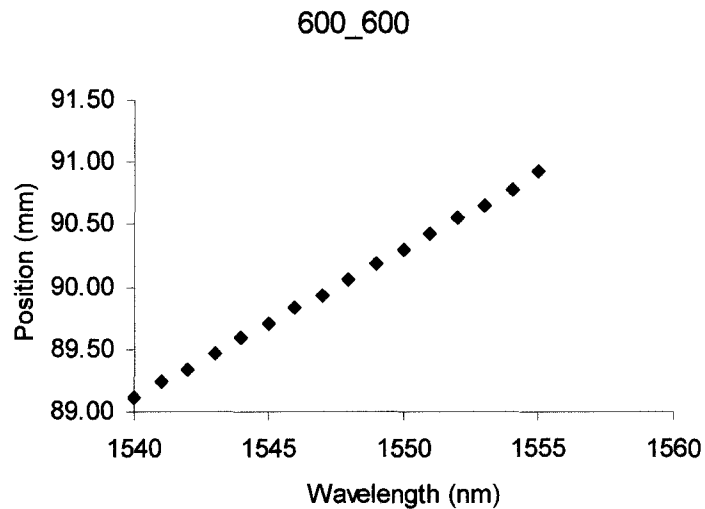


Figure 33: Peak power positions of each wavelength for the two 600 grooves/mm grating in series for the final setup measurement.

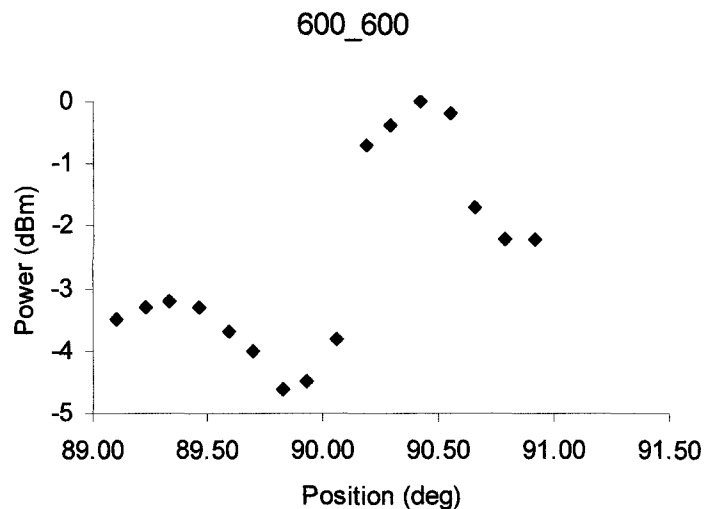


Figure 34: Peak power measurement for each wavelength for the two 600 grooves/mm grating in series for the final setup measurement.

two 600 grooves/mm grating in series is shown in Figure 34. As before, the power fluctuated for each wavelength; however, the fluctuations between the each wavelength were not as severe compared to the previous measurements. On average, the peak power of each channel fluctuated  $\Delta P/\Delta\lambda \approx 0.57$  dBm/nm from the neighboring channels. The power difference between the highest power channel and the lowest power channel was 4.6 dBm.

### 4.3.3 Results for the 600 grooves/mm Grating and the 1st Chirped Grating in Series

The measurements from 600 grooves/mm grating series with first chirped grating, having groove density varying from 300 grooves/mm to 600 grooves/mm, are shown in

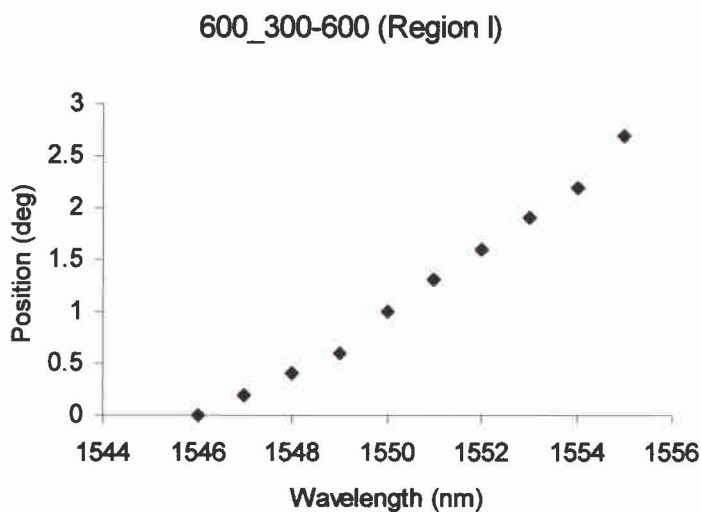


Figure 35: Peak power position of each wavelength for dual grating. 600 grooves/mm and 1<sup>st</sup> chirped grating in series for the testing setup measurement. (at region I of chirped grating)

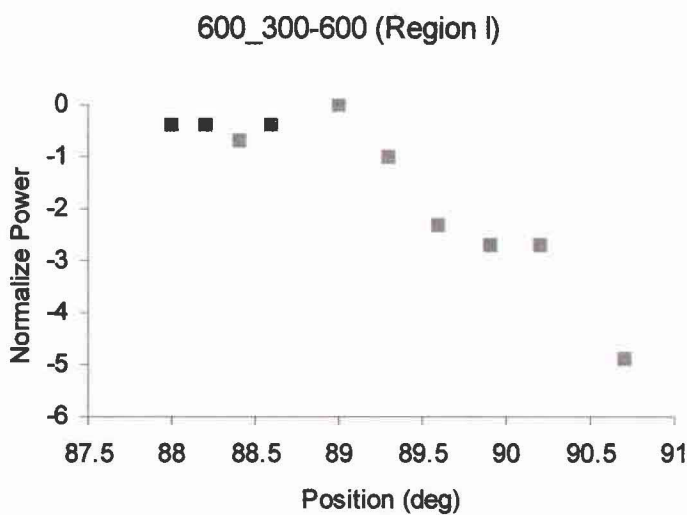


Figure 36: Actual peak power measurement for each wavelength for the 600 grooves/mm and 1<sup>st</sup> chirped grating in series for the testing setup measurement. (at region I of chirped grating).

Figures 35, 36, 37 38, 39, and 40.

#### 4.3.3.1 Results at Region I of the 1st Chirped Grating

The normalized position of each channel for the 600 grooves/mm grating in series with region I of the first chirped grating is shown in Figure 35. The average spatial angular separation between each channel's peak power position was  $\Delta\theta/\Delta\lambda \approx 0.3$  deg/nm.

The actual power measurements from the 600 grooves/mm grating and region I of the 1st chirped grating are shown in Figure 36. On average, the peak power of each channel fluctuated  $\Delta P/\Delta\lambda \approx 0.66$  dBm/nm from the

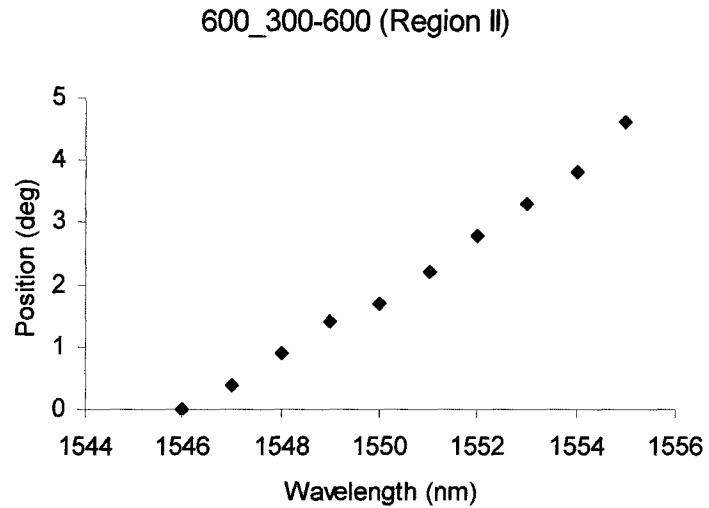


Figure 37: Peak power position of each wavelength for dual grating. 600 grooves/mm and 1<sup>st</sup> chirped grating in series for the testing setup measurement. (at region II of chirped grating)

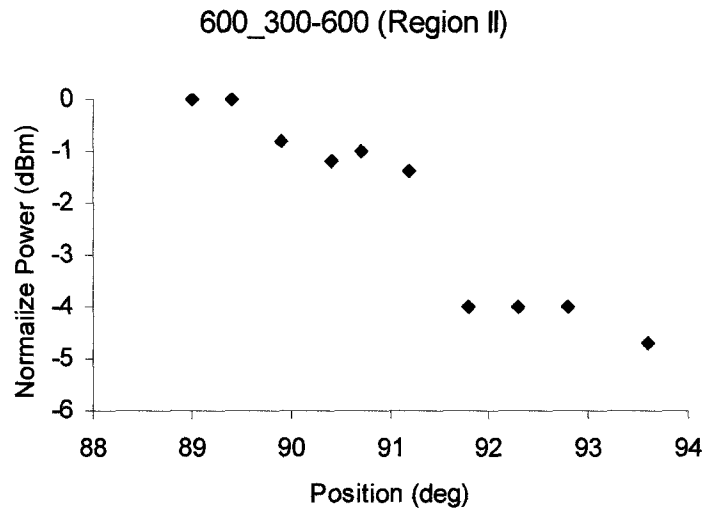


Figure 38: Actual peak power measurement for each wavelength for the 600 grooves/mm and 1<sup>st</sup> chirped grating in series for the testing setup measurement. (at region II of chirped grating).

neighboring channels. The power difference between the highest power channel and the lowest power channel was 4.9 dBm.

#### 4.3.3.2 Results at Region II of the 1st Chirped Grating

The normalized position of each channel for the 600 grooves/mm grating in series with region II of the first chirped grating is shown in Figure 37. The average angular separation between each channel's peak power position was  $\Delta\theta/\Delta\lambda \approx 0.51 \text{ deg/nm}$ .

The actual power measurements of the 600 grooves/mm grating and region II of the 1st chirped grating

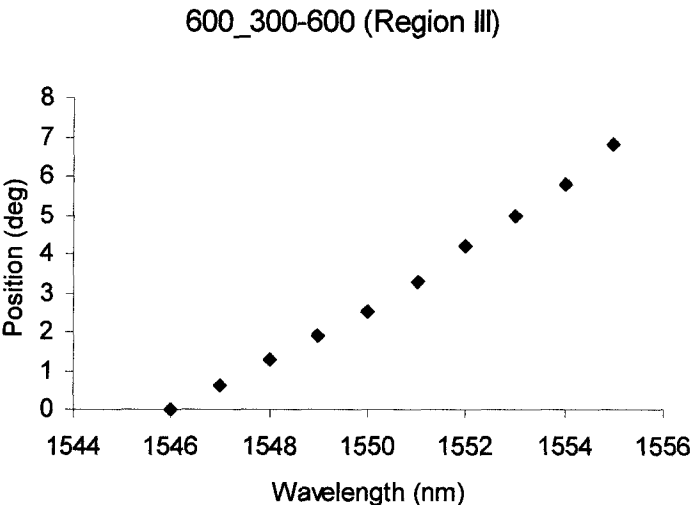


Figure 39: Peak power position of each wavelength for dual grating. 600 grooves/mm and 1<sup>st</sup> chirped grating in series for the testing setup measurement. (at region III area of chirped grating)

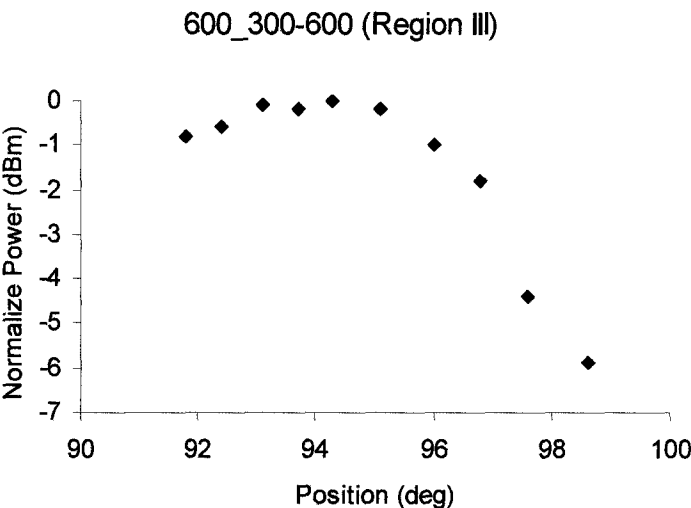


Figure 40: Actual peak power measurement for each wavelength for the 600 grooves/mm and 1<sup>st</sup> chirped grating in series for the testing setup measurement. (at region III area of chirped grating).

are shown in Figure 38. On average, the peak power of each channel fluctuated  $\Delta P/\Delta\lambda \approx 0.56$  dBm/nm from the neighboring channels. The power difference between the highest power channel and the lowest power channels was 4.7 dBm.

#### **4.3.3.3 Results at the Region III of 1st Chirped Grating**

The normalized position of each channel for the 600 grooves/mm grating in series with region III of the 1st chirped grating, grooves density varying from 500 grooves/mm to 600 grooves/mm, is shown in Figure 39. The average angular separation between each channel's peak power position was  $\Delta\theta/\Delta\lambda \approx 0.76$  deg/nm.

The actual power measurements from the 600 grooves/mm grating and region III of 1st chirped grating are shown in Figure 40. On average, the peak power of each channel fluctuated  $\Delta P/\Delta\lambda \approx 0.77$  dBm/nm from the neighboring channels. The power difference between the highest power channels and the lowest power channel was 5.9 dBm.

#### **4.3.4 Results for the 600 grooves/mm Grating and the 2nd Chirped Grating in Series**

The measurements from 600 grooves/mm grating in series with 2nd chirped grating, having groove density varying from 100 grooves/mm to 600 grooves/mm, are shown in Figure 41, 42, 43, 44, 45, and 46.

##### **4.3.4.1 Results at the Region I of 2nd Chirped Grating**

The normalized position of each channel for the 600 grooves/mm grating series with region I area of the 2nd chirped grating is shown in Figure 41. The average angular separation between each channel's peak power position was  $\Delta\theta/\Delta\lambda \approx 0.48$  deg/nm.

The actual power measurements from the 600 grooves/mm grating and region I of the 2nd chirped grating are shown in Figure 42. On average, the peak power of each channel fluctuated  $\Delta P/\Delta \lambda \approx 1.16$  dBm/nm from the neighboring channels. The power difference between the highest power channel and the lowest power channel was 6.1 dBm.

#### 4.3.4.2 Results at

#### Region II Area of the 2nd Chirped Grating

The normalized position of each channel for the for 600 grooves/mm grating in series with region II of the 2nd chirped grating, having groove density varying from 250 grooves/mm to 400 grooves/mm, is shown in Figure 43. The average angular separation between each channel's peak power position was

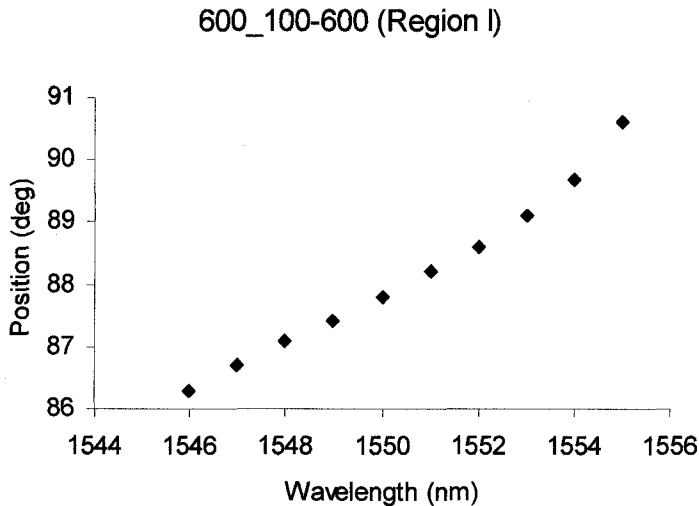


Figure 41: Peak power position of each wavelength for dual grating. 600 grooves/mm and 2<sup>nd</sup> chirped grating in series for the testing setup measurement. (at region I area of chirped grating)

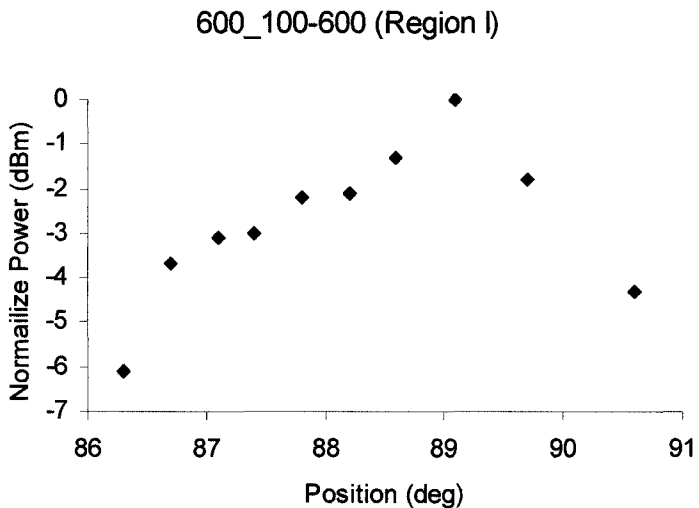


Figure 42: Actual peak power measurement for each wavelength for the 600 grooves/mm and 2<sup>nd</sup> chirped grating in series for the testing setup measurement. (at region I area of chirped grating).



$$\Delta\theta/\Delta\lambda \approx 0.84 \text{ deg/nm.}$$

The actual power measurements from the 600 grooves/mm grating and region II of the 2nd chirped grating are shown in Figure 44. On average, the peak power of each channel fluctuated  $\Delta P/\Delta\lambda \approx 0.84$

dBm/nm from the

neighboring channels.

The power difference

between the highest

power channel and the

lowest power channel

was 3.9 dBm.

600\_100-600 (Region II)

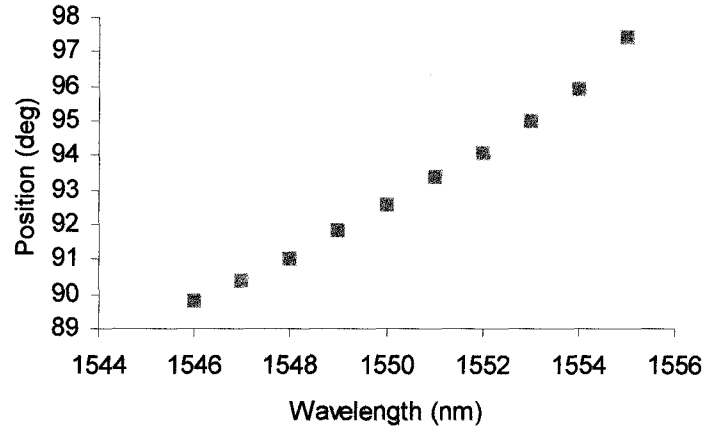


Figure 43: Peak power position of each wavelength for dual grating. 600 grooves/mm and 2<sup>nd</sup> chirped grating in series for the testing setup measurement. (at region II of chirped grating)

#### 4.3.4.3 Results at

#### Region III of the 2nd

#### Chirped Grating

The normalized position of each channel for the 600 grooves/mm grating in series with region III of the 2nd chirped grating is shown

in Figure 45. The

600\_100-600 (Region II)

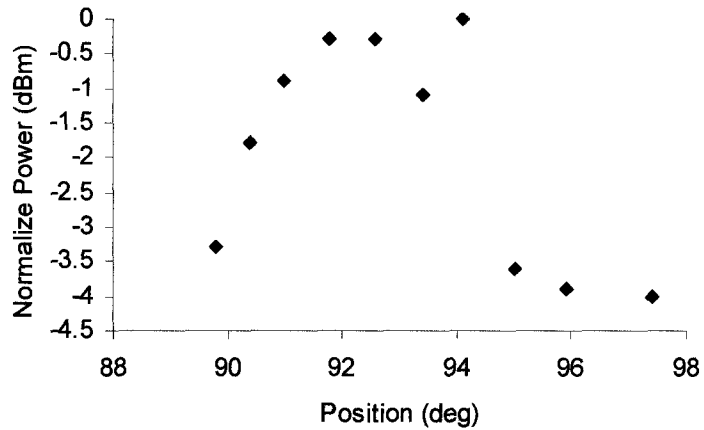


Figure 44: Actual peak power measurement for each wavelength for the 600 grooves/mm and 2<sup>nd</sup> chirped grating in series for the testing setup measurement. (at region II area of chirped grating).

average angular separation between each channel's peak power position was  $\Delta\theta/\Delta\lambda \approx 1.07 \text{ deg/nm}$ .

The actual power measurements from the 600 grooves/mm grating and region III of the 2nd chirped grating are shown in Figure 46. On average, the peak power of each channel fluctuated  $\Delta P/\Delta\lambda \approx$

0.47 dBm/nm from the neighboring channels.

The power difference between the highest power channel and the lowest power channel was 2.3 dBm.

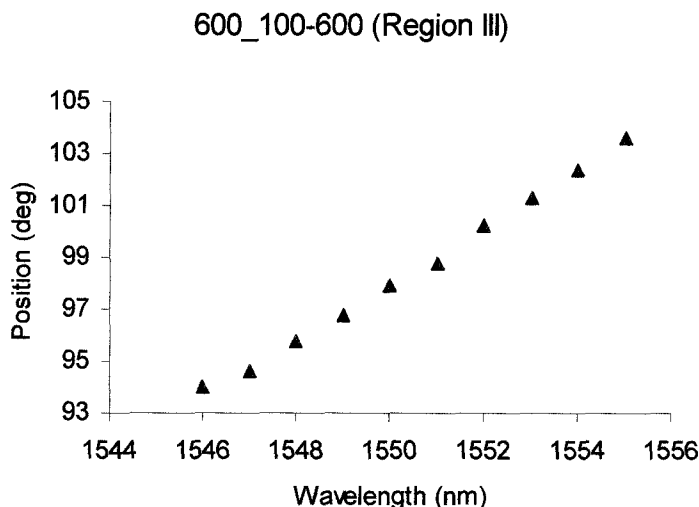


Figure 45: Peak power position of each wavelength for dual grating. 600 grooves/mm and 2<sup>nd</sup> chirped grating in series for the testing setup measurement. (at region III area of chirped grating)

#### 4.4 Wavelength

#### Routing Properties of the Dual Grating System

These results also show how each channel's peak power position shifted depending on the

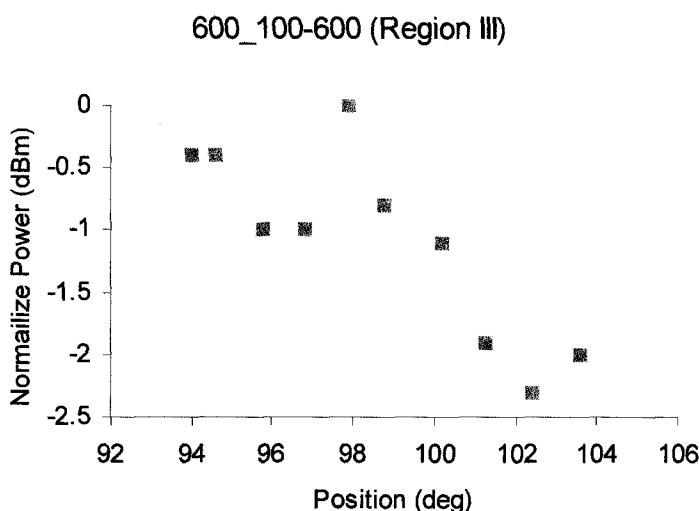


Figure 46: Actual peak power measurement for each wavelength for the 600 grooves/mm and 2<sup>nd</sup> chirped grating in series for the testing setup measurement. (at region III area of chirped grating).

grooves density of the second grating. This shows ability to shift (or move) channel's peak power position just by varying the groove density of second grating, which for the chirped grating can be accomplished by lateral translation.

#### 4.4.1 Results from Lateral Setup Results

The shifting of the channel's peak power positions for the different groove densities of second grating in the first setup is shown in Figure 47 and 48.

Due to the large power fluctuation in chirped grating measurements, the full range of test wavelengths could not be measured. However, even with the limited wavelengths analyzed it

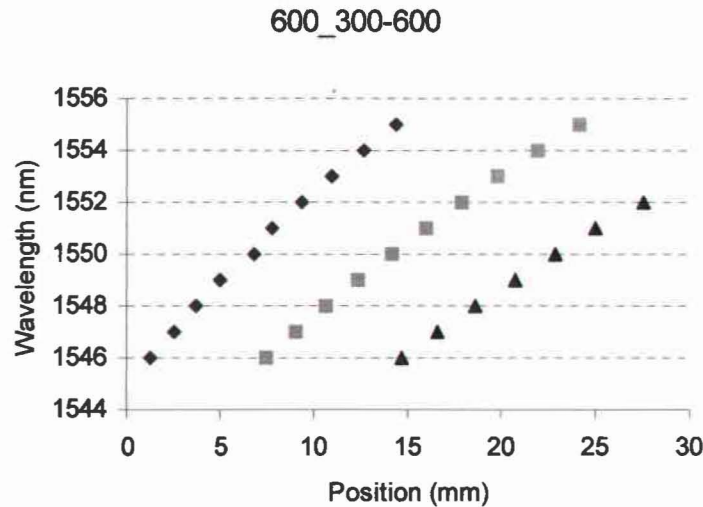


Figure 47: Channel's peak power position shifting as the groove density of 1<sup>st</sup> chirped grating varies from region I to region II and region II to region III.

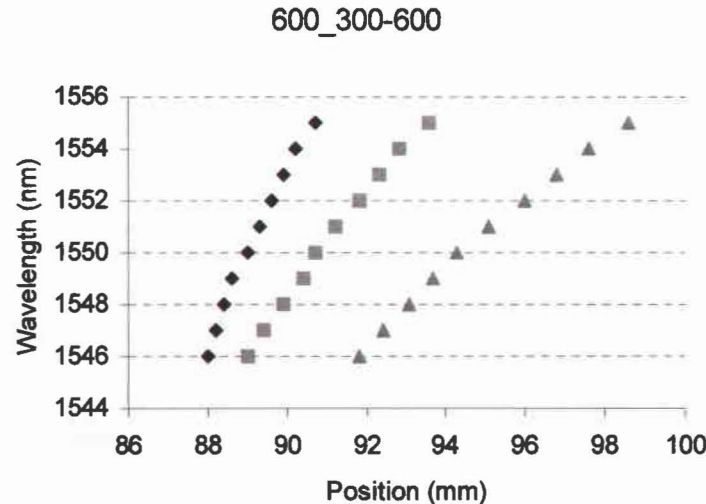


Figure 48: Channel's peak power position shifting as the groove density of 1<sup>st</sup> chirped grating varies from region I to region II and region II to region III.

is clearly shown that each channel's peak power position shifts from one place to another based on the groove density.

#### 4.4.1.1 Position Shifting of 1st Grating

The position shifting of each channel's peak power for the 1st chirped grating, having groove densities varying from 300 grooves/mm to 600 grooves/mm, is shown in Figure 49.

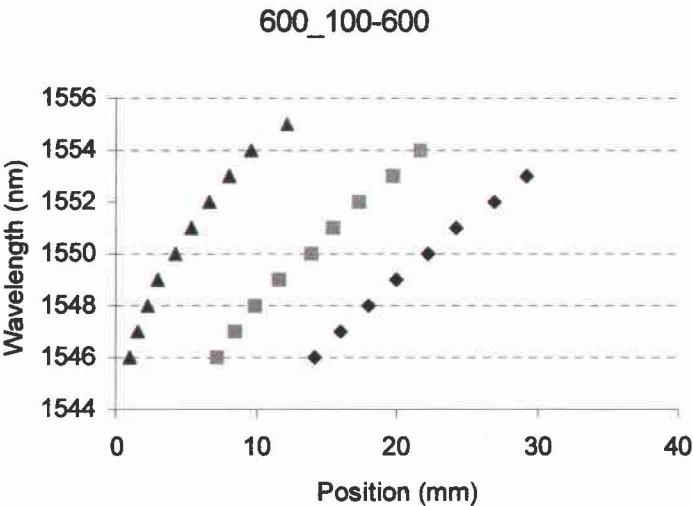


Figure 49: Channel's peak power position shifting as the groove density of 2<sup>nd</sup> chirped grating varies from region I to region II and region II to region III.

#### 4.4.1.2 Position Shifting of 2nd Grating

The position shifting of each channel's peak power for the 2nd chirped grating, having groove density varying from 100 grooves/mm to 600 grooves/mm, is

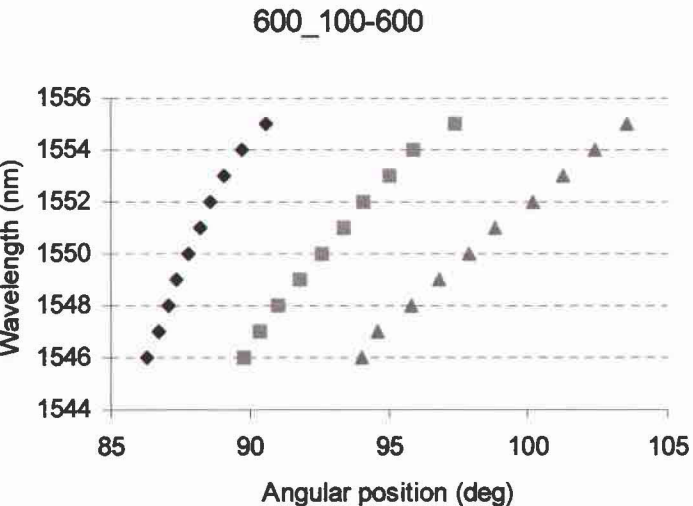


Figure 50: Channel's peak power position shifting as the groove density of 2<sup>nd</sup> chirped grating varies from region I to region II and region II to region III.

shown in Figure 50.

#### **4.4.2 Final Setup Results**

The angular shifting of the channel's peak power positions for different groove densities on the second grating for final setup is shown in Figures 49 and 50.

Unlike previous measurements, where the power fluctuations became larger as the separation between the wavelengths increased, measurements for the full range of wavelengths were collected because power fluctuations were small.

##### **4.4.2.1 Position Shifting of 1st Grating**

The position shifting of each channel's peak power for the 1st chirped grating, having groove density varying from 300 grooves/mm to 600 grooves/mm, is shown in Figure 49.

##### **4.4.2.2 Position Shifting of 2nd Grating**

The position shifting of each channel's peak power for the 2nd chirped grating, having groove densities varying from 100 grooves/mm to 600 grooves/mm, is shown in Figure 50.

In Chapter 5, all the data given in this chapter will be compared and discuss.

## **Chapter 5**

### **Discussion of Results**

#### **5.1 Wavelength Channel's Peak Power Separations**

A summary of the wavelength channel separation for all experimental setups is given in Table 1.

##### **5.1.1 Single Grating (Reference Measurement)**

Using a single 600 grooves/mm grating, reference measurements were conducted to examine the channel separation property of the diffraction grating and to compare the results with the other setups. Reference measurements were conducted for all the various setups, however, for the final setup, due to limited control over the fine angular movement (angle less than 0.05 degree) and limited precision from the angle measurement equipment, measurements of individual wavelength channel separations were not possible.

In setups where single grating measurements were possible, the results showed an average spatial separation of 0.06 deg/nm for the initial setup and 0.06 deg/nm for the testing setup. Even though the two measurements show slight difference in separation, this difference is within measurement error, which was about 0.01 deg/nm for the setups. In addition, these differences could be the result of slight changes in distance between the grating and collection fiber, since the setup was reconstructed for every measurement.

The measurement results show that the single grating setup is ideally suited for wide channel systems, with spacing of  $\Delta\lambda > 1\text{nm}$ , within a reasonable size because it is simple, robust, and cost effective. However, for DWDM systems, which require wavelength

	Theory testing setup	1 <sup>st</sup> Setup using continuous chirped grating setup	Final setup results
	Average Separation between the wavelength ( $\Delta\theta/\Delta\lambda$ ) ( $\Delta x/\Delta\lambda$ )	Average Separation between the wavelength ( $\Delta\theta/\Delta\lambda$ ) ( $\Delta x/\Delta\lambda$ )	Average Separation between the wavelength ( $\Delta\theta/\Delta\lambda$ ) ( $\Delta\theta/\Delta\lambda$ )
Single grating (600 grooves/mm)	$0.06 \pm 0.01$ deg $0.24 \pm 0.05$ mm	$0.06 \pm 0.01$ deg $0.22 \pm 0.05$ mm	NA
Dual grating (Two 600 grooves/mm)	$0.10 \pm 0.01$ deg $0.44 \pm 0.05$ mm	$0.1 \pm 0.01$ deg $0.44 \pm 0.05$ mm	$0.12 \pm 0.01$ deg $0.49 \pm 0.05$ mm
Dual grating (600 and 1 <sup>st</sup> chirped grating) at region I	NA	$0.32 \pm 0.01$ deg $1.46 \pm 0.05$ mm	$0.3 \pm 0.01$ deg $1.15 \pm 0.05$ mm
Dual grating (600 and 1 <sup>st</sup> chirped grating) at region II	NA	$0.38 \pm 0.01$ deg $1.86 \pm 0.05$ mm	$0.51 \pm 0.01$ deg $1.96 \pm 0.05$ mm
Dual grating (600 and 1 <sup>st</sup> chirped grating) at region III	NA	$0.41 \pm 0.01$ deg $2.15 \pm 0.05$ mm	$0.76 \pm 0.01$ deg $2.91 \pm 0.05$ mm
Dual grating (600 and 2 <sup>nd</sup> chirped grating) at region I	NA	$0.28 \pm 0.01$ deg $1.24 \pm 0.05$ mm	$0.48 \pm 0.01$ deg $1.84 \pm 0.05$ mm
Dual grating (600 and 2 <sup>nd</sup> chirped grating) at region II	NA	$0.37 \pm 0.01$ deg $1.81 \pm 0.05$ mm	$0.84 \pm 0.01$ deg $3.23 \pm 0.05$ mm
Dual grating (600 and 2 <sup>nd</sup> chirped grating) at region III	NA	$0.4 \pm 0.01$ deg $2.14 \pm 0.05$ mm	$1.07 \pm 0.01$ deg $4.11 \pm 0.05$ mm

Table 1: Average separation between the channels' peak power. For the theory and 1<sup>st</sup> setup measurement, both measured separations in metric term and calculated value of separation in angular terms are given. For the final setup measurement, both measured angular separations and calculated value of separation in metric terms are given. The calculations were based on the individual experiment's geometry. The calculations were based on the individual experiment's geometry.

channel spacings of  $\Delta\lambda < 1\text{ nm}$ , it would not be suitable. Even though the resolution of the channels can be increased by increasing the distance between the grating and output fiber and/or changing the angle of incidence of the input to the grating, this result illustrates the typical lower limit of channel spacing for a single grating setup with a reasonable distance between the input and output.

### **5.1.2 Dual Grating Measurement Results**

As can be seen from the Table 1, all of the dual grating setups improved the average wavelength channel separation compared to the single grating setup. The improvement of separation ranges from 160% to 1700% depending on the setup, which is shown in Table 2.

#### **5.1.2.1 Two 600 groove/mm Gratings in Series**

For the dual grating configuration the spatial separation between each wavelength channel was larger than the single grating setup, as was expected. In the initial measurement setup, dual gratings resulted in greater than 160% improvement over the single grating. In the testing measurement, improvement between the single grating and the dual grating was about 200 %.

The differences in these results could be due to different factors. One such factor is due to the small difference in the separation between the first and the second grating. This difference will result in a difference in incident angles on the second grating, as the separation between the first and second grating increases, the range of the incident angles into the second grating increases. This will result in larger separation.



Secondly, however small the difference might be, the total distance traveled by the separated light will increase the wavelength separations due to angular spread of the light from the grating. This is unavoidable and results in a larger spread in wavelength.

However, the difference in the wavelength separation is within the measurement error in this experiment. The difference in percentage seems larger since the separation between the wavelengths is small compared to the measurement error range.

#### 5.1.2.2 Dual Grating (1<sup>st</sup> Chirped grating)

	1 <sup>st</sup> Setup using continuous chirped grating setup	Final setup results
	% Improved compared to the reference measurements	% Improved compared to the reference measurements
Dual grating (Two 600 groove/mm)	160	200
Dual grating (600 and 1 <sup>st</sup> chirped grating) at region I	533	500
Dual grating (600 and 1 <sup>st</sup> chirped grating) at region II	633	850
Dual grating (600 and 1 <sup>st</sup> chirped grating) at region III	683	1267
Dual grating (600 and 2 <sup>nd</sup> chirped grating) at region I	466	800
Dual grating (600 and 2 <sup>nd</sup> chirped grating) at region II	616	1400
Dual grating (600 and 2 <sup>nd</sup> chirped grating) at region III	667	1783
Table 2: Wavelength channels separation improvement compared to the average reference measurement in percent		

Use of the 1<sup>st</sup> chirped grating, having groove density varying from 300 grooves/mm to 600 grooves/mm, improved the wavelength channel separations in both the testing setup and final setups.

#### **5.1.2.2.1 Testing Setup**

Using the 600 grooves/mm grating, as a master grating, and the different density areas of the 1<sup>st</sup> chirped grating, having groove density varying from 300 grooves/mm to 600 grooves/mm, as the slave grating, in series results in improved wavelength channel separation. The separation between the wavelength channels improved by 530% to 680% depending on the groove density of the chirped grating compared to the average separations of the wavelength channels for the reference measurements, as shown in Table 2.

#### **5.1.2.2.2 Final Setup**

Using the 600 grooves/mm grating, as a master grating, and the different density area of the 1<sup>st</sup> chirped grating, groove density varying from 300 grooves/mm to 600 grooves/mm, as the slave grating, in series results in improving wavelength channel separations. The separations between the wavelength channels improved by 500% to 1200% depending on the groove density of the chirped grating area compared to the average separations of the wavelength channels for the reference measurements, as shown in Table 2.

The large increase in average wavelength separation in the final setup is partly due to a

larger separation in longer wavelengths ranging from 1553 nm to 1555 nm. In previous measurements from the testing setup, the full range of the wavelength channels could not be measured due to the large power attenuation at the larger wavelength, especially in 1555 nm range. However, in the final setup, it was possible to measure these longer wavelengths. This resulted in an increase of the average separation of the wavelength channels due to the longer wavelength combined with the higher groove density of slave grating. Thus for these wavelengths, the separation between the channels was larger than the other wavelength, which increased the average separation. Still, the final setup performed better overall.

#### **5.1.2.3 Dual Grating Setup (2<sup>nd</sup> Chirped Grating)**

Use of the 2<sup>nd</sup> chirped grating improved the channel separation in both the testing setup and final setups.

##### **5.1.2.3.1 Testing Setup**

Using the 600 grooves/mm grating, as a master grating, and the different density areas of the 2<sup>nd</sup> chirped grating, groove density varying from 100 grooves/mm to 600 grooves/mm, as the slave grating, in series results in improving wavelength channel separations. The separation between the wavelength channels improved by 450% to 660% depending on the groove density of the chirped grating, when compared to the average separations of the channels for the reference measurements, as shown in Table 2.

##### **5.1.2.3.2 Final Setup**

Using the 600 grooves/mm grating, as a master grating, and the different density area

of the 2<sup>nd</sup> chirped grating, having groove density varying from 100 grooves/mm to 600 grooves/mm, as the slave grating, in series results in improving channel space separation as well. The separation between the wavelength channels improved by 800% to 1750% depending on the groove density of the chirped grating, when compared to the average separations of the wavelength channels for the reference measurements, as shown in

	Theory testing setup	1 <sup>st</sup> Setup using continuous chirped grating setup	Final setup results
	Average power fluctuation between the neighboring channels ( $\Delta P/\Delta\lambda$ ) [ dBm/nm]	Average power fluctuation between the neighboring channels ( $\Delta P/\Delta\lambda$ ) [ dBm/nm]	Average power fluctuation between the neighboring channels ( $\Delta P/\Delta\lambda$ ) [ dBm/nm]
Single grating (600 grooves/mm)	$3.26 \pm 0.1$	$0.55 \pm 0.1$	NA
Dual grating (Two 600 grooves/mm)	$0.67 \pm 0.1$	$0.67 \pm 0.1$	$0.57 \pm 0.1$
Dual grating (600 and 1 <sup>st</sup> chirped grating) at region I	NA	$1.13 \pm 0.1$	$0.66 \pm 0.1$
Dual grating (600 and 1 <sup>st</sup> chirped grating) at region II	NA	$1.6 \pm 0.1$	$0.56 \pm 0.1$
Dual grating (600 and 1 <sup>st</sup> chirped grating) at region III	NA	$1.35 \pm 0.1$	$0.77 \pm 0.1$
Dual grating (600 and 2 <sup>nd</sup> chirped grating) at region I	NA	$0.86 \pm 0.1$	$1.16 \pm 0.1$
Dual grating (600 and 2 <sup>nd</sup> chirped grating) at region II	NA	$0.74 \pm 0.1$	$0.84 \pm 0.1$
Dual grating (600 and 2 <sup>nd</sup> chirped grating) at region III	NA	$1.76 \pm 0.1$	$0.47 \pm 0.1$
Table 3: Average power fluctuation between the wavelength channels' peak power.			

Table 2.

### 5.1.3 Dual Grating Measured Results verse Calculated Results

In the calculations, the position of each wavelength channel was predominately controlled by the groove density of second grating.

The relationships between the groove density, the wavelengths, and the position of each wavelength channels are shown in Figure 51 and 52. Figure 51 show, each wavelength channel's

position for the different slave (second) gratings: constant 600 grooves/mm, 1<sup>st</sup> chirped grating, with groove density varying from 600 grooves/mm to 300 grooves/mm, and 2<sup>nd</sup> chirped grating, with

Calculation of Wavelength Channel Position

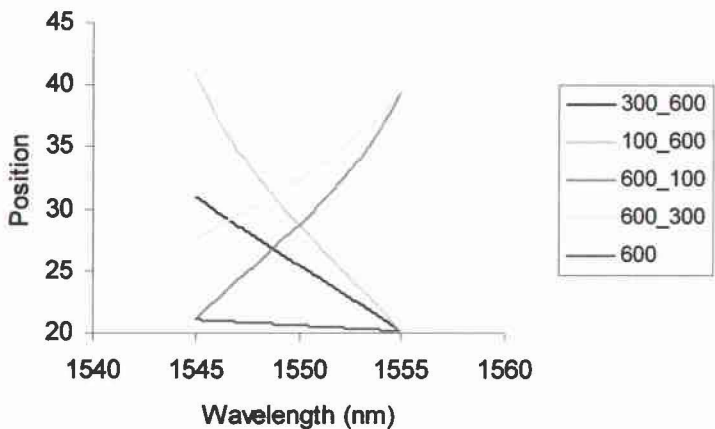


Figure 51: Calculated Position of wavelength channel for 1<sup>st</sup> and 2<sup>nd</sup> chirped grating.

Calculated Wavelength Channel Position

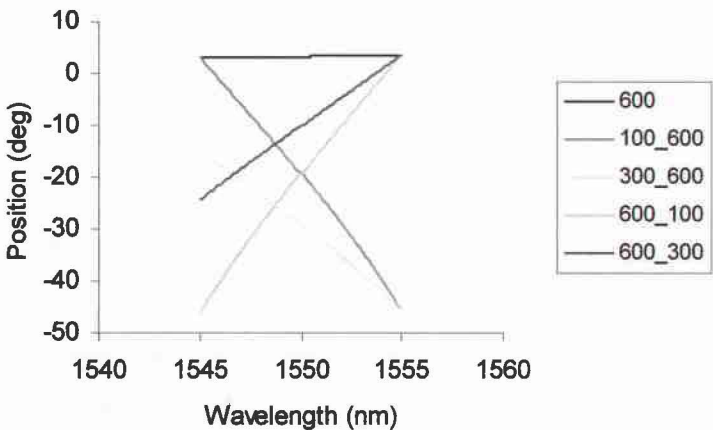


Figure 52: Calculated angular position of wavelength channel for 1<sup>st</sup> and 2<sup>nd</sup> chirped grating.

groove density varying from 600 grooves/mm to 100 grooves/mm. Figure 52 shows each wavelength channel's position for the different slave (second) gratings: constant 600 grooves/mm, 1<sup>st</sup> chirped grating, with groove density varying from 300 grooves/mm to 600 grooves/mm, and 2<sup>nd</sup> chirped grating, with groove density varying from 100 grooves/mm to 600 grooves/mm.

As can be seen from Figures 51 and 52, for a constant groove density on the second (600 grooves/mm) grating, the position of each channel was determined by the wavelength, but the amount of position change between each channel was small.

However, for the chirped grating, the position of each wavelength channel was predominately controlled by the groove density of the second (chirped) grating. For example, in the case when the chirped grating density varied from low to high, as the wavelength increases, from 1545 nm to 1555 nm, the position of the each channel was determine by the groove density not by the wavelength. For the case when the groove

density of the chirped grating decreases as the wavelength increases, the

calculated results show a mirror image from top to bottom of the case when the groove density of the chirped grating increases as the wavelength

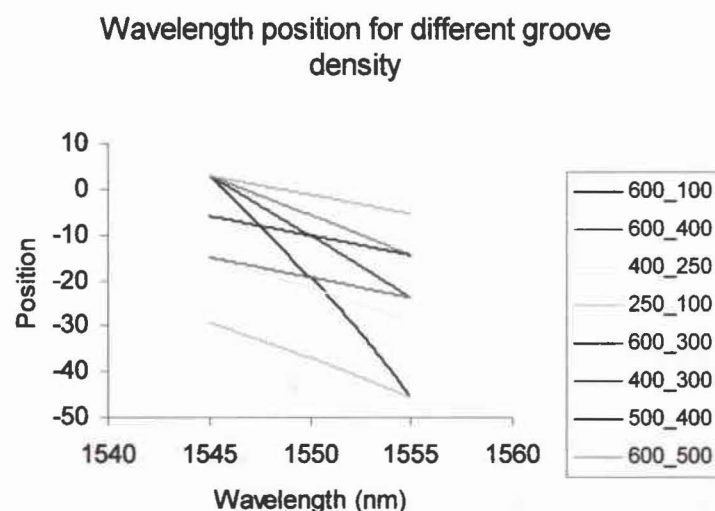


Figure 53: Calculated position of wavelength channel for 1<sup>st</sup> and 2<sup>nd</sup> chirped grating for the different region.

increase, except the position is shift by the effect of 1<sup>st</sup> (master) grating's spectral spreading.

However, in the actual measurement, when the direction of the density gradient was switched, the results did not give mirror images of each other. When the groove density of the chirped grating increased as the wavelength increased, the result could not be obtained due to the wide beam broadening effect. However, in the case when the groove density of the chirped grating decreased as the wavelength increased, there was less broadening. This broadening effect will be discussed later on.

In the measurement, each chirped grating was divided into three sections, each with different groove density. Each groove density period resulted in different wavelength channel separation abilities, some sections showing larger separation abilities than others. However, in the calculations, the three sections seem to show similar abilities, except for the lower end (groove density around 100 grooves/mm) of the grating, which shows slightly better performance, see Figure 53.

## **5.2 Power Fluctuation**

### **5.2.1 Initial Setup**

The power fluctuation in the measurements is partially due to the ineffective coupling into the output single-mode fiber, due to the small numerical aperture. The loss is also attributed to the angle of incidence for the single-mode fiber, which differs for each wavelength. The angle of incidence for light coupling into output fiber was difficult to control due to small angle changes for each wavelength; therefore, the output fiber was

fixed at a single angle relative to the grating, while light came from slightly different angles. Also, the power from the input fiber was not completely uniform over the wavelength range tested, which was a function of the laser source and amplifier.

### **5.2.2 Testing Setup**

The output (collected) power for the testing setup fluctuated due to problems with coupling, as mentioned before. For the first measurement, this power fluctuation was not as severe as the other two measurements, since the separation between the wavelengths was not as large, and thus, the incident angle of light on the fiber did not vary as much. But, for mid and high density areas, the power fluctuation between the wavelengths was severe as the wavelength separation increased. The highest power of the wavelength channel occurs at one wavelength position, where the incident angle of the light on fiber was optimum, and the power decreased as the position shifted away from this optimum angle. For this reason, the measurement of power for longer wavelengths incident on the high density area of grating was not possible, since the power dropped below the detectable limit of the wave-meter.

### **5.2.3 Final Setup**

In the final setup measurements, the power fluctuated as well. However, the power fluctuation in the final setup differed from the other setups. Unlike the other setups, where there were one or two distinctive peak powers and a gradual lowering of the power for the adjacent wavelength channels, the final power fluctuated without a distinctive pattern.



Even though there were power fluctuations within the measurements, the fluctuations were not as severe as in the testing measurements, especially when considering the difference between the highest power and the lowest power received by the collection fiber. The power fluctuations from the final setup could arise for different reasons. It could be due to the differences

in incident angles of the beams into the fiber, which is caused by small differences in the origin of the rotating axis where the collection fiber is placed. The difference in the rotation axis occurs from the distribution of the wavelength

channels at the second (slave) grating, since no matter how small the distribution of the wavelength channels are, there can only be one origin of the rotational axis for collection fiber. In addition, any power fluctuations in the input channel will appear directly on

Position shift as groove density varies

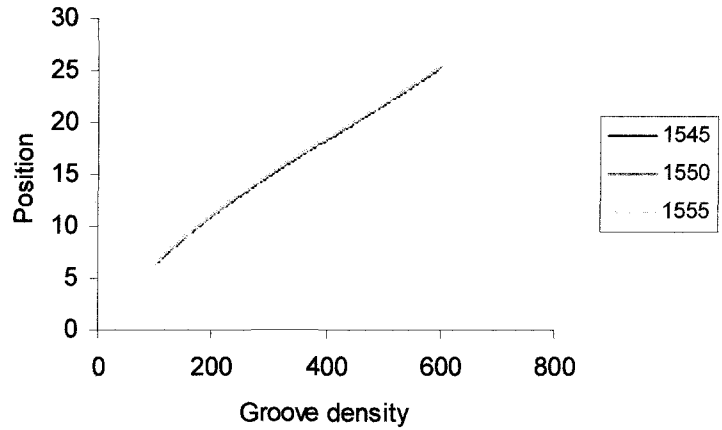


Figure 54: Calculated position of each wavelength channel as the groove density varies for testing setup

Angular position shifting as the groove density varies

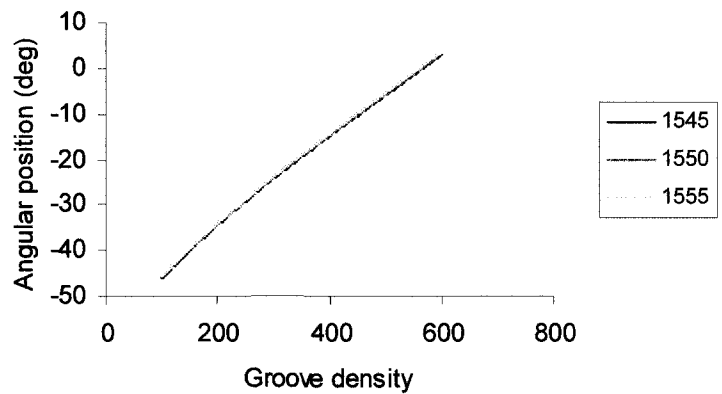


Figure 55: Calculated angular position of each wavelength channel as the groove density varies for the final setup

the output. Furthermore, there was a limit to resolution of the angular movement of the output fiber, which made positioning of the output fiber at the peak power position difficult.

### 5.3 Wavelength Routing Properties

#### 5.3.1 Routing of Wavelength Channels in the Testing Setup

The position shifts for each wavelength channel in the testing setup are shown in Table 3 and 4.

##### 5.3.1.1 1<sup>st</sup> Chirped Grating

The position shift of each wavelength channel for the 1<sup>st</sup> chirped grating is shown in

	Theory testing setup	1 <sup>st</sup> Setup using continuous chirped grating setup	Final setup results
	Amount of position shifted as chirped grating is moved from region I to region II (deg)	Amount of position shifted as chirped grating is moved from region II to region III (deg)	Amount of position shifted as chirped grating is moved from region I to region III (deg)
1546 nm	$1.41 \pm 0.02$	$1.56 \pm 0.02$	$2.97 \pm 0.02$
1547 nm	$1.48 \pm 0.02$	$1.59 \pm 0.02$	$3.07 \pm 0.02$
1548 nm	$1.55 \pm 0.02$	$1.64 \pm 0.02$	$3.18 \pm 0.02$
1549 nm	$1.61 \pm 0.02$	$1.68 \pm 0.02$	$3.29 \pm 0.02$
1550 nm	$1.57 \pm 0.02$	$1.72 \pm 0.02$	$3.29 \pm 0.02$
1551 nm	$1.73 \pm 0.02$	$1.72 \pm 0.02$	$3.46 \pm 0.02$
1552 nm	$1.76 \pm 0.02$	$1.81 \pm 0.02$	$3.57 \pm 0.02$
1553 nm	$1.79 \pm 0.02$	NA	NA
1554 nm	$1.83 \pm 0.02$	NA	NA
1555 nm	$1.88 \pm 0.02$	NA	NA

Table 4: The wavelength channels' peak power position shift as change in the 1<sup>st</sup> chirped grating density for the testing setup.

Table 4. The position shifting of each wavelength channel is not linear, but does monotonically increase as the wavelength increases. The change in the amount of the position shifting for different wavelengths is due to a change in the incident position of the light within the region. This is expected as seen from the calculation result in Figure 54 and Figure 55. This figure shows the position of a wavelength channel as the groove density changes in the 2<sup>nd</sup> (slave) grating.

### 5.3.1.2 2<sup>nd</sup> Chirped Grating

The position shift of each wavelength channel for the 2<sup>nd</sup> chirped grating is shown in Table 5. The position shifting is not linear, but again increases monotonically as the wavelength increases, which is due to the changes in incident position within the region. This is expected as seen from calculations, in Figure 54 and 55. However, for the longer wavelengths, the amount of shift per channel increased progressively more than what the

	Amount of position shifted as chirped grating is moved from region I to 2egion II (deg)	Amount of position shifted as chirped grating is moved from region II to region III (deg)	Amount of position shifted as chirped grating is moved from region I to region III (deg)
1546 nm	1.46± 0.02	1.49 ± 0.02	2.95 ± 0.02
1547 nm	1.60± 0.02	1.57 ± 0.02	3.17 ± 0.02
1548 nm	1.75± 0.02	1.67 ± 0.02	3.42 ± 0.02
1549 nm	1.94± 0.02	1.68 ± 0.02	3.63 ± 0.02
1550 nm	2.11± 0.02	1.66 ± 0.02	3.78 ± 0.02
1551 nm	2.15± 0.02	1.7 ± 0.02	3.86 ± 0.02
1552 nm	2.24± 0.02	1.8 ± 0.02	4.04 ± 0.02
1553 nm	2.39± 0.02	1.75 ± 0.02	4.14 ± 0.02
1554 nm	NA	NA	NA
1555 nm	NA	NA	NA
Table 5: The wavelength channels' peak power position shift as change in the 2 <sup>nd</sup> chirped grating density for the testing setup.			

calculations predicted. This could be due to difference in the incident angle of the shorter wavelength and the longer wavelength on to the second grating since the longer wavelength is diffracted at larger incident angle than the shorter wavelength in the experiment.

### 5.3.2 Routing of Wavelength Channel in Final Setup

The amount of the position shift of each wavelength channel for the final setup is shown in Tables 6 and 7.

#### 5.3.2.1 1<sup>st</sup> Chirped Grating

The position shift of each wavelength channel for the 1<sup>st</sup> chirped grating is shown in Table 6. As with the previous setups, the position shifting of the wavelength channel was not linear and monotonically increased with wavelength, which was predicted by the

	Amount of position shifted as chirped grating is moved from region I to 2egion II (deg)	Amount of position shifted as chirped grating is moved from region II to region III (deg)	Amount of position shifted as chirped grating is moved from region I to region III (deg)
1546 nm	1	2.8	3.8
1547 nm	1.2	3	4.2
1548 nm	1.5	3.2	4.7
1549 nm	1.8	3.3	5.1
1550 nm	1.7	3.6	5.3
1551 nm	1.9	3.9	5.8
1552 nm	2.2	4.2	6.4
1553 nm	2.4	4.5	6.9
1554 nm	2.6	4.8	7.4
1555 nm	2.9	5	7.9
Table 6: The wavelength channels' peak power position shift as change in the 1 <sup>st</sup> chirped grating density for the final setup.			

calculations in Figure 54 and 55. The figure shows position of a wavelength channel as the groove density changes in the 2<sup>nd</sup> (slave) grating.

### 5.3.2.2 2<sup>nd</sup> Chirped Grating

The position shift of each wavelength channel for the 2<sup>nd</sup> chirped grating is shown in Table 7. The position shifting of the wavelength channel is not linear, but does increase as the wavelength increases. In addition, the amount of the position shifting is different between positions due to change in the region groove density. This is expected as seen from the calculations, shown in Figure 54 and 55. This figure shows the position of a wavelength channel as the groove density changes in the 2<sup>nd</sup> (slave) grating. However, for the higher wavelengths, the amount of shifting of each channel position increased progressively more than what the calculation predicted. As before, this could be due to difference in the incident angle of the shorter wavelength and the longer wavelength.

	Amount of position shifted as chirped grating is moved from region I to region II (deg)	Amount of position shifted as chirped grating is moved from region II to region III (deg)	Amount of position shifted as chirped grating is moved from region I to region III (deg)
1546 nm	3.5	4.2	7.7
1547 nm	3.7	4.2	7.9
1548 nm	3.9	4.8	8.7
1549 nm	4.4	5	9.4
1550 nm	4.8	5.3	10.1
1551 nm	5.2	5.4	10.6
1552 nm	5.5	6.1	11.6
1553 nm	5.9	6.3	12.2
1554 nm	6.2	6.5	12.7
1555 nm	6.8	6.2	13

Table 7: The wavelength channels' peak power position shift as change in the 2<sup>nd</sup> chirped grating density for the final setup.

## 5.4 Beam Broadening

Due to the limitations in controlling the beam waist of the light incident on the chirped grating, a noticeable

increase of beam waist at

the output was observed.

Even though it is possible

to focus or collimate the

light beam into small spot

size, there was a limit to

minimum output spot size

that could be achieved, due

to the wavelength of the

light as well as diffraction

effects from the optics.

Therefore, when the beam

hit the chirped grating in

which the groove density

varies continuously, each

part of the beam is incident

on a slightly different

portion of the grating, and

Beam broadening

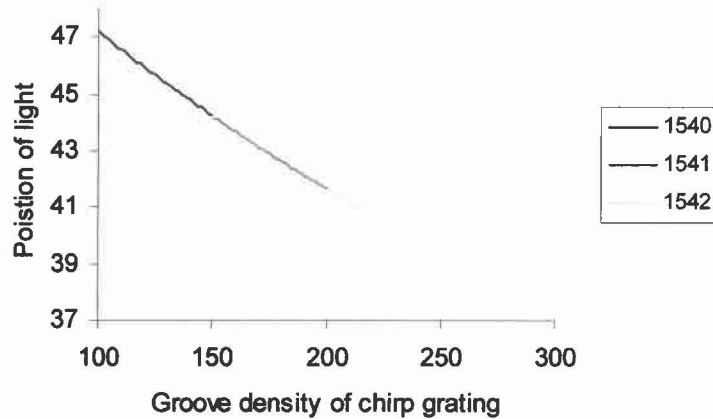


Figure 56: Calculated position of wavelength channel for the case when the wavelength channel interacted over the range of the chirped grating without overlapping the same groove density area.

Overlapping of the wavelength

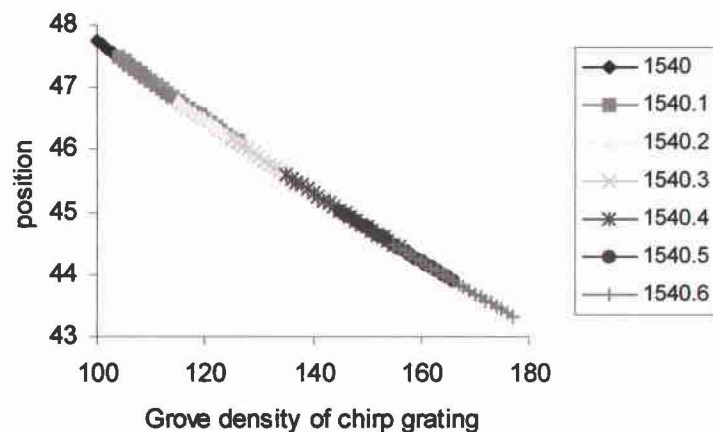


Figure 57: Calculated position of wavelength channel for the case when the wavelength channel interacted over the range of the chirped grating with overlapping the same groove density area.

thus encounters various groove densities. As the beam spot size increased, the area of chirped grating hit by the light increased. For example, if the spot diameter for the light containing only a single wavelength and with evenly distributed power is comparable to the length of the chirp on the grating, then the diffracted angle would be different for each spatial location along the length of the grating. This would result in spreading of light at different angles according to groove density. Figure 56 shows the affect of grove density variation on the final position of an individual wavelength channel.

In the experiment, due to the beams of closely spaced channels physically overlapping following diffraction from the first grating, some of the same area of the chirped grating is shared by the different channels. This results in over lapping of the wavelengths at the final destination (output), as shown in Figure 57. As the area shared by each wavelength channel at the chirped grating increases, the overlapping of each channel at the output increases.

The spatial overlapping of the wavelengths leads to high levels of cross-talk between the channels. In order to minimize the effect of overlapping of the beam on the chirped grating, it would be necessary to focus each channel's beam at the chirped grating to reduce the area shared by each wavelength.

## **Chapter 6**

### **Conclusion**

The fast paced increase in the need for higher bandwidth in current communication systems has led to the development optical networks. However, today's communication technologies do not completely utilize the full potential of optic communication systems, due to limiting constraints from the optical components. Even with the advancement in optical components within optical communication systems, the available wavelength channel ranges are limited. This limitation arises from the optical fiber, which has narrow wavelength ranges with low loss coefficients centered at 0.8  $\mu\text{m}$ , 1.3  $\mu\text{m}$ , and 1.5  $\mu\text{m}$ . In addition to the limitations of the optical fiber, the optical amplifiers currently in used, such as the erbium dope fiber amplifier (EDFA), also limit the maximum channel spacing due to the limited range of wavelengths it can amplify uniformly, typically about 35-40 nm [23]. Therefore, in order to increase the efficiency of optical communication systems, the number of channels within the available wavelength ranges needs to be increased.

One means to accomplish this is wavelength division multiplexing. However, in today's optical communication systems, the demultiplexer is one of the factors which limits the number of channels that can be transmitted through the optical fiber, since it can only demultiplex wavelength channels with certain wavelength separations, typically larger than 0.5 nm. Therefore, to increase the number of the wavelength channels, there is a need for the demultiplexer that is capable of separating closely packed wavelength



channels. To meet this need, this thesis discussed the research and development of a demultiplexer constructed with cascading diffraction gratings to achieve a robust and cost-effective demultiplexer that is capable of separating the closely packed wavelength channels, with separation less than 0.5 nm.

## **6.1 Testing of Grating System**

In the initial stage of the research, a single 600 grooves/mm grating was used for reference measurements. These measurements were conducted to examine the wavelength channel separation property of diffraction gratings and to compare the results with other demultiplexer setups published in the literature. Reference measurements were conducted with this configuration for all the different experimental setups examined in this thesis.

The initial reference measurement results showed that the single grating setup, within reasonable size, is ideally suited for wide channel systems, with spacing of  $\Delta\lambda > 1\text{nm}$  because it is simple, robust, and cost effective. However, for DWDM systems, which require wavelength channel spacings of  $\Delta\lambda < 1\text{nm}$ , it would not be suitable. Even though the resolution of the channels can be increased by increasing the distance between the grating and collection fiber and/or changing the angle of incidence of the input to the grating, this results in achieving only the typical lower limit of channel density for a setup with a reasonable distance between input and output.

## **6.2 Testing of Dual Grating System**

### **6.2.1 First Stage**

In the beginning of this research, the feasibility of a demultiplexer using dual grating

in series was tested [25]. Once the feasibility was proven, two proto-type chirped gratings were fabricated, by Oceanic Inc., one chirped grating with groove density varying from 300 grooves/mm to 600 grooves/mm and another chirped grating with groove density varying from 100 grooves/mm to 600 grooves/mm.

With these two proto-type chirped gratings, testing of two different setups were conducted; the testing setup and then final setup. In this research, two different measurement setups were conducted due to the power fluctuation problems in the first setup, called the testing setup.

### **6.2.2 Testing Setup**

Using the 600 grooves/mm grating, as a master grating, and the different groove density areas of the chirped grating that had groove density varying from 300 grooves/mm to 600 grooves/mm, as the slave grating, in series resulted in improved wavelength channel separations. Following this test, the 1<sup>st</sup> chirped grating was replaced by the 2<sup>nd</sup> chirped grating, having groove density varying from 100 grooves/mm to 600 grooves/mm. In both case, the separations between the wavelength channels improved by 450% to 850% depending on the groove density, when compared to the average separations of the wavelength channels for the reference measurements.

However, even though this testing setup showed improvement of the physical separation between the wavelengths, the power of each channel fluctuated depending on the position of receiving fiber. This power fluctuation in the measurements was partially due to the ineffective coupling into the output single-mode fiber, which has small numerical aperture. The loss is also due to the angle of incidence for the single-mode

fiber, which differs for each wavelength. The angle of incidence for light coupling into the collection fiber was difficult to control due to small angle changes for each wavelength; therefore, the output fiber was fix at a single angle, while light came from slightly different angles.

### **6.3 Final Setup**

To reduce the power fluctuations in the testing stage of this research, a different setup was used. Identical to the configuration of the testing setup, the 600 grooves/mm grating was used as a master grating, and 1<sup>st</sup> chirped grating, having groove density varying from 300 grooves/mm to 600 grooves/mm, was used as the slave grating. The two gratings in series resulted in improved wavelength channel separation. Then, as it was done with testing setup, the 1<sup>st</sup> chirped grating was replaced by the 2<sup>nd</sup> chirped grating, having groove density varying from 100 grooves/mm to 600 grooves/mm. In this setup, the separations between the wavelength channels improved by 370% to 1700% for the 1<sup>st</sup> chirped grating and 800% to 1780% for the second chirped grating, depending on the groove density, when compared to the average separations of the wavelength channels for the reference measurements.

Compared to the first setup, which had more than 10 dB difference between the highest power and the lowest power, the second setup reduced the power fluctuation between the highest and the lowest power to less than 10 dB. However, the improvement in received power came at the cost of additional measurement error due to a larger limitation on movement control. In the design of an actual demultiplexer device, this could be compensated for by precise control of the arrangement of the output fiber.

#### **6.4 Dual Grating Measured Results verse Calculated Results**

From the calculations, it was evident that the position of the each wavelength channel was predominately controlled by the groove density of second grating. This is attributed to the difficulty encountered in controlling the accuracy of the light from the first grating to hit the area of the desired groove density of the second grating. Through the experiment using the chirped grating as a routing element, the relationship of wavelength and the groove density was partly verified.

#### **6.5 Routing Property**

In addition to the demultiplexing capability of the chirped grating, it was tested for the routing property.

The position shifting of the wavelength channel was found to be non-linear, but monotonically increasing as was expected. The position of the selected wavelength changed as the groove density increased and decreased. These position changes were different between the 1<sup>st</sup> and 2<sup>nd</sup> chirped gratings, where 2<sup>nd</sup> chirped grating had a larger groove density change. This routing of the wavelength also verified that position shifting of the given wavelength is depended on groove density.

#### **6.7 Unwanted Effects of Chirped Grating**

Due to the limitation in controlling the beam waist of the light going into the chirped grating, an increase of beam waist was observed. Even though it is possible to focus or collimate the light beam into small spot size, there was a limit to minimum size, achieved in this experiment. Therefore, when the beam hit the continuously chirped grating, the

light interacted with various groove densities, and as the beam spot size increased, the area illuminated on the chirped grating increased. This resulted in spreading of light in different direction according to groove density. This effect is more severe for the setup where the chirped grating was used compared to the uniform groove density grating.

The beam broadening effect caused large cross talk between the neighboring wavelength channels, since the each wavelength coming out of the master grating could not be easily separated before the chirped grating (slave grating).

Other than the beam broadening, the typical loss due to the coupling the light into the output fiber was large, typically about 20 dB. This can be significantly reduced by inserting collection optics in front of each fiber, which is common technique employed in fiber optic systems.

## **Closing**

This research shows that all of the dual grating setup improved the average wavelength channel separation compare to the single grating systems. The improvements of the wavelength separation ranges from 50% to 1700% depending on the setup, which clearly shows capability of the system of separating the wavelength channel spacing of less than 0.5 nm for reasonably sized demultiplexer.

## Reference

- [1] D. R. Wisely, *Electron. Lett.* **27**, 520 (1991).
- [2] Jean-Pierre Lande, "DWDM Fundamentals, Components, and Applications", Artech House, 2002,
- [3] Rajiv Ramaswan, Kumar N. Sivarajar, "Optical Networks, A Practical Perspective 2<sup>nd</sup>", Academic Press, 2002
- [4] Takada, K., Abe, M., Shibata, T., Ishii, T., Inoue, H., Yamada, Y., Hibino, Y., and Okamoto, K., "10-GHz-spaced 1010-channel AWG filter achieved by tandem connection of primary and secondary AWGs", ECOC 200, Munich, 2000, Postdeadline Paper PD3-8
- [5] Takada, K., Abe, M., Shibata, T., Okamoto, K., "Low-loss 10-GHz-spaced tandem multi/demultiplexer with more than 1000 channels using a 1×5 interference multi/demultiplexer as a primary filter", *IEEE Photonics Technology Letters* , Volume: 14 Issue: 1 , Jan 2002 Page(s): 59 –61
- [6] Takada, K., Abe, M., Shibata, T., Okamoto, K., "Three-stage ultra-high-density multi/demultiplexer covering low-loss fibre transmission window 1.26-1.63  $\mu\text{m}$ ", *Electronic Letters* , Volume: 39 No. 9, April 2002, Page(s): 405-406
- [7] Sun, Z.J., McGreer, K.A., Broughten, J.N., "Demultiplexer with 90 channels and 0.3 nm channel spacing Vertical-Cavity Lasers, Technologies for a Global Information Infrastructure, WDM Components Technology, Advanced Semiconductor Lasers, Gallium Nitride Materials, Processing", 1997 Digest of the IEEE/LEOS Summer Topical Meetings , 11-15 Aug 1997, Page(s): 52 -53
- [8] Stavdas, A., "A single WDM multi/demultiplexer for all SMF transmission windows in 1280-1680 nm", *IEEE Photonics Technology Letters* , Volume: 14 Issue: 11 , Nov 2002, Page(s): 1542 –1544
- [9] William B. Jones Jr., "Introduction to Optical Fiber Communication System", Holt, Rinehart and Winston, Inc., 1988
- [10] Robert J. Hoss, Edward A. Lacy, "Fiber Optics", PTR Prentice-Hall Inc., NJ, 1993
- [11] Josep Prat, Pere E Balaguer, Joan M. Gene, Oscar Diaz, Sergi Figuirola, "Fiber to the Home Technologies", Academic Publishers, 2002
- [12] Katsunari Okamoto, "Fundamentals of Optical Waveguides", Academic Press, 2000

- [13] Robert J. Hoss, "Fiber Optic Communications: Design Handbook", Prentice Hall Inc., 1990
- [14] John P. Powers, "Introduction to Fiber Optic Systems", Aksen Association Inc., 1993
- [15] Andreas Othonos, Kyriacos Kalli, "Fiber Bragg Grating: Fundamentals and Applications in Telecommunications and Sensing", Artech House Publishers, 1999
- [16] William O. Grant, "Understanding Lightwave Transmission: Applications of Fiber Optics", Harcourt Brace Jovanovich, 1988
- [17] Thomas E. Stern, Krishna Bala, "Multiwavelength Optical Network: A Layered Approach", Addison Wesley Longman, Inc., 1999
- [18] Dr. Martin Amersfoort, "Arrayed Waveguide Grating", Concept to Volume b.v., 15 June 1998
- [19] P.D. Rinh, S. Yegnanarayanan, F. Coppinger, B. Jalali, "Silicon-on-insulator Phased-Array waveguide grating WDM filter", OFC '97 Technical Digest, p301-302, 1997
- [20] Tsunetoshi Saito, Toshihiko Ota , Tomoaki Toratani, Yoshimi Ono, "16-ch Arrayed Waveguide Grating Module with 100-GHz Spacing", Furukawa Review, No. 19. 2000
- [21] C. Dragone, "Planar 1 N Optical Multiplexer With Nearly Ideal Response", IEEE Photonics Technology Letters, VOL. 14, NO. 11, pp.1545-1547, NOVEMBER 2002
- [22] Alexandros Stavdas, "A Single WDM Multi/Demultiplexer for All SMF Transmission Windows in 1280–1680 nm", IEEE Photonics Technology Letters, VOL. 14, NO. 11, pp1542-1542, NOVEMBER 2002
- [23] Tizhi Huang, Jeff Huang, Yueai Liu, Ming Xu, Yatao Yang, Minchun Li, Chongchang Mao and Jung-Chih Chiao, "Performance of a Liquid-Crystal Optical Harmonic Equalizer", 2001 Optical Fiber Communications Conference, TX, March 2001
- [24] Stamatios V. Kartalopoulos, "DWDM Networks, Devices, and Technology", IEEE Press, NJ., 2003

- [25] Ray Park, Audra Bullock, Multigrating Demultiplexer, Optical Devices for Fiber Communication IV; Michel J. Digonnet; Ed Proc. SPIE Vol. 4989, p 168-173, June 2003.



MULTI-GRATING DEMULTIPLXER UTILIZING  
CHIRPED GRATING

A THESIS SUBMITTED TO THE GRADUATED DIVISION OF THE  
UNIVERSITY OF HAWAI'I IN PARTIAL FULFILLMENT  
OF THE REQUIREMENTS FOR THE DEGREE OF

MASTER OF SCIENCE

IN

ELECTRICAL ENGINEERING

NOVEMBER 2004

By  
Ray J. Park

Thesis Committee:

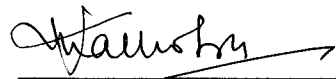
Audra Bullock, Chairperson  
Victor M. Lubecke  
Vinod Malhotra

**RECEIVED**  
**AS**  
**FOLLOWS**

We certify that we have read this thesis and that, in our opinion, it is satisfactory in scope and quality as a thesis for the degree of Master of Science in Electrical Engineering

THESIS COMMITTEE

  
Chairperson





## **Acknowledgement**

I would like to thank Dr. Bullock for her support throughout the project.

I would also like to thank Dr. Malhotra and Dr. Lubecke for being on thesis member.

## **Abstract**

In today's optical communication systems, the demultiplexer limits the number of channels that can be transmitted through the optical fiber, since its wavelength channels demultiplexing limit is typically larger than 0.5 nm. To increase this limitation of the demultiplexer, this thesis discusses the research and development of a demultiplexer constructed with cascading diffraction gratings.

To achieve larger channel separation, a multi-grating demultiplexer was developed using diffraction gratings with different profile in different configurations. With different configuration utilizing different grating, an improvement of 50% to 1700% in separation of wavelength channels was achieved compared to the single grating system. In addition routing properties of the chirped grating were researched.

Over all, the research presented here demonstrates that it is possible to increase the wavelength channel spacing and route the channels using multi-grating system.

## TABLE OF CONTENT

Acknowledgement.....	iii
Abstract.....	iv
List of Tables.....	viii
List of Figures.....	vi
Chapter 1: Communication Network.....	1
Introduction.....	1
1.1 Communication technologies.....	2
1.2 Fiber optic communication setup.....	3
1.3 Components of fiber optic communication system.....	4
1.3.1 Light source.....	4
1.3.2 Channel.....	5
1.3.2.1 Multimode fiber.....	5
1.3.2.2 Single-mode fiber.....	6
1.3.3 Amplifier.....	6
1.3.4 Multiplexing of Optical signal.....	7
1.3.4.1 Multiplexing scheme in hybrid communication system.....	7
1.3.4.2 Multiplexing scheme in all optical system.....	8
1.3.5 Multiplexer and Demultiplexer.....	8
1.3.6 Router/Switch.....	9
1.3.7 Receiver.....	9
1.4 Wavelength add/drop multiplexer (WADM).....	9
Chapter 2: Different Grating Technologies.....	11
2.1 Bragg grating (FBG).....	11
2.2 AWG (Arrayed Waveguide Grating).....	13
2.3 Diffraction grating.....	16
2.4 Improvements made in the diffraction grating.....	18
Chapter 3: Theory and Calculation.....	19
3.1 Theory.....	19
3.1.1 Chirped grating.....	20
3.2 Calculations.....	21
3.2.1 Initial testing of the Theory.....	22
3.2.2 Final setup calculation.....	25
Chapter 4: Setup and Procedures, Setups and Measurement.....	28
4.1 Testing of the theory.....	28
4.1.1 Layout of the measurement setup.....	29
4.1.2 Reference setup.....	30
4.1.2.1 Actual dimensions for first setup.....	31

4.1.2.2 Measurement technique in first setup	32
4.1.2.3 Reference setup results (Single grating)	33
4.1.3 Dual grating setup	34
4.1.3.1 Results for the two 600 grooves/mm gratings in series	36
4.2 First experiment with continuous chirped grating (Lateral measurement setup)	36
4.2.1 Reference setup results (Single grating)	38
4.2.2 Results for the two 600 grooves/mm gratings in series	39
4.2.3 Results for the 600 grooves/mm grating and the 1st chirped grating in series	40
4.2.3.1 Results at region I of the 1st chirped grating	41
4.2.3.2 Results at region II of the 1st chirped grating	42
4.2.3.3 Results at region III of the 1st chirped grating	43
4.2.4 Results for the 600 grooves/mm grating and the 2nd chirped grating in series	44
4.2.4.1 Results at region I of the 2nd chirped grating	44
4.2.4.2 Results at region II of the 2nd chirped grating	45
4.2.4.3 Results at region III of the 2nd chirped grating	46
4.3 Final setup with continuous chirped grating (Circular measurement setup)	47
4.3.1 Reference Setup (Single grating)	48
4.3.1.1 Actual setup dimensions for final setup	49
4.3.1.2 Measurement technique final setup	50
4.3.2 Dual grating setup	51
4.3.2.1 Results for the two 600 grooves/mm gratings in series	52
4.3.3 Results for the 600 grooves/mm grating and the 1st chirped grating in series	53
4.3.3.1 Results at region I of the 1st chirped grating	54
4.3.3.2 Results at region II of the 1st chirped grating	55
4.3.3.3 Results at region III of the 1st chirped grating	56
4.3.4 Results for the 600 grooves/mm grating and the 2nd chirped grating in series	56
4.3.4.1 Results at region I of the 2nd chirped grating	56
4.3.4.2 Results at region II area of the 2nd chirped grating	57
4.3.4.3 Results at region III of the 2nd chirped grating	58
4.4 Wavelength routing properties of the dual grating system	59
4.4.1 Results from lateral setup results	60
4.4.1.1 Position shifting of 1st grating	61
4.4.1.2 Position shifting of 2nd grating	61
4.4.2 Final setup results	62
4.4.2.1 Position shifting of 1st grating	62
4.4.2.2 Position shifting of 2nd grating	62
Chapter 5: Discussion of Results	63

5.1 Wavelength channel's peak power separations	63
5.1.1 Single grating (Reference measurement)	63
5.1.2 Dual grating measured results	65
5.1.2.1 Two 600 groove/mm in series	65
5.1.2.2 Dual grating (1st Chirp grating)	66
5.1.2.2.1 Testing Setup	67
5.1.2.2.2 Final setup	67
5.1.2.3 Dual grating (2nd Chirp grating)	68
5.1.2.3.1 Testing Setup	68
5.1.2.3.2 Final Setup	68
5.1.3 Dual grating measured results vs. calculated results	70
5.2 Power fluctuation	72
5.2.1 Initial setup	72
5.2.2 Testing setup	73
5.2.3 Final setup	73
5.3 Wavelength routing properties	75
5.3.1 Routing of wavelength channel in testing setup	75
5.3.1.1 1st Chirp grating	75
5.3.1.2 2nd Chirp grating	76
5.3.2 Routing of wavelength channel in final setup	77
5.3.2.1 1st Chirp grating	77
5.3.2.2 2nd Chirp grating	78
5.4 Beam Broadening	79
Chapter 6: Conclusion	81
6.1 Testing of grating system	82
6.2 Testing of dual grating system	82
6.2.1 First Stage	82
6.2.2 Testing Setup	83
6.3 Final setup	84
6.4 Dual grating measured results vs. calculated results	85
6.5 Routing Property	85
6.7 Unwanted Effects of Chirped grating	85
Closing	86
Reference	87



## LIST OF TABLES

<u>Table</u>	<u>Page</u>
1. Average separation between the channels' peak power.....	64
2. Wavelength channels separation improvement.....	66
3. Average power fluctuation between the wavelength channels' peak power.....	69
4. The wavelength channels' peak power position shift as change in the 1 <sup>st</sup> chirped grating density for the testing setup.....	75
5. The wavelength channels' peak power position shift as change in the 2 <sup>nd</sup> chirped grating density for the testing setup.....	76
6. The wavelength channels' peak power position shift as change in the 1 <sup>st</sup> chirped grating density for the final setup.....	77
7. The wavelength channels' peak power position shift as change in the 2 <sup>nd</sup> chirped grating density for the final setup.....	78

## LIST OF FIGURES

<u>Figure</u>	<u>Page</u>
1. Arrayed Waveguide Grating (AWG).....	13
2. Diffraction grating.....	16
3. Diffraction behavior of wavelength.....	20
4. Geometry of initial dual grating setup.....	22
5. Geometry of final dual grating setup.....	25
6. Schematic of the measurement setup.....	28
7. Dimensions of the setup.....	29
8. Measurement.....	30
9a. Reference measurement setup.....	32
9b. Dual standard ruled grating (DS configuration), both grating with 600 grooves/mm.....	32
9c. Standard/chirped ruled grating (SC configuration), initial grating with 600 grooves/mm and groove-spacing varying grating for second grating.....	32
10. Actual measurement for each wavelength for single 600 grooves/mm (Reference measurement).....	33
11. Peak power position of each wavelength for single 600 grooves/mm. (Reference measurement).....	31
12. Peak power position of each wavelength for dual grating. Two 600 grooves/mm grating in series.....	33
13. Actual measurement for each wavelength for dual grating. Two 600 grooves/mm in series.....	33
14. Peak power position of each wavelength for single 600 grooves/mm. For the testing setup measurement (Reference measurement).....	37
15. Actual measurement for each wavelength for single 600 grooves/mm. For the testing setup measurement (Reference measurement).....	38
16. Peak power position of each wavelength for dual grating. Two 600 grooves/mm grating in series for the testing setup measurement.....	39
17. Actual power measurement for each wavelength for the two 600 grooves/mm in series. For the testing setup measurement.....	39
18. Peak power position of each wavelength for dual grating. 600 grooves/mm and 1 <sup>st</sup> chirp grating in series for the testing setup measurement. (at region I of chirped grating).....	40

19. Actual power measurement for each wavelength for the 600 grooves/mm and 1 <sup>st</sup> chirped grating in series for the testing setup measurement. (at region I of chirped grating)	40
20. Peak power position of each wavelength for dual grating. 600 grooves/mm and 1 <sup>st</sup> chirped grating in series for the testing setup measurement. (at region II of chirped grating)	41
21. Actual power measurement for each wavelength for the 600 grooves/mm and 1 <sup>st</sup> chirped grating in series for the testing setup measurement. (at region II of chirped grating)	41
22. Peak power position of each wavelength for dual grating. 600 grooves/mm and 1 <sup>st</sup> chirped grating in series for the testing setup measurement. (at region III of chirped grating)	42
23. Actual power measurement for each wavelength for the 600 grooves/mm and 1 <sup>st</sup> chirped grating in series for the testing setup measurement. (at region III of chirped grating)	42
24. Peak power position of each wavelength for dual grating. 600 grooves/mm and 2 <sup>nd</sup> chirped grating in series for the testing setup measurement. (at region I of chirped grating)	43
25. Actual power measurement for each wavelength for the 600 grooves/mm and 2 <sup>nd</sup> chirped grating in series for the testing setup measurement. (at region I of chirped grating)	43
26. Peak power position of each wavelength for dual grating. 600 grooves/mm and 2 <sup>nd</sup> chirped grating in series for the testing setup measurement. (at region II of chirped grating)	45
27. Actual power measurement for each wavelength for the 600 grooves/mm and 2 <sup>nd</sup> chirped grating in series for the testing setup measurement. (at region II of chirped grating)	45
28. Peak power position of each wavelength for dual grating. 600 grooves/mm and 2 <sup>nd</sup> chirped grating in series for the testing setup measurement. (at region III of chirped grating)	46
29. Actual power measurement for each wavelength for the 600 grooves/mm and 2 <sup>nd</sup> chirped grating in series for the testing setup measurement. (at region III of chirped grating)	46
30. Final measurement setup	47
31. The dimension for the final setup	48
32. Final setup measurement technique	49
33. Peak power positions of each wavelength for the two 600 grooves/mm grating in series for the final setup measurement	52
34. Peak power measurement for each wavelength for the two 600 grooves/mm grating in series for the final setup measurement	52
35. Peak power position of each wavelength for dual grating. 600 grooves/mm and 1 <sup>st</sup> chirped grating in series for the testing setup measurement. (at region I of chirped grating)	53

36. Actual peak power measurement for each wavelength for the 600 grooves/mm and 1 <sup>st</sup> chirped grating in series for the testing setup measurement. (at region I of chirped grating).....	53
37. Peak power position of each wavelength for dual grating. 600 grooves/mm and 1 <sup>st</sup> chirped grating in series for the testing setup measurement. (at region II of chirped grating).....	54
38. Actual peak power measurement for each wavelength for the 600 grooves/mm and 1 <sup>st</sup> chirped grating in series for the testing setup measurement. (at region II of chirped grating).....	54
39. Peak power position of each wavelength for dual grating. 600 grooves/mm and 1 <sup>st</sup> chirped grating in series for the testing setup measurement. (at region III area of chirped grating).....	55
40. Actual peak power measurement for each wavelength for the 600 grooves/mm and 1 <sup>st</sup> chirped grating in series for the testing setup measurement. (at region III area of chirped grating).....	55
41. Peak power position of each wavelength for dual grating. 600 grooves/mm and 2 <sup>nd</sup> chirped grating in series for the testing setup measurement. (at region I area of chirped grating).....	57
42. Actual peak power measurement for each wavelength for the 600 grooves/mm and 2 <sup>nd</sup> chirped grating in series for the testing setup measurement. (at region I area of chirped grating).....	57
43. Peak power position of each wavelength for dual grating. 600 grooves/mm and 2 <sup>nd</sup> chirped grating in series for the testing setup measurement. (at region II of chirped grating).....	58
44. Actual peak power measurement for each wavelength for the 600 grooves/mm and 2 <sup>nd</sup> chirped grating in series for the testing setup measurement. (at region II area of chirped grating).....	58
45. Peak power position of each wavelength for dual grating. 600 grooves/mm and 2 <sup>nd</sup> chirped grating in series for the testing setup measurement. (at region III area of chirped grating).....	59
46. Actual peak power measurement for each wavelength for the 600 grooves/mm and 2 <sup>nd</sup> chirped grating in series for the testing setup measurement. (at region III area of chirped grating).....	59
47. Channel's peak power position shifting as the groove density of 1 <sup>st</sup> chirped grating varies from region I to region II and region II to region III.....	60
48. Channel's peak power position shifting as the groove density of 1 <sup>st</sup> chirped grating varies from region I to region II and region II to region III.....	60
49. Channel's peak power position shifting as the groove density of 2 <sup>nd</sup> chirped grating varies from region I to region II and region II to region III.....	61
50. Channel's peak power position shifting as the groove density of 2 <sup>nd</sup> chirped grating varies from region I to region II and region II to region III.....	61

51. Calculated Position of wavelength channel for 1 <sup>st</sup> and 2 <sup>nd</sup> chirped grating.....	70
52. Calculated angular position of wavelength channel for 1 <sup>st</sup> and 2 <sup>nd</sup> chirped grating.....	70
53. Calculated position of wavelength channel for 1 <sup>st</sup> and 2 <sup>nd</sup> chirped grating for the different region.....	71
54. Calculated position of each wavelength channel as the groove density varies for testing setup.....	74
55. Calculated angular position of each wavelength channel as the groove density varies for the final set.....	74
56. Calculated position of wavelength channel for the case when the wavelength channel interacted over the range of the chirped grating without overlapping the same groove density area.....	79
57. Calculated position of wavelength channel for the case when the wavelength channel interacted over the range of the chirped grating with overlapping the same groove density area.....	79

## **Chapter 1**

### **Introductions and Communication Network**

#### **Introduction**

Fast paced increase in the need for the higher bandwidth in communication systems has led to the development optical networks. While moving to an optical network topology has increased the available bandwidth, today's communication technologies still do not fully utilize the potential of optic communication systems, due to limiting constraints in the optical system components. All optical network systems have the potential to dramatically increase the efficiency of communication networks however, due to high cost and power loss today's communication networks still rely on optical-to-electrical and electrical-to-optical conversion network elements. The difficult task in creating all optic networks is the development cost effective, flexible, and reliable Wavelength Add Drop Multiplex (WADM) components capable of demultiplexing/multiplex a highly dense signal efficiently.

Even with the advancement in optical components within the optical communication systems, the available wavelength channel ranges are limited. These limitations arise from the optical fiber, which has narrow wavelength ranges with low loss centered at wavelength, 0.8  $\mu\text{m}$ , 1.3  $\mu\text{m}$  and 1.5  $\mu\text{m}$ . In addition to the limitations of the optical fiber,

the optical amplifiers, such as the erbium dope fiber amplifier (EDFA), currently in used also limit the minimum channel spacing due to the limited range of wavelengths it can amplify uniformly, typically about 35-40 nm [23]. Therefore, in order to increase the efficiency of optical communication systems, the number of channels within the available wavelength ranges needs to be increased. However, in today's optical communication systems, the demultiplexer is one of the factors which limits the number of channels that can be transmitted through the optical fiber, since it can only demultiplex wavelength channels with wavelength separations larger than 0.5 nm. Therefore, to increase the number of the wavelength channels, there is a need for a demultiplexer that is capable of separating closely packed wavelength channels. To meet this need, this thesis discuss the research and development of a demultiplexer constructed with cascading diffraction gratings to achieve a demultiplexer that is capable of separating the closely packed, less than 0.5 nm, wavelength channels.

## **1 Communication Network**

### **1.1 Communication Technologies**

Current communication systems consist of two types of technologies, wireless and wired. For the wireless technology, microwaves or radiowaves are used to transmit information over the air. For wired technology, we use metal-based transmission media or fiber optic-based media to transmit information over the land. When comparing the two wired technologies, fiber optic-based technology offers many advantages over metal base technology. Compared to metal-based technology, fiber optic-based technology

offers larger bandwidth, lower loss, no electromagnetic interference, smaller cross-talk, and higher security. Also, optical fiber is smaller and lighter than the metallic counter part, and consequently, it is much easier to install than metallic-based connections.

## **1.2 Fiber Optic Communication Setup**

The basic communication system setup consists of a signal transmitter, channel, and receiver. First, the signal is modulated on a carrier frequency using one of many different modulation methods. Second, the modulated signal is transmitted over the channel. Finally, the modulated signal is received at the receiver and demodulated.

Currently, most of the communication system setups are a mixture of metallic-based connections and fiber optic based connections. Typically in short-haul communications, metallic-based channel media are used and for the long haul, some metallic and fiber optic channels are used to transmit signals. In long-haul transmission using fiber optics, the information source is converted into electrical signals then converted into optical signals and transmitted over the fiber optic cables.

Even with introduction and development of many different technologies in optical communication systems, full capabilities of the optic networks are not utilized due to limitations of the individual components within the optical systems. These limitations include: dispersion of wavelengths while traveling in the optical fiber, lack of stable and narrow spectral widths, and incapability of separating closely packed wavelengths.

Still with the limitations of the optical system components, current communication systems do not fully utilizes the potential of fiber optic technologies that are available. The biggest cause of these limitations is the mixture of metallic (electrical) and optic



(light) based components. With all the improvements and developments, current communication systems still depends on the electrical signals within the networks (e.g. at routers, regenerator, and repeater), which limits the bandwidth and speed. This limitation arises mostly at the nodes within the communication-network. As the signal reaches the nodes of the network, each signal is distributed (routed) through the network. Current communication systems still depend on an electrical means to distribute (route) the communication signal to a designated point instead of routing the light signal directly to the intended path or channel. This means that the optical signal must be transformed into an electrical signal each time it reaches a node of the communication network and then routed to its designated node or receiver.

In order to use the full bandwidth of optical technologies available, an all optical approach in such networks is desirable. To realize the all optical network, some of the key optical system components within the system are in need of improvement.

### **1.3. Components of Fiber Optic Communication System**

In the fiber optic communication system there are many different components that are essential, including, light source, optical fiber, multiplexer, demultiplexer, optical amplifier, router/switch, and receiver [14].

#### **1.3.1 Light Source**

In order to send a signal over the fiber optic system, the signal needs to be converted from an electrical signal to an optical signal before launching it into the fiber. To convert the electrical signal to an optical signal, some type of light source is required. The light

sources currently used with fiber optics are semiconductor light source; either a light emitting diode (LED) or a semiconductor laser. Using either LED or laser, the signal is modulated with different modulation schemes, either internally or externally depending on the required bandwidth, and then the signal is transmitted over the channels (transmission media).

Of the two light sources available, laser-based sources are more widely used due to their high power and narrow spectral width, even though they are more costly than the LEDs. Still some systems requiring low to moderate data rates use LED base light sources, since LEDs offer relatively low cost and are less sensitive to temperature [14].

### **1.3.2 Channel**

To deliver a light signal, fiber optic cable is used to guide the optical signal through the systems. In fiber optic systems, there are two general classifications of fiber optic cable, multimode and single mode fiber. Multimode fibers are still used for some applications calling for moderated distances and/or data rates. But, due to the limitations of the multimode transmission, single mode fiber currently dominates the market, even though single mode fibers are more costly, more difficult to fabricate within certain tolerances requirement, and more difficult to couple light into from the source [11].

#### **1.3.2.1 Multimode Fiber**

In the early stages of optical communication systems, the multimode fibers were used. Typically, the multimode has core size of 50  $\mu\text{m}$  and cladding size of 125  $\mu\text{m}$ . This large core size allows many modes of propagation to exist within the fiber, which gives rises to

the modal dispersion, a condition where different propagation modes of the light pulse (signal) travel different paths resulting in temporal spreading of the pulse. This type of modal dispersion limits the data rate of multimode fiber to less than 100 Mb/s.

#### **1.3.2.2 Single-mode Fiber**

To reduce the effect of modal dispersion in fiber, single mode fibers were developed. Typically, single-mode fiber has core size of 9  $\mu\text{m}$  and cladding size of 125  $\mu\text{m}$ . Theoretically, this core size allows only one mode of propagation to exist within the fiber at a given wavelength that minimizes dispersion [29]. However, even the single propagation mode still suffers from chromatic dispersion [24], a condition arising from the spectral spread in the light and the spectral dependence of the refractive index of the material. In chromatic dispersion the different frequency components travel at different phase velocities within the waveguide medium, the fiber core. Nevertheless, single mode fiber allows at much higher data rate, 10 to 40 Gb/s, than the multimode. Further, single mode fiber can be designed not to have net dispersion at a given wavelength (or over a narrow wavelength range). These qualities make single mode fiber the transmission medium of choice for high bandwidth applications.

#### **1.3.3 Amplifier**

Most times in long-haul communications, the signal needs to be amplified between connections. Prior to the advent of optical amplifiers, amplification of an optical signal required that it be converted to an electrical signal, reconditioned and amplified electrically, and converted back to an optical signal to be launched in the network again.

However, since the introduction of the erbium doped fiber amplifier (EDFA), which allows optical amplification of the signal, it has been possible to transmit optical signals over long haul without having to introduce electrical nodes that slow the data rate [9]. Still, for extremely long-haul networks, optical signals need to be reshaped (regenerated), due to distortion caused by the optical amplifiers and fiber, including amplified spontaneous emission (ASE) and dispersion.

#### **1.3.4 Multiplexing of Optical Signals**

To efficiently use the available bandwidth, typically, different channels are multiplexed into a single channel. Electronically, signals are multiplexed in the time or frequency domain, known as TDM (time division multiplexing) for time domain and FDM (frequency division multiplexing) for frequency domain. Also CDM (code division multiplexing) is used in many of today's communication systems. Each of these multiplexing schemes lends themselves best to certain modulation approaches. Optically, signals are multiplexed in the wavelength domain, known as WDM (wavelength division multiplexing), which is complimentary to the other multiplexing schemes. In addition to WDM, all optical multiplexing scheme utilizing TDM and CDM are currently implemented [13].

##### **1.3.4.1 Multiplexing Scheme in Hybrid Communication System**

In hybrid communication networks, where electrical and optical systems are used together, WDM alone cannot satisfy the all the needs of a large network, especially when a single carrier wavelength is used for single channel. Therefore, signals in current

communication network are multiplexed electronically into either TDM or CDM signals and further multiplexed with WDM as the electrical signal are converted into an optical signal.

#### **1.3.4.2 Multiplexing Scheme in All Optical System**

Based on electrical multiplexing schemes, optical signals are also being multiplexed using TDM, CDM, and WDM [10]. In OTDM (optical time division multiplexing), unlike electrical TDM, where signals are divided in time slots, electrical pulses are converted into optical pulses and then optical pulses are compressed using special fiber [10]. In WDM, each wavelength is used as a carrier for a signal. Finally, in OCDM (optical code division multiplexing), a signal is coded and decoded using similar technique as the electrical counter part [11].

#### **1.3.5 Multiplexer and Demultiplexer**

In optical systems, ability to combine (multiplex) and separate (demultiplex) the closely spaced carriers into each wavelength channel is crucial. As the capability of separating closely spaced wavelength channels increases, the capacity for sending more information over the fiber increases. However, there is a limit to bit rate which can be transmitted, as the bit rate increases the channel spacing has to increase, but current technology has not yet reached the maximum channel spacing for available bit rates.

There are many different methods in which the light signals are separated according to wavelengths. The technologies most often used to demultiplex/multiplex optical signals in current optic systems, employing DWDM (dense wavelength division multiplexing) re

methods base on reflective/refractive gratings, array waveguide gratings, and fiber Bragg gratings (FBG) [2].

### **1.3.6 Router/Switch**

Once the optical signals have been delivered to a node of the network and the mixed signals have been demultiplexed, each signal is routed to its designated destination. To route the optic signals, there are several different methods utilized, which depend on the number of channels and channel spacing. For a low number of channels, FBG based routers or simple mirror-based routers are used to direct the signals. Currently, for moderate to high density channels spacing, MEMS (microelectronic mechanical systems) are being implemented.

Routers and switches are the main cause of delay in the optical network, especially when mechanical-based routers are used (e.g. routers using motors to rotate the mirrors).

### **1.3.7 Receiver**

Once the optical signal reaches the destination, it is detected, demodulated, and decoded in electrical form by the receiver. To the convert optical signal to an electrical signal, semiconductor-based photo detectors are used. The electrical signal is amplified and passed along for equalization and discriminated by electrical circuitry [14].

## **1.4 Wavelength add/drop multiplexer (WADM)**

One of the key components in the optical network system is WADM (wavelength add/drop multiplexer), also known as OADM (optical add/drop multiplexer). WADM

allows the signals to be dropped or added at the nodes of the system network, allowing efficient use of the optical fiber network. Without an OADM, it would be necessary to place additional optical cable for each path between the nodes in the optical network.

In next chapter, Chapter 2, more detail about the gratings used in today optical communication technologies will be discuss along with their use in this project.

## **Chapter 2**

### **Different Grating Technologies**

There are three primary types of gratings used to develop multiplexer and demultiplexer systems: Bragg gratings, arrayed waveguide gratings, and diffraction gratings. Each grating type offers unique properties, which can be used to develop diverse multiplexer/demultiplexer characteristics for different requirements within optical systems. The following sections will describe each of these.

#### **2.1 Bragg grating**

For simple or less dense WDM systems, a multiplexer/demultiplexer is constructed using a Fiber Bragg Grating (FBG). The FBG offers both narrow and broad wavelength demultiplexing/multiplexing capabilities. Typical FBG multiplexer/demultiplexer structures consists of a Bragg grating and a 3-dB coupler.

The fiber Bragg grating is a periodic (or near periodic) distribution of alternating regions of higher and lower refractive index. The effect of the alternating refractive index produces a narrowband mirror, which reflects a narrow range of wavelengths around the Bragg wavelength (given in Eq.1) and allows all other wavelengths to pass through. At the interface between the alternating refractive index a portion of the forward going signal is reflected and the rest is passed. At each successive junction, another portion of the forward going signal gets reflected back. At or near the grating's matched



wavelength, known as the Bragg wavelength or Bragg frequency, all of the reflected waves add in phase and as a result the signal is nearly completely reflected [15].

The Bragg wavelength is given in Eq. 1,

$$\lambda_B = 2n_0\Lambda \quad (1)$$

where  $n_0$  is the average refractive index of the propagation modes and  $\Lambda$  is the period of index modulation.

Currently the most common method of producing fiber Bragg gratings is through the use of a silica phase mask and ultraviolet light (UV). First, the proper grating size is etched onto the phase mask and the fiber is exposed to UV light. Due to the UV sensitivity of the fiber core, when the core is exposed to UV light, the index of refraction of the core changes. This change in refractive index creates a periodic structure of varying index of refraction, which acts as the Bragg grating. Another method of fabrication without the use of a phase mask is through the use of two UV sources. In this method, two UV sources are shone across the optical fiber and the fringes produced by the interference of the two sources cause the change in refractive index.

Normally a FBG is able to reflect a narrow range of the wavelengths near or at Bragg wavelength. However, through used of a chirped Bragg grating, where the periodic structure of the altering refractive index changes from low to high with distance through the grating, broad wavelength ranges can be reflected.

Even though the FBG-based demultiplexer is capable of demultiplexing a narrow range of wavelengths, the FBG is only capable of demultiplexing a single wavelength

range at a time. Therefore, in order to demultiplex a multi-channel system, multiple FBG demultiplexers are needed in series. For example, in order to demultiplex a 16 channel signal, a minimum of 8 FBG demultiplexers are required in a cascade configuration, with each FBG having a different Bragg wavelength. Because of this characteristic, FBG-based demultiplexers are typically used for less dense WDM systems.

Since a demultiplexer using FBG is capable of demultiplexing a single wavelength range at a time, there have not been many improvements made to FBG-based demultiplexers recently. Most of the improvements to the FBG technologies have been in development of efficient and cost effective ways of creating accurate periodic structures for FBGs.

## 2.2 AWG (Arrayed Waveguide Grating)

One of the most widely used multiplexer/demultiplexer technologies is the AWG multiplexer/demultiplexer. The AWG consists of input and output waveguides, typically star couplers, with the arrayed waveguide between them, having a constant path-length difference between neighboring

waveguides, see Figure 1.

As the multi-channel signal enters the input section of the AWG, it is distributed evenly throughout the input waveguides, due to the power distribution characteristic of the star



Figure 1: Arrayed Waveguide Grating (AWG)

coupler [12]. As the redistributed light beams enter the arrayed waveguide section of the AWG, each light beam travels a slight different path length, where the difference is given in Eq. 2.

$$\Delta L = \frac{n_s d D \lambda_0}{N_c f(\Delta \lambda)} \quad (2)$$

Here,  $D$  is the lateral separation of the input waveguides,  $d$  is the arrayed waveguide separation,  $f$  is the radius of curvature of the star coupler,  $N_c$  is the group index of the effective core index  $n_c$ ,  $n_s$  is the effective index of slab region,  $\lambda_0$  is the center wavelength of the WDM system, and  $\Delta \lambda$  is the channel spacing of the WDM system. As the light travels through the arrayed waveguide, it experiences a phase shift due to the different path lengths traveled. This relative phase shift between each channel at the exit of arrayed waveguide is given by Eq. 3.

$$\Delta \phi = \frac{\Delta L}{\lambda} \quad (3)$$

As the light exits the arrayed waveguide section of the AWG, each of the light beams constructively interfere into single focal points on the second slab. The location of the focal point for each channel depends on its carrier wavelength. The physical length separation of the wavelengths for the AWG is given by Eq. 4.

$$\frac{\Delta x}{\Delta \lambda} = \frac{N_c f(\Delta L)}{n_s d \lambda_0} \quad (4)$$

In the AWG, the number of array waveguides is increased in order to minimize the loss.

Also, the number of the array waveguides is increased as the number of channel increases.

In an attempt to increase the demultiplexing-abilities of AWGs, Takada et al [4][5], used two AWGs, one as the primary and the other as the secondary in tandem. In an improved version [5], a 1 X 5 multiplexer/demultiplexer with flat-top interference filter and five 1 X 288 AWGs with a 10 GHz channel spacing as second filters were used.

The primary AWG separated the signals into 5 channels in succession according to the wavelength. Then the 5 channels were demultiplexed using the secondary 1 X 288 AWG for each channel.

Even though Takada et al. [5] were able to develop a lower transmission loss demultiplexer/multiplexer, capable of separating signals with channel spacing of 10 GHz, the method of using two-stage AWG had its down falls. In order to demultiplex the 288 channels in the secondary AWGs, a 5-inch wafer was required to make a single secondary AWG due to the large number of arrayed waveguides and long focal length. The secondary AWG needed more than 1000 arrayed waveguides and more than 4 cm of spacing for focal area.

To optimize the performances of the tandem AWG demultiplexer/multiplexer, additional processes were implemented on secondary AWG. The temperature of the secondary AWG's substrate had to be controlled in order to obtain all the channels from the output of the secondary AWG. In addition, UV irradiation was used to sharpen the pass band of AWG to compensate for the phase error. Even with the phase error compensation with UV irradiation, larger side lobes were present on the higher bands, which led to higher phase error.

In further development of cascading AWGs in tandem, Takada et al. were able to increase the number of channels separated using 3-stages [6], without sacrificing much in transmission loss. In the 3-stage configuration, Takada was able to reduce the size of the biggest AWG, but a number of different parameter AWGs had to be fabricated individually.

## 2.3 Diffraction Grating

Another common method used in multiplexer and demultiplexer technology is the use of diffraction gratings. The diffraction grating is simply a reflective or transmitting surface with periodic grooves, see Figure 2. There are two types of diffractive gratings commonly used in today's multiplexer and demultiplexer scheme, ruled and holographic. Even though both types of gratings consist of closely spaced, straight-line grooves in parallel on the substrates, there are differences between the two. The differences between the ruled and holographic grating arise from not only the way each grating is manufactured but also by the physical profile of each groove [23]. The ruled gratings have a saw tooth-shaped groove profiles tilted at a specific angle (the blaze angle) that is designed to have maximum efficiency at a specific (blaze) wavelength. The holographic grating has a sinusoidal groove profile. Because the holographic grating has a sinusoidal pattern groove, holographic gratings cannot be blazed easily and the

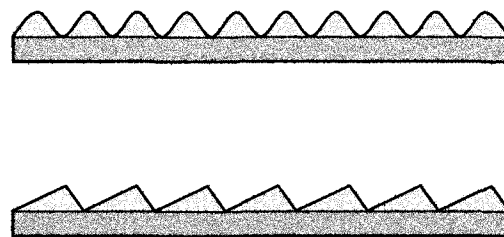


Figure 2: Diffraction grating, holographic grating profile on top and ruled grating on the bottom

efficiency is usually less than a comparable ruled grating. However, when the groove spacing-to-wavelength ratio is nearly one, holographic gratings have virtually the same efficiency as ruled gratings and they can be fabricated with much higher groove densities.

Both ruled and holographic diffraction gratings separate a multi-wavelength source into its component wavelengths by diffraction, a process in which light incident on a surface with dimensions similar in size to its wavelength is dispersed at certain angles. As the multiple wavelengths hit the grating, each wavelength is diffracted into a different angle. It is this difference in diffraction angle that separates light into each spectral component.

In a transmission grating the diffracted light is passed through at an angle equal to the diffraction angle. For reflective gratings, the light is first diffracted as it is reflected by the coating on the surface of the grooves at an angle equal to the diffraction angle.

The relationship between the incident angle, wavelength, and groove density to the diffraction angle is given by grating the equation in Eq. 5.

$$n\lambda = \Lambda(\sin(\theta_i) \pm \sin(\theta_n)) \quad (5)$$

Here,  $n$  is the integer diffraction mode-order for the light,  $\Lambda$  is the spatial period of the groove on the grating,  $\theta_i$  is the incident angle,  $\theta_d$  is the diffracted angle, and  $\lambda$  is the wavelength of the light. This grating equation is the same for both the ruled and the holographic grooves in reflective and transmission gratings. The grating equation can be rewritten in the form given by Eq. 6 to show the relationship between the incident angle and diffracted angle. Equation 6 shows that, the diffracted angle depends on the

wavelength, groove period, and incident angle. As wavelength increases and or the groove period decreases, the diffracted angle increases.

$$\theta_d = \sin^{-1} \left( \frac{n\lambda}{\Lambda} - \sin(\theta_i) \right) \quad (6)$$

Currently, not much attention has been given to the diffraction grating scheme since the diffraction of light is well studied and diffraction by a single grating is limited by the grating Equation. Therefore, there has not been much room to improve the diffraction grating. Most of the efforts associated with diffraction gratings have been in manufacturing process, to increase the consistency of groove profile and groove spacing. Other improvements in diffractive grating technology have been in shaping of gratings to focus light without using lenses or to line up the light to couple into fiber.

## **2.4 Improvement of Diffraction Grating Demultiplexer**

Of the three types of gratings, the diffraction grating was chosen for this thesis to construct a tunable demultiplexer. In the Chapter 3, the theory and calculations supporting the design will be discussed to show the feasibility of the demultiplexer developed through this research. The system presented here, which is capable of demultiplexing wavelength channels that are separated by less than 0.5 nm, was engineered by cascading two diffraction gratings, one normal ruled grating and a chirped grating. In later chapters, Chapter 4 and Chapter 5, the experiment setup and measured data will be presented. Finally, in Chapter 6, the results of the data will be discussed.

## Chapter 3

### Theory and Calculation

#### 3.1 Theory

Most diffraction based multiplexers and demultiplexers schemes use a single grating to separate the WDM signals. Yet, a single grating system with limited space, however it is configured, can only resolve limited wavelength channel spacing. In order to increase the demultiplexing capability of a single grating system, the physical space between the grating and the output fiber has to be increased, since angular separation between the wavelengths is limited by the diffraction equation (see Eqs. 5 and 6).

As can be seen from Eq. 6, for a single grating system, only two factors can be controlled to increase the separation between the wavelengths, incident angle and groove density. However, the values of incident angle and groove density are limited by the Eq. 7, given below that expresses the range of angles over which diffraction is possible. If Eq. 7 is not satisfied, the values of the all the diffraction angles becomes imaginary, which signifies that only the mirror reflection or total internal reflection/refraction exist.

$$\frac{n\lambda}{\Lambda} - \sin(\theta_i) \leq 1 \quad (7)$$

In addition, the groove density of the grating is limited by the wavelength since as the grating's groove period gets smaller than the wavelength, the grating does not diffracts



the light, but reflects it as mirror would. Therefore, once this limitation is reached, the separation can only be increased by increasing the distance between the output fiber and grating. Doing so is not ideal since prevailing demand is for smaller, more reliable, and cost effective systems.

To increase the separation between the wavelengths for a given device size using the grating system, multiple gratings in series are used. By having a series of gratings, the incident angle and/or the groove density for each of the individual wavelength channel changes at the second grating, giving rise to an increase in separation, as shown in Figure 3. As Figure 3 shows, the wavelengths are initially separated by the first grating, then the separated wavelengths travel different paths to the second grating, where the shorter wavelengths travel to a second grating with smaller diffracted angles than the longer wavelengths. This wavelength-dependent change in incident angle for the second grating gives rise to larger diffraction angle changes in the second grating, and hence, larger angular separation of the wavelengths. The drawback to using such a configuration is the loss that is encountered by using two gratings in series. This issue will be addressed in later chapters. For now, we proceed with the derivation of the resolution performance for dual grating demultiplexers.

### 3.1.1 Chirped Grating

In order to increase the effectiveness of the dual grating system, the chirped grating

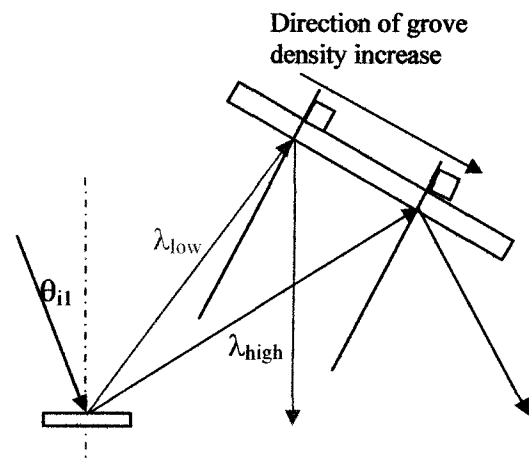


Figure 3: Diffraction behavior of wavelength

is introduced in this research. The idea of the chirped grating, a grating fabricated such that groove density varies from one position to another position within the same grating, arose from grating equation. This equation shows that diffraction angle is greatly influenced by the groove density of the grating, and thus, by changing the groove density as a function of the wavelength one can control the diffraction angle. By controlling the diffraction angle, the channels can be routed to a desired location. In order to accomplish this routing, a dual grating system must be implemented. By placing the chirped grating at the position of first (master) grating would not make much sense, since at the first grating, all channel would interact within the same area, since each channels travels as a single beam. However, once the multi-channel beam diffracts from the first grating, each wavelength is spatially separated. Therefore, by introducing a chirped grating at the second (slave) grating position, where each wavelength interact with a different location on the second grating, it would be possible to diffract each channel with a different groove density. Thus by changing the location of incidence for each channel on the chirped grating, either by rotation of the master grating or translation of the slave grating, one can route a particular channel to desired location. Further, the additional diffraction of the channels form the second grating can effectively introduce additional separation of the channel, which will be shown in the calculation in this chapter.

### **3.2 Calculations**

Using the grating equation (see Eqs. 5 and 6), two different setup calculations were made to predict the position of each WDM channel as travels through the series of diffraction grating.

### 3.2.1 Initial testing setup calculation

To test the theory before the chirped grating could be fabricated, a dual-grating setup, as shown in Figure 4, was setup and tested. For the initial setup, the following calculations were done to predict the position of the each wavelength.

The experiment was setup such that for given angle at the second grating, the diffracted angle would be in the increasing x-axis direction.

Recall that Eq. 6 is, given as:

$$\theta_{d1} = \sin^{-1} \left( \frac{\lambda_i}{\Lambda_1} - \sin(\theta_{i1}) \right) \quad (6)$$

where  $\lambda_i$  is the wavelengths,  $\theta_{i1}$  is the incident angle on first grating, and  $\Lambda_1$  is the groove density of the first grating. Using this diffracted angle as the incident angle for a second grating, the second diffracted angle  $\theta_{i2}$  is given by Eq. 8:

$$\theta_{d21} = \sin^{-1} \left( \frac{\lambda_i}{\Lambda_2} - \sin(\theta_{d1} - \theta_g) \right) \quad (8)$$

Here  $\theta_{i2}$  (labeled as angle b in Figure 4) is the incident angle of the light on the second grating, and  $\Lambda_2$  is the groove density of the second grating.

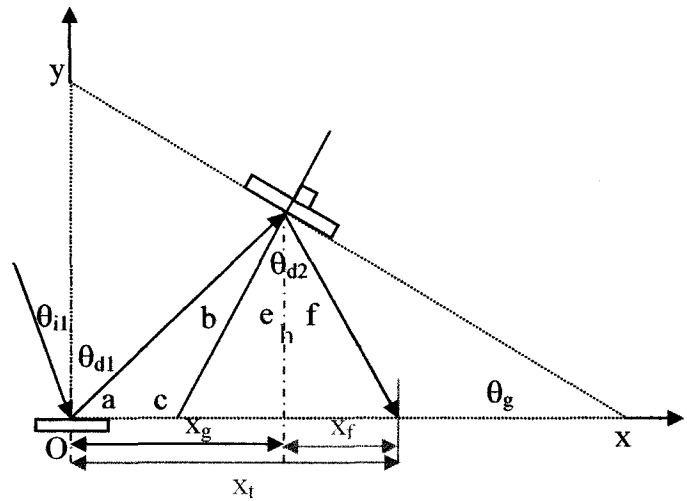


Figure 4: Geometry of initial dual grating setup

Given the angle of second grating ( $\theta_{d2}$ ) and the height of the grating  $h_{y0}$ , which is the vertical distance between the x-axis and the position of the reference wavelength  $\lambda_0$  at second grating, the line equation of the second grating position is written as:

$$y = (-m_g \cdot x) + h_{y0} - (x_{x0} \cdot m_g) \quad (9)$$

Then the line equation of the light path between the first grating and second grating can be written as:

$$y = m_a \cdot x \quad (10)$$

Here  $m_g$  is slope of second grating path equation,  $m_a$  is the slope of the light path between the first and second gratings,  $h_{y0}$  is the y position of the reference wavelength at the second grating,  $\lambda_0$  is the reference wavelength, and  $x_{x0}$  is the x position of reference wavelength.

Combining the two equations above results in:

$$y = \frac{m_g \cdot x_{g0} + h_{y0}}{1 + \frac{m_g}{m_a}} \quad (11)$$

where the slopes can be written as:

$$m_a = \tan(\theta_a) \quad (12)$$

$$m_g = \tan(\theta_g) \quad (13)$$

Then by using trigonometric relations, the x position of second grating is given as

$$x_g = \frac{\tan(\theta_g) \cdot x_{g0} + h_{y0}}{1 + \frac{\tan(\theta_g)}{\tan(\theta_a)}} \cdot \tan(\theta_{d1}) \quad (14)$$

and the horizontal distance between each wavelength from the grating to the final position on the x-axis where the output fiber is positioned is given as:

$$x_f = y \cdot \tan(\theta_{d2} - \theta_g) \quad (15)$$

Thus, the final x position of the each wavelength is the sum of the  $x_g$  and  $x_f$ , which is written as:

$$x_t = y \cdot (\tan(\theta_{d1}) + \tan(\theta_{d2} - \theta_g)) \quad (16)$$

Substituting for y gives the final equation:

$$x_t = \left[ \frac{\tan(\theta_g) \cdot x_{g0} + h_{y0}}{1 + \frac{\tan(\theta_g)}{\tan(\theta_a)}} \right] [\tan(\theta_{d1}) + \tan(\theta_{d2} - \theta_g)] \quad (17)$$

This final position  $x_f$  gives location of each wavelength relative to the position of initial light incident area of the first grating, which is defined as the origin.

### 3.2.2 Final Setup Calculation

The final dual-grating setup is set as shown in Figure 5. Unlike the initial measurement, the output fiber was placed in the y-axis. For the final setup, the following calculations were done to predict the output position of each wavelength.

The experiment was setup such that for a given angle at the second grating, the diffracted angle would be in the increasing y-axis direction, see Figure 5.

Since the diffracted angle of second grating is in the increasing y-direction, the diffracted angle of second grating is different from the initial setup, where diffracted angle of second grating is now written as:

$$\theta_{d23} = \sin^{-1}\left(\frac{\lambda_t}{\Lambda_2} - \sin(\theta_g - \theta_{d1})\right) \quad (18)$$

Using the same method as the initial calculations with the line equation of the wavelength path and grating path position, and combining the two equations gives:

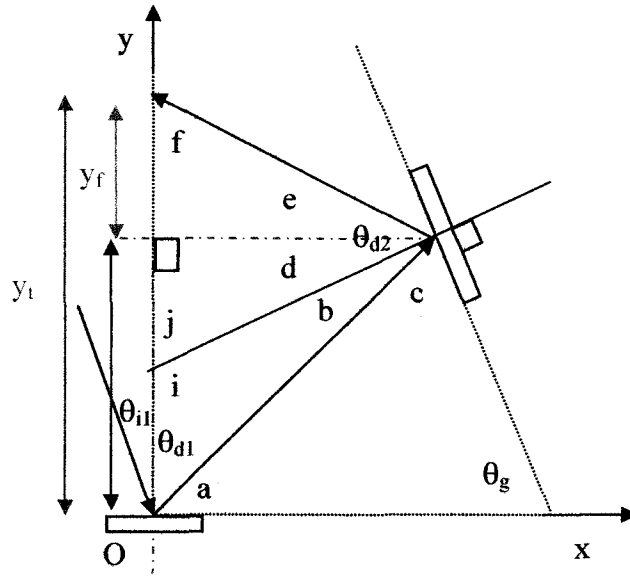


Figure 5: Geometry of final dual grating setup

$$x = \frac{m_g \cdot h_{x0} + y_{g0}}{m_g + m_a} \quad (19)$$

Again using trigonometric relations the y-position of second grating is given as;

$$y_g = x \frac{\sin(b+d)}{\sin(\theta_{d1})} \quad (20)$$

or

$$y_g = x \frac{\cos(\theta_{d1})}{\sin(\theta_{d1})} = x \cdot \cot(\theta_{d1}) \quad (21)$$

The vertical distance between the each wavelength from the grating to the final position on the y-axis, where the output fiber is positioned is given as:

$$y_f = x \frac{\sin(e)}{\sin(f)} \quad (22)$$

or

$$y_f = x \cdot \cot(\theta_{d2} + \theta_g) \quad (23)$$

Thus, the final y-axis position of each wavelength is the sum of  $y_g$  and  $y_f$ , which is written as

$$y_t = x \cdot (\cot(\theta_{d1}) + \cot(\theta_{d1} + \theta_g)) \quad (24)$$

Substituting x into the about equation gives:

$$y_t = \left[ \frac{\tan(\theta_g) \cdot h_{x0} + y_{g0}}{\tan(\theta_g) + \tan(\theta_a)} \right] [\cot(\theta_{d1}) + \cot(\theta_{d2} + \theta_g)] \quad (25)$$

From the equations 17 and 25 both gives calculated position of the each channel for each configuration. As it can be seen by the equations, the relationship between the channel's wavelength and position is not linear, which is undesirable. However, by controlling the grating density variation of second grating (chirped), the position of each channel could be come more linear.

In next chapter, Chapter 4, where all the data will be presented that show the non-linearity of dual grating system.



## Chapter 4

### Experiment Procedures, Setups and Measurement

To test the theory of the dual grating system, multiple experiments were set up using two gratings in series. The following sections detail the various setups, experimental procedures, and results.

#### 4.1 Testing of the Theory

To test the efficacy of the multiplexer/demultiplexer scheme, various measurements were made with different components in one of two basic measurement configurations.

For the first measurement configuration, a single grating system, consisting of

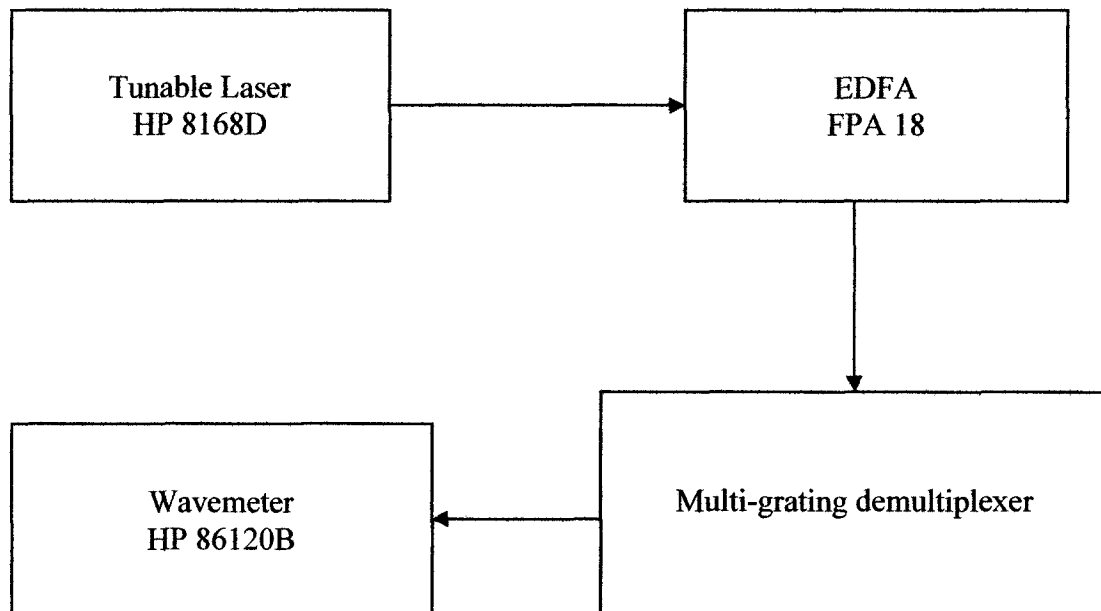


Figure 6: Schematic of the measurement setup

collimating optics and a uniform ruled grating (600 grooves/mm), was set up and tested as a reference. Then a second configuration using a dual grating system was set up and tested. In this second configuration, the original ruled grating was used along with one of the following gratings to increase the physical separation between the wavelengths:

1. Uniform 600 grooves/mm
2. Chirped grating

Groove spacing varied from 300 grooves/mm to 600 grooves/mm for the chirped grating (using segmented grating, which is described in a later section of this chapter)

#### 4.1.1 Layout of the Measurement Setup

A schematic of the experimental setup is shown in Figure 6, and the physical dimensions of this

setup are shown in

Figure 7. For the

laser source, a

tunable laser HP

8168D was used.

Since the maximum

output power from

the tunable laser

was 350  $\mu$ W (-4.6

dBm), an EDFA,

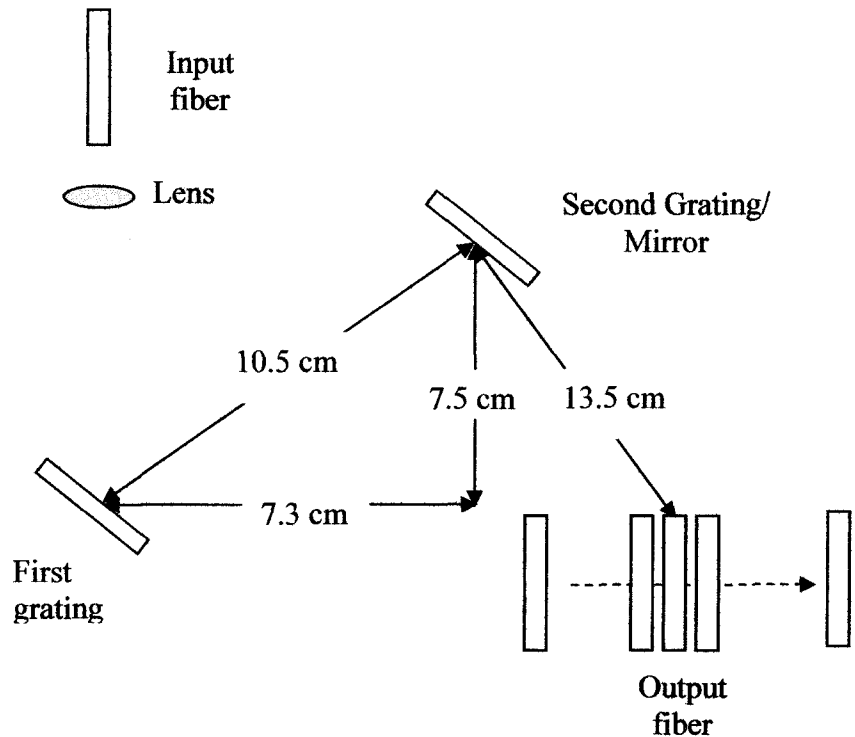


Figure 7: Dimensions of the setup

Newport FPA18, was used to amplify the tunable laser to 18 dBm. However, this caused the unwanted effect of spectral spreading of the laser due to ASE (amplified spontaneous emission), which could not be compensated for with the available equipment and shows up in the experimental results as broadened channel width. The experimental setup is shown in Figure 8. The amplified light was focused through the lens and transmitted through the multi-grating system. After the incoming signal was separated by the demultiplexing systems, the diffracted wavelengths were collected into single-mode fiber, designated in Figure 8 as the Output fiber. The output power was measured with a wavemeter, HP 86120B

#### 4.1.2 Reference Setup

First, to compare the results between the single and dual grating configurations, measurements using a single grating were performed (see Figure 9a). In this

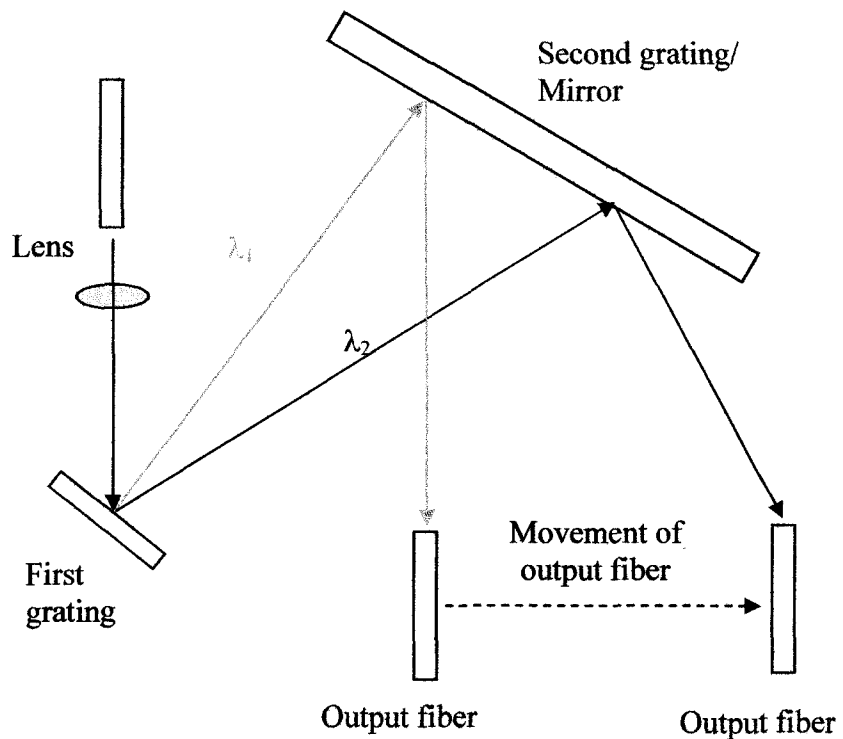


Figure 8: Measurement

setup, the input signal containing multiple wavelengths was diffracted via a gold-coated ruled grating with 600 grooves/mm (Edmund Optics). Since the separation of the channels increased as the distance between the grating and collection fiber increased, from the angular spreading of light from the first grating, the distance between the initial grating and output fiber needed to be held constant for all the setups. Therefore, in order to minimize the affect of the variation of the distance between the first grating and the output fiber, a mirror was placed between the first grating and the output fiber. This insured that all setups, both single and dual grating, had the same overall physical length.

#### **4.1.2.1 Actual Dimensions for First Setup**

In the setup, the components were placed such that they would minimize the distance between the each other. The dimension of the setup is as follows (also shown in Figure 7). The horizontal distance between the first grating and the second grating was 7.3 cm, which is labeled  $x_g$  in Figure 4. The vertical distance between the first grating and the second grating was 7.5 cm, which is labeled  $h$  in Figure 4. The distance between center of the first grating and center of the second grating was 10.5 cm. The distance between center of the second grating and the position of the output fiber where the middle wavelength's peak power was measure was 13.5 cm.

The system was constructed this way for following reasons. First, it was desirable to reduce the total size of the demultiplexer scheme. Second, in order to transmit the light over the total path length of the demultiplexer the light needed to be collimated. However, collimating the light required a second lens to be placed at the output fiber to refocus the light into the fiber. The placement of an additional lens (ball lens) in front of the output

fiber was difficult, though, and ultimately ineffective due to the lack of a stable lens holder that would fit within the allotted space and allow adjustment of the ball lens position to focus the light into the output fiber. Therefore, an additional lens in front of the output fiber was not used. Further, the minimization of the demultiplexer size in turn caused a constraint in the working area, which allowed only one lens to be used in front of the input fiber of the system to focus the light into output fiber after it had been transmitted through the demultiplexer scheme.

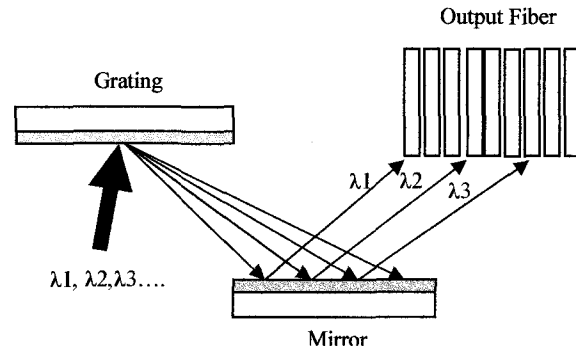


Figure 9a: Reference measurement setup.

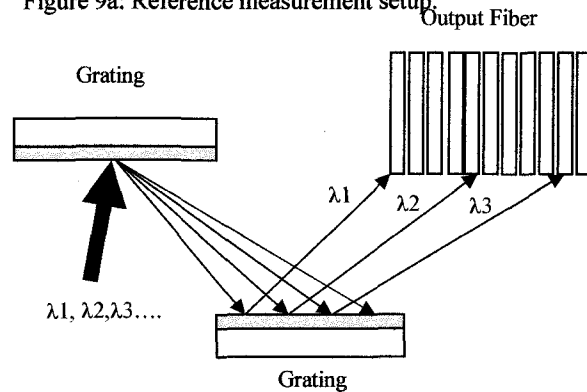


Figure 9b: Dual standard ruled grating (DS configuration), both grating with 600 grooves/mm

#### 4.1.2.2 Measurement Technique in First Setup

Using a tunable laser in series with an EDFA, a single wavelength, starting at the lowest laser wavelength (1545 nm), was transmitted through the multi-grating system. The actual power was measured using the

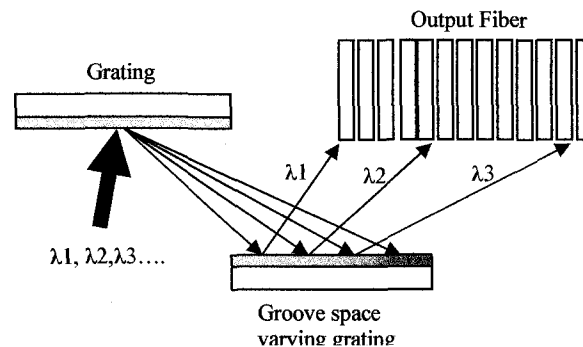


Figure 9c: Standard/chirped ruled grating (SC configuration), initial grating with 600 grooves/mm and groove-spacing varying grating for second grating

wavemeter by sweeping the output fiber in small intervals (0.05 mm) horizontally. Then, the power at each position was recorded with the HP wavemeter. Once the full beam width of the wavelength was measured, the individual channel wavelength was increased by 1 nm and this procedure was repeated until the wavelength reached 1555 nm.

#### 4.1.2.3 Reference Setup Results (Single Grating)

The following sections present the results of the experiments. The data for each of the setups are shown in Figures 10, 11, 12, and 13.

In the single 600 grooves/mm grating measurement, the spatial separation between each wavelength channel was small. The average spatial separation between each channel's peak power position was  $\Delta x / \Delta \lambda \approx$

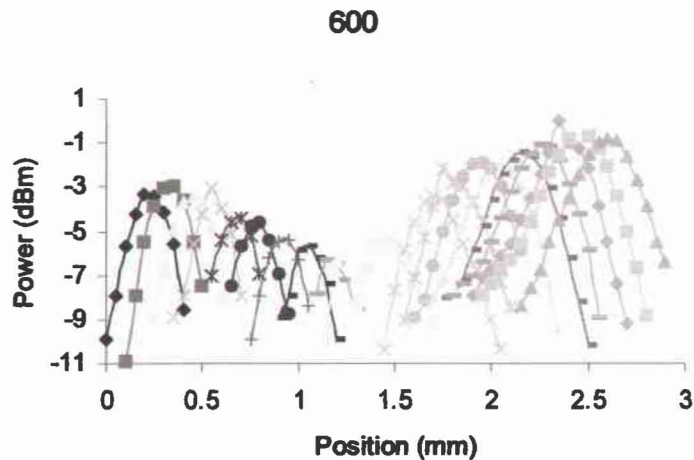


Figure 10: Actual measurement for each wavelength for single 600 grooves/mm. (Reference measurement)

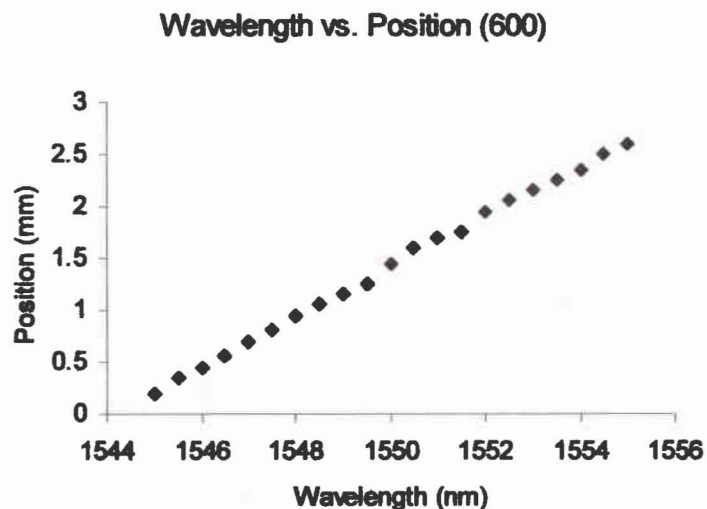


Figure 11: Peak power position of each wavelength for single 600 grooves/mm. (Reference measurement)

0.24 mm/nm. The optical channels ranged in wavelength from 1545 nm (at the initial position on x-axis) to 1555 nm in increments of 0.5 nm, see Figure 10.

The actual power measurement for each channel with the single 600 grooves/mm grating is shown in Figure 11. In the measurements, the power fluctuated between neighboring channels. On average, the peak power of each channel fluctuated  $\Delta P/\Delta\lambda \approx 0.67$  dBm/nm from the neighboring channels. The power difference between the highest power channel and the lowest power channel was 2.8 dBm. This power fluctuation in the measurements, which occurred in all the measurements, was partially due to the ineffective coupling into the output single-mode fiber, due to the small numerical aperture. More on this will be discussed in Chapter 5.

#### **4.1.3 Dual Grating Setup**

For the first dual grating measurement, the mirror was replaced with a second gold-coated ruled grating with 600-grooves/mm (see Figure 9b). An increase in the separation of the channels was expected in this case due to the change of incident angle of light on the second grating as well as from the additional diffraction resulting from the grating itself.

For the second dual grating measurement, the mirror was replaced with a segmented chirped grating with groove spacing varying from 300 to 600 grooves/mm, see Figure 9c. In this setup, a continuous chirped grating was not available, so the chirped grating was constructed by placing different groove spaced gratings next to each other. This in turn created a defect area at the joining of gratings. Because of this defect, measuring small wavelength spacing was not possible; however, a demonstration of the concept was

achievable.

The measurements were taken by moving a single fiber laterally from one end of the output to other. The measurement started from the position closest to the second grating, where the shortest wavelength was measured, and continued to the farthest output position, where the longest wavelength was measured. Measurements for all setups were conducted in same manner

to minimize the measurement variation. Also, the position of shortest wavelength was kept constant to avoid additional separation due to differences in path length.

For all measurements, the power transmitted to first grating was set at 5 dBm and the first-order diffraction mode was chosen to separate the signals.

Physical wavelength position, starting from the

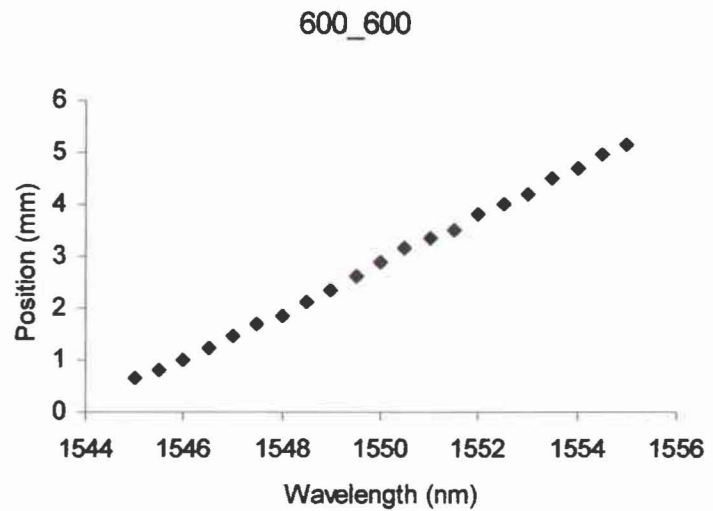


Figure 12: Peak power position of each wavelength for dual grating. Two 600 grooves/mm grating in series

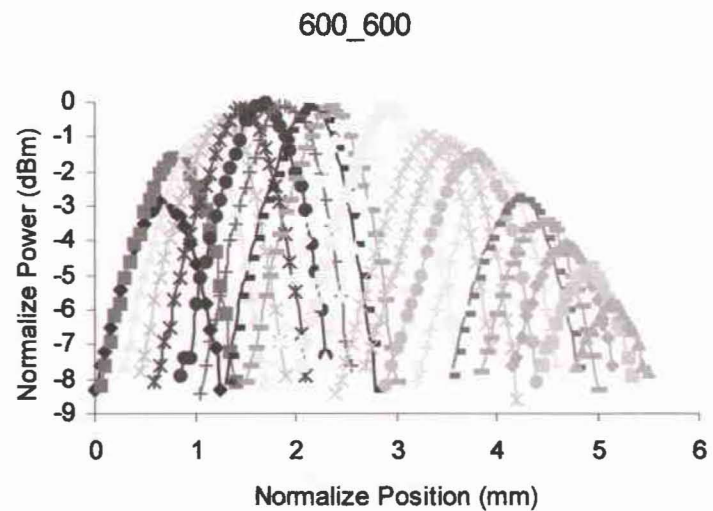


Figure 13: Actual measurement for each wavelength for dual grating. Two 600 grooves/mm in series.



shortest wavelength and continuing to the longest wavelength, is shown in Figures 9a, 9b, and 9c for both the dual standard-ruled grating (DS) and standard/chirped-ruled grating (SC) configurations, respectively. The position of shortest wavelength measured using the single grating and mirror configuration was set as a reference point for all other measurements. The channel wavelength separations were kept at  $\Delta\lambda = 0.5$  nm for the single grating and dual grating setups due to the minimum resolution of the wavemeter used in the experiment. For the segmented chirped grating configuration, the maximum channel separation was 1545 nm at the low end and 1555 nm at the high end. This large wavelength separation was selected in order to avoid the defects that occurred at the edges of the gratings, as well as to control groove density encountered by each of the wavelengths.

#### **4.1.3.1 Results for the Two 600 grooves/mm Gratings in Series**

The normalized position of the peak powers for each channel from the two gratings in series with 600 grooves/mm is shown in Figure 12. The average spatial separation between each channel's peak power position was  $\Delta x/\Delta\lambda \approx 0.44$  mm/nm.

The actual power measurements from the two grating in series are shown in Figure 13. On average, the peak power of each channel fluctuated  $\Delta P/\Delta\lambda \approx 0.67$  dBm/nm from the neighboring channels. The power difference between the highest power channel and the lowest power channel was 2.8 dBm.

## **4.2 First Experiment with Continuous Chirped Grating (Lateral Measurement Setup)**

After testing the dual grating system, two chirped gratings were fabricated, one grating with groove density varying from 300 grooves/mm to 600 grooves/mm and a second grating with groove density varying from 100 grooves/mm to 600 grooves/mm. Both gratings' groove density increased continuously over a 5 mm length. However, since the initial separation from the first grating (600 grooves/mm) did not separate the channels

wide enough to cover the full length of the chirped grating, each chirped grating was divided into three sections. The chirped grating with groove density varying from 300

grooves/mm was divided into sections consisting of

groove density varying from 300 grooves/mm to 400 grooves/mm, 400 grooves/mm to 500 grooves/mm, and 500 grooves/mm to 600 grooves/mm. The chirped

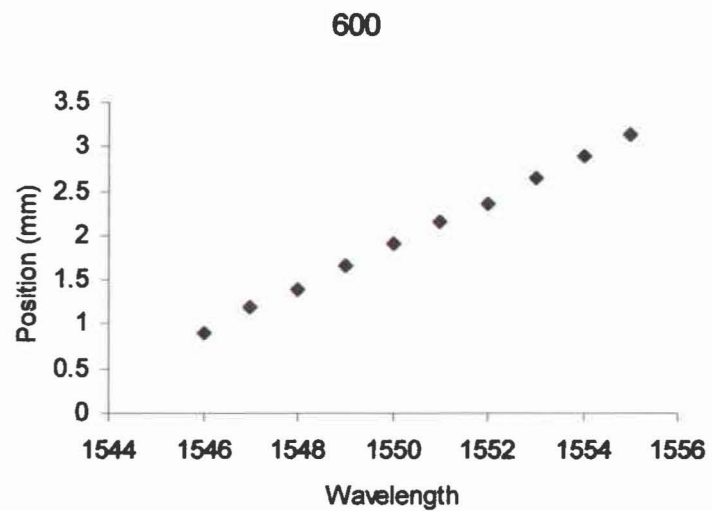


Figure 14: Peak power position of each wavelength for single 600 grooves/mm. For the testing setup measurement (Reference measurement)

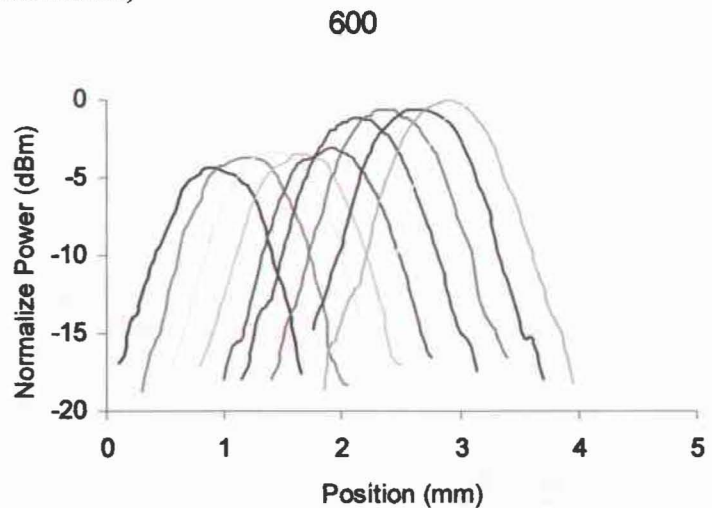


Figure 15: Actual measurement for each wavelength for single 600 grooves/mm. For the testing setup measurement (Reference measurement)

grating with groove density varying from 100 grooves/mm to 600 grooves/mm was divided into sections consisting of groove density varying from 100 grooves/mm to 275 grooves/mm, 275 grooves/mm to 450 grooves/mm, and 450 grooves/mm to 600 grooves/mm.

With these new chirped gratings, the previous experimental procedures were repeated. All the measurement including the single grating (reference measurement) and two 600 grooves/mm gratings in series were repeated to insure that any in advertent changes to the variables within the setup were accounted for in all tests. For example, in this second testing series, the position between the gratings were reduced to increase the power delivered to the collection fiber. However, this resulted in limited range in the incident angle for the first grating due to the geometry of the setup and the physical size of the grating.

#### 4.2.1 Reference Setup Results (Single Grating)

The normalized position of each channel for the single 600 grooves/mm grating is shown in Figure 14. The average spatial separation between each channel's peak power position was  $\Delta x/\Delta\lambda \approx$

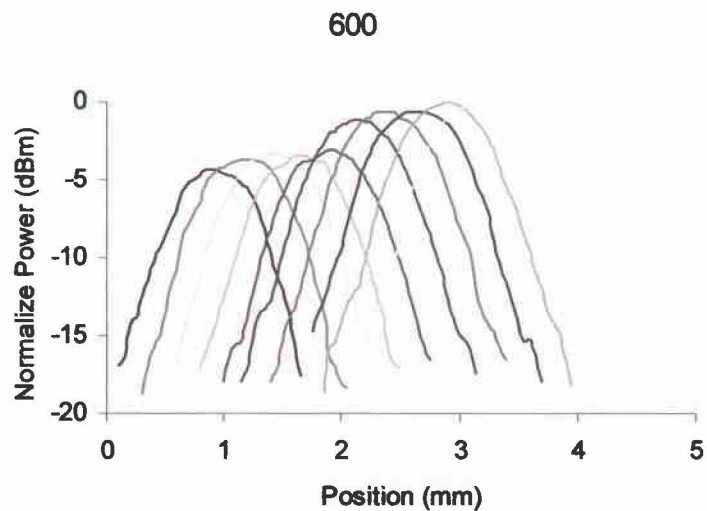


Figure 15: Actual measurement for each wavelength for single 600 grooves/mm. For the testing setup measurement (Reference measurement)

0.25mm/nm from the neighboring channels. The results of this reference measurement differed from the previous measurement due to slight difference in distance between the input and output (or collection) fiber.

The actual power measurements from the single 600 grooves/mm as the reference measurement for this setup is shown in Figure 15. On average, the peak power of each channel fluctuated  $\Delta P/\Delta\lambda \approx$

0.55 dBm/nm from the neighboring channels. The power difference between the highest power channel and the lowest power channel was 4.4 dBm.

#### 4.2.2 Results for the Two 600 grooves/mm Gratings in Series

The normalized position of each channel for the two 600 grooves/mm grating in series is shown in Figure 16. The average spatial separation between each

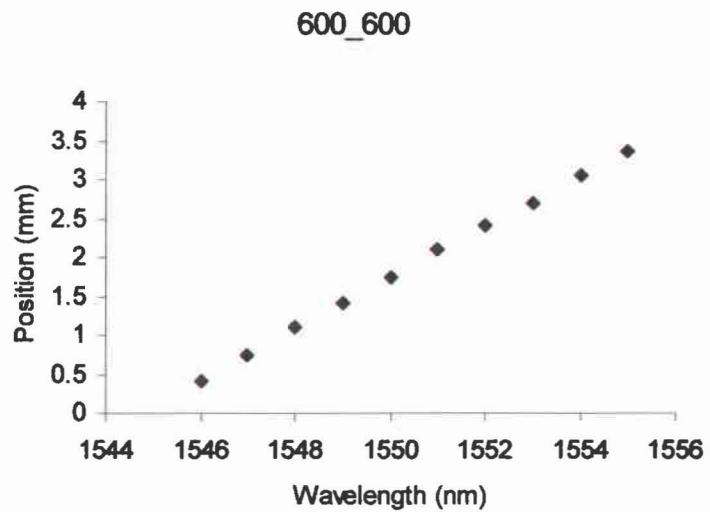


Figure 16: Peak power position of each wavelength for dual grating. Two 600 grooves/mm grating in series for the testing setup measurement.

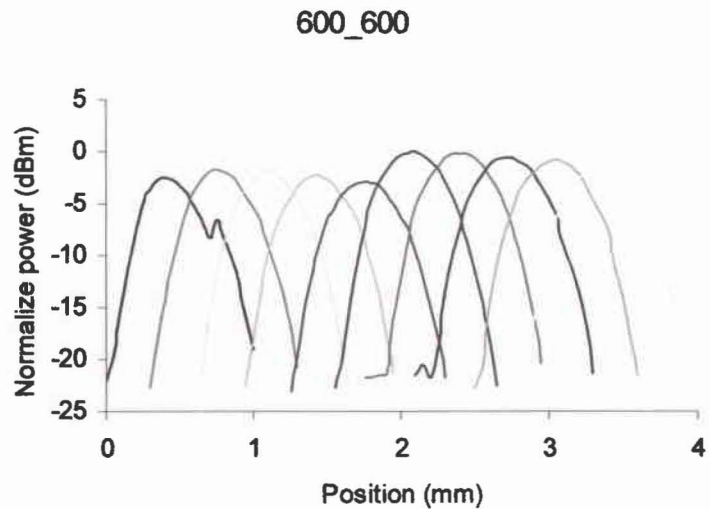


Figure 17: Actual power measurement for each wavelength for the two 600 grooves/mm in series. For the testing setup measurement.

channel's peak power position was  $\Delta x/\Delta\lambda \approx 0.33$  mm/nm.

The actual power measurements from the two 600 grooves/mm gratings in series are shown in Figure 17. On average, the peak power of each channel fluctuated  $\Delta P/\Delta\lambda \approx 0.67$  dBm/nm from the neighboring channels.

The power difference between the highest power channel and the lowest power channel was 2.8 dBm.

#### 4.2.3 Results for the 600 grooves/mm Grating and the 1st Chirped Grating in Series

The measurements from the 600 grooves/mm grating in series with the 1st chirped grating, having a grooves density that

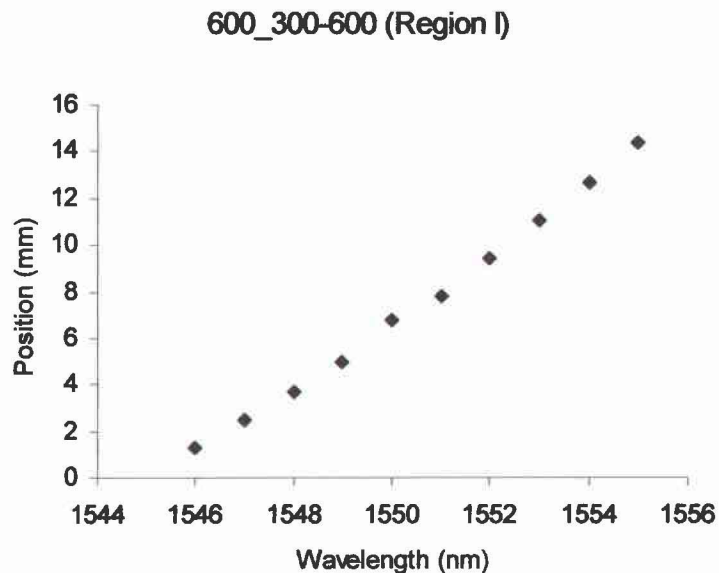


Figure 18: Peak power position of each wavelength for dual grating. 600 grooves/mm and 1<sup>st</sup> chirp grating in series for the testing setup measurement. (at region I area of chirped grating)

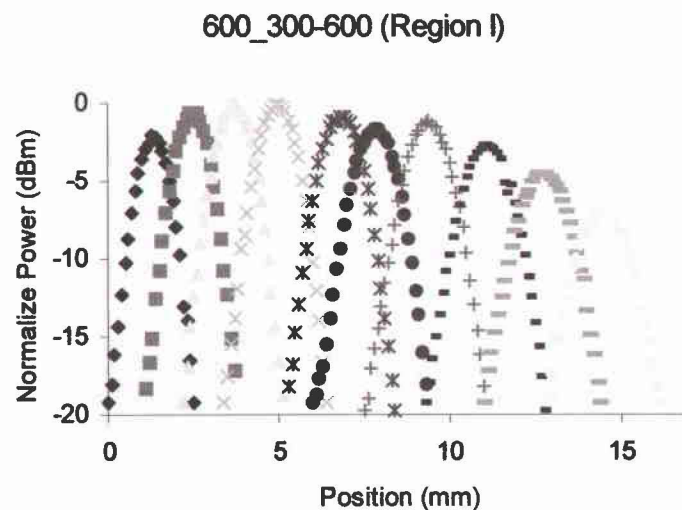


Figure 19: Actual power measurement for each wavelength for the 600 grooves/mm and 1<sup>st</sup> chirped grating in series for the testing setup measurement. (at region I area of chirped grating).



varying from 300 grooves/mm to 600 grooves/mm, are shown in Figures 18, 19, 20, 21, 22 and 23. Due to the small separation of the channels from the first grating (600 grooves/mm), the chirped grating was divided into three sections, region I (RI: 300 grooves/mm to 400 grooves/mm), region II (RII: 400 grooves/mm to 500 grooves/mm), and region III (RIII:

500 grooves/mm to 600 grooves/mm), each with different groove densities. The division of the groove density on the grating was an approximation base on the fact that

each grating's density varied constantly from one end to other. This was done for all of the following chirped grating measurements for same reason.

#### 4.2.3.1 Results at

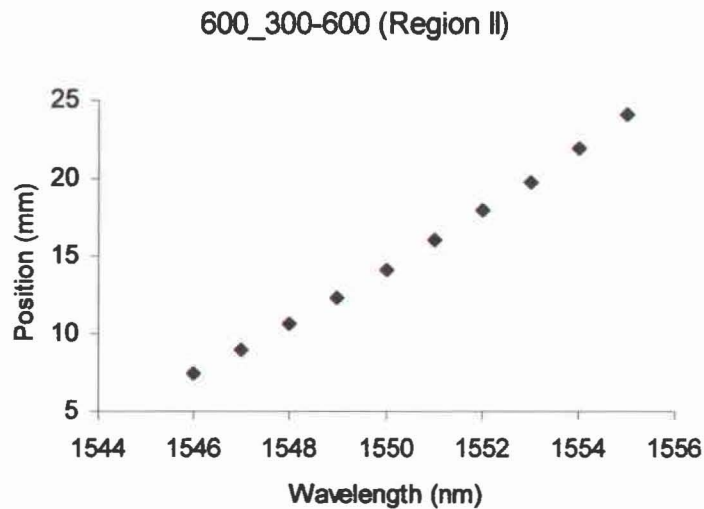


Figure 20: Peak power position of each wavelength for dual grating. 600 grooves/mm and 1<sup>st</sup> chirped grating in series for the testing setup measurement. (at region II of chirped grating)

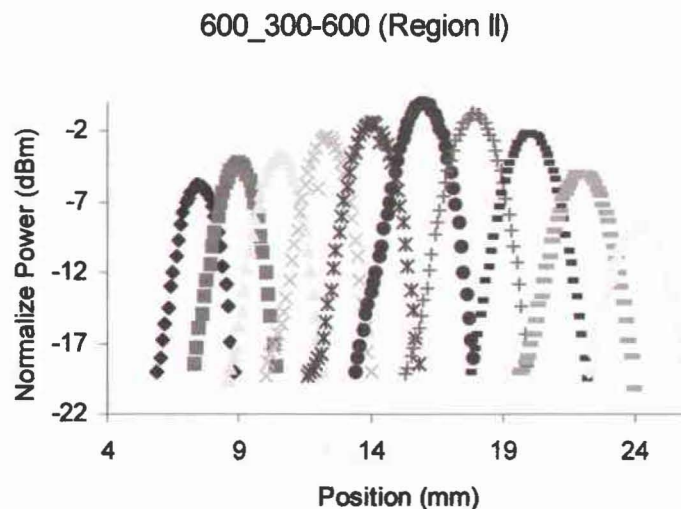


Figure 21: Actual power measurement for each wavelength for the 600 grooves/mm and 1<sup>st</sup> chirped grating in series for the testing setup measurement. (at region II of chirped grating).

### Region I of the 1st Chirped Grating

The normalized position of each channel for the 600 grooves/mm grating in series with region I of the 1st chirped grating is shown in Figure 18. The average spatial separation between each channel's peak power position was  $\Delta x/\Delta\lambda \approx 1.46$  mm/nm.

The actual power measurements from the 600 grooves/mm grating and region II of 1st chirped grating in series are shown in Figure 19. On average, the peak power of each channel fluctuated  $\Delta P/\Delta\lambda \approx 1.13$  dBm/nm from the neighboring channels. The power difference between the highest power channel and the lowest power channel was 7.1 dBm.

#### 4.2.3.2 Results at the

600\_300-600 (Region III)

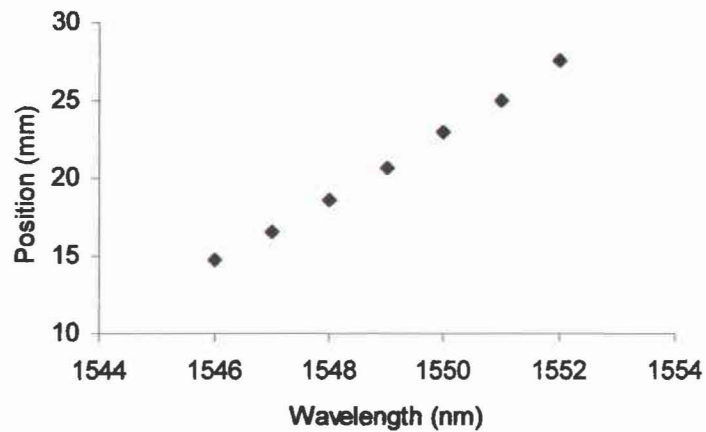


Figure 22: Peak power position of each wavelength for dual grating. 600 grooves/mm and 1<sup>st</sup> chirped grating in series for the testing setup measurement. (at region III of chirped grating)

600\_300-600 (Region III)

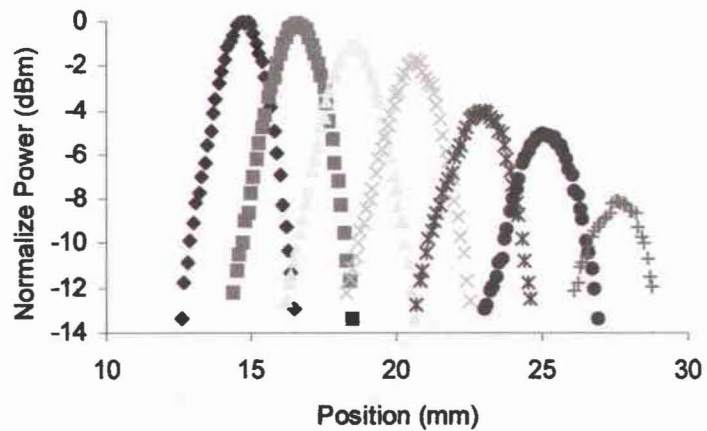


Figure 23: Actual power measurement for each wavelength for the 600 grooves/mm and 1<sup>st</sup> chirped grating in series for the testing setup measurement. (at region III of chirped grating).

## Region II of 1st Chirped Grating

The normalized position of each wavelength for the 600 grooves/mm grating in series with region II of the 1st chirped grating are shown in Figure 20. The average spatial separation between each channel's peak power position was  $\Delta x/\Delta\lambda \approx 1.86$  mm/nm.

The actual power measurements from the 600 grooves/mm grating and region II of the 1st chirped grating is shown in Figure 21. On average, the peak power of each channel fluctuated  $\Delta P/\Delta\lambda \approx 1.6$  dBm/nm from the neighboring channels. The power difference between the highest power channel and the lowest power channel was 8.6 dBm.

### 4.2.3.3 Results at

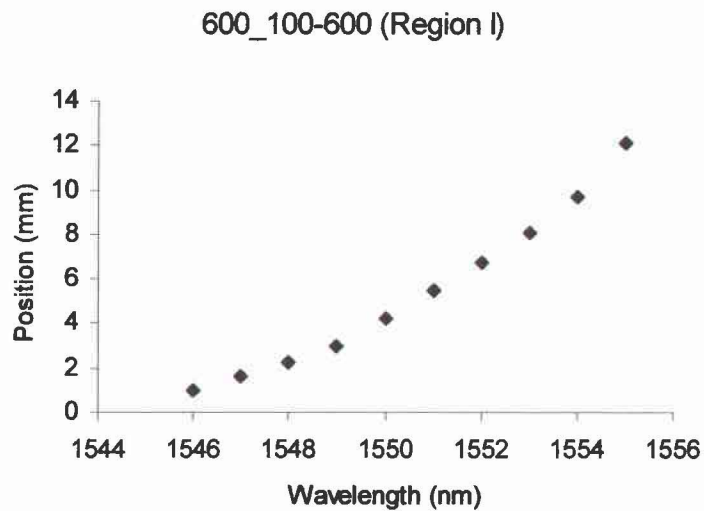


Figure 24: Peak power position of each wavelength for dual grating. 600 grooves/mm and 2<sup>nd</sup> chirped grating in series for the testing setup measurement. (at region I of chirped grating)

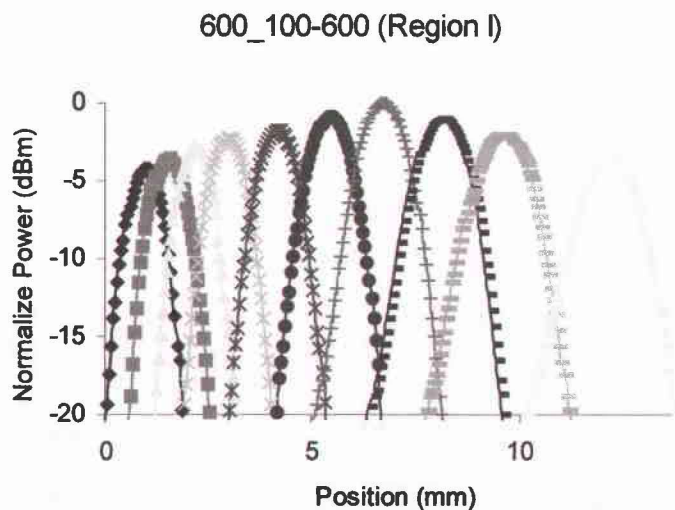


Figure 25: Actual power measurement for each wavelength for the 600 grooves/mm and 2<sup>nd</sup> chirped grating in series for the testing setup measurement. (at region I of chirped grating).



### **Region III of the 1st Chirped Grating**

The normalized position of each channel for the 600 grooves/mm grating series with region III of the 1st chirped grating is shown in Figure 22. The average spatial separation between each channel's peak power position was  $\Delta x/\Delta \lambda \approx 2.15$  mm/nm.

The actual power measurements from the 600 grooves/mm grating and region III of the 1st chirped grating are shown in Figure 23. On average, the peak power of each channel fluctuated  $\Delta P/\Delta \lambda \approx 1.35$  dBm/nm from the neighboring channels. Due to the large power fluctuations, some of the channels could not be measured. The power difference between the highest power channel and the lowest power channel in 1546 nm to 1552 nm ranges was 8.1 dBm.

### **4.2.4 Results for the 600 grooves/mm Grating and the 2nd Chirped Grating in Series**

The measurements from 600 grooves/mm grating series with the 2nd chirped grating having groove density varying from 100 grooves/mm to 600 grooves/mm is shown in Figures 24, 25, 26, 27, 28, and 29.

#### **4.2.4.1 Results at Region I of the 2nd Chirped Grating**

The normalized position of each channel for the 600 grooves/mm grating in series with region I of the 2nd chirped grating is shown in Figure 24. The average spatial separation between each channel's peak power position was  $\Delta x/\Delta \lambda \approx 1.24$  mm/nm.

The actual power measurements from the 600 grooves/mm grating and region I of the 2nd chirped grating are shown in Figure 25. On average, the peak power of each channel fluctuated  $\Delta P/\Delta \lambda \approx 0.86$  dBm/nm from the neighboring channels. The power difference

between the highest power channel and the lowest power channel in 1546 nm to 1554 nm range was 4.2 dBm.

#### 4.2.4.2 Results at Region II of the 2nd Chirped Grating

The normalized position of each channel for the 600 grooves/mm grating series with region II of the second chirped grating is shown in Figure 26. The average spatial separation between each channel's peak power position was  $\Delta x/\Delta\lambda \approx 1.81$  mm/nm.

The actual power measurements from the 600 grooves/mm grating and the region II of 2nd chirped grating are shown in Figure 27. On average, the peak power

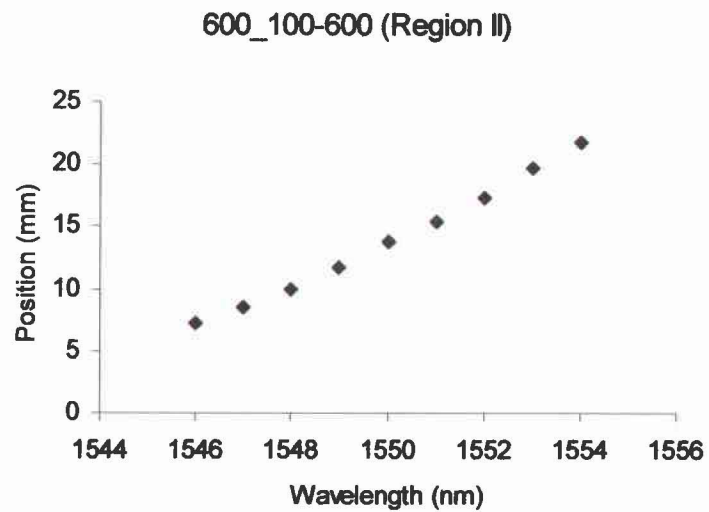


Figure 26: Peak power position of each wavelength for dual grating. 600 grooves/mm and 2<sup>nd</sup> chirped grating in series for the testing setup measurement. (at region II of chirped grating)

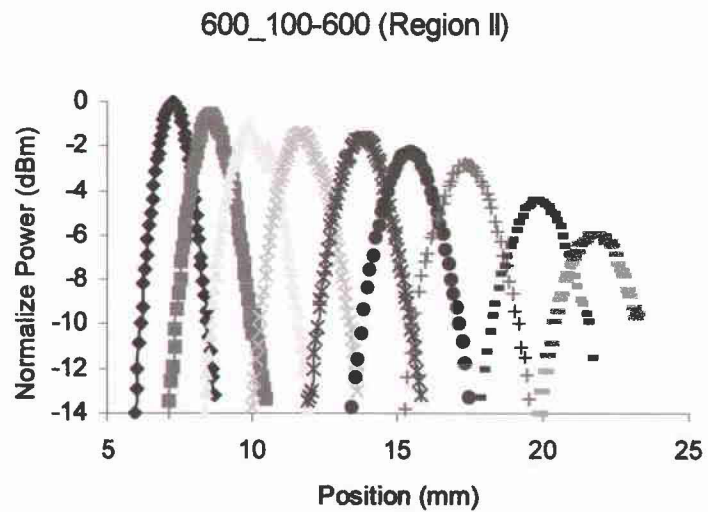


Figure 27: Actual power measurement for each wavelength for the 600 grooves/mm and 2<sup>nd</sup> chirped grating in series for the testing setup measurement. (at region II of chirped grating).

of each channel fluctuated  $\Delta P/\Delta \lambda \approx 0.74 \text{ dBm/nm}$  from the neighboring channels. As was the in region III measurements of the 1st chirped grating, the full range of the channels could not be measured because the power dropped too low to be measured by the wavemeter for some of them. The power difference between the highest power channel and the lowest

measured power in the 1546 nm to 1554 nm range was 5.9 dBm.

#### 4.2.4.3 Results at Region III of the 2nd Chirped Grating

The normalized position of each channel for the 600 grooves/mm grating series with the region III of the second chirped grating is shown in Figure 28.

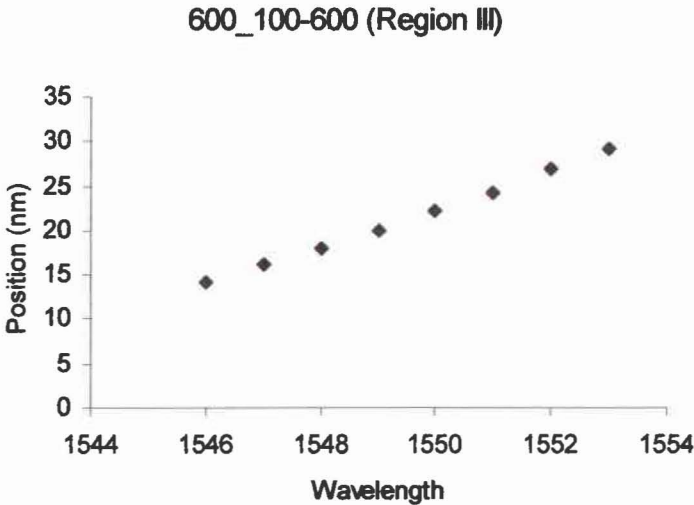


Figure 28: Peak power position of each wavelength for dual grating. 600 grooves/mm and 2<sup>nd</sup> chirped grating in series for the testing setup measurement. (at region III of chirped grating)

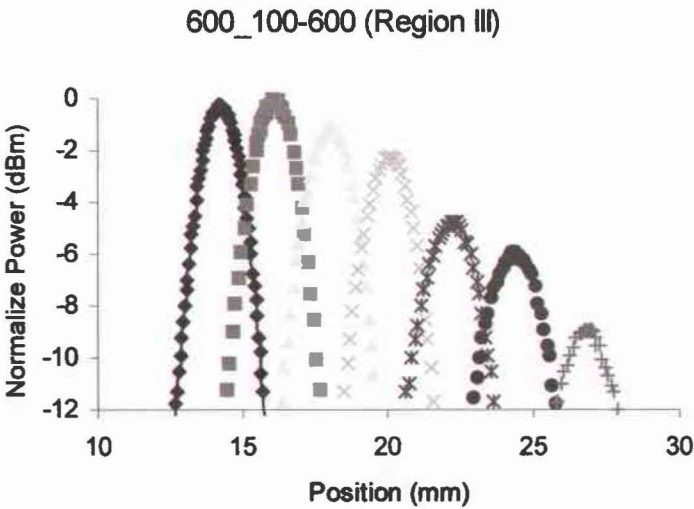


Figure 29: Actual power measurement for each wavelength for the 600 grooves/mm and 2<sup>nd</sup> chirped grating in series for the testing setup measurement. (at region III of chirped grating).

The average spatial separation between each channel's peak power position was  $\Delta x/\Delta\lambda \approx 2.15 \text{ mm/nm}$ .

The actual power measurements from the 600 grooves/mm grating and the region III of 2nd chirped grating are shown in Figure 29. On average, the peak power of each channel fluctuated  $\Delta P/\Delta\lambda \approx 1.76 \text{ dBm/nm}$  from the neighboring channels. As in the previous measurements, the full range of channels could not be measured. The power difference between the highest power channel and the lowest measured power channel in 1546 nm to 1553 nm ranges was 12.1 dBm. This large power fluctuation arises from the incident angle of the light entering the output fiber that is caused by the large spectral separation. More will be discussed in a later chapter.

#### 4.3 Final Setup with Continuous Chirped Grating (Circular Measurement Setup)

To reduce the variation of the power collected by the output fiber caused by the increase in entrance angle as this output fiber was moved laterally, the set up for the output fiber was changed as shown in Figure 30. As was done for all the previous measurements, the

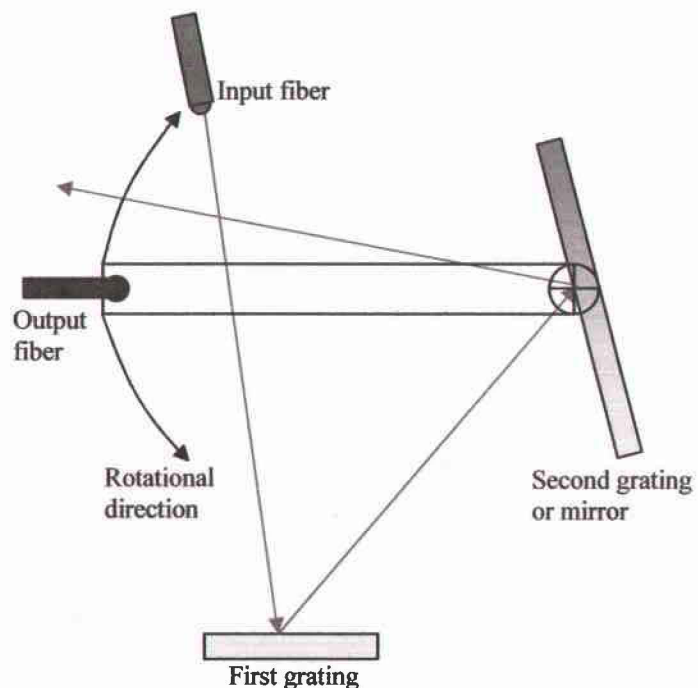


Figure 30: Final measurement setup

single grating system was set up and tested to be used as a reference measurement. Then the second configuration using the dual grating system was setup and measured as well. In the second setup, the following gratings were used as the second grating to increase the physical separation between the wavelengths:

1. Uniform 600 grooves/mm
2. Chirped grating

Groove density varied from 300 grooves/mm to 600 grooves/mm for the first chirped grating and from 100 grooves/mm to 600 grooves/mm for the second, which was divided into three

sections as it was in previous configuration.

#### 4.3.1 Reference Setup (Single Grating)

First, measurements using a single grating were repeated, as was done in all of the

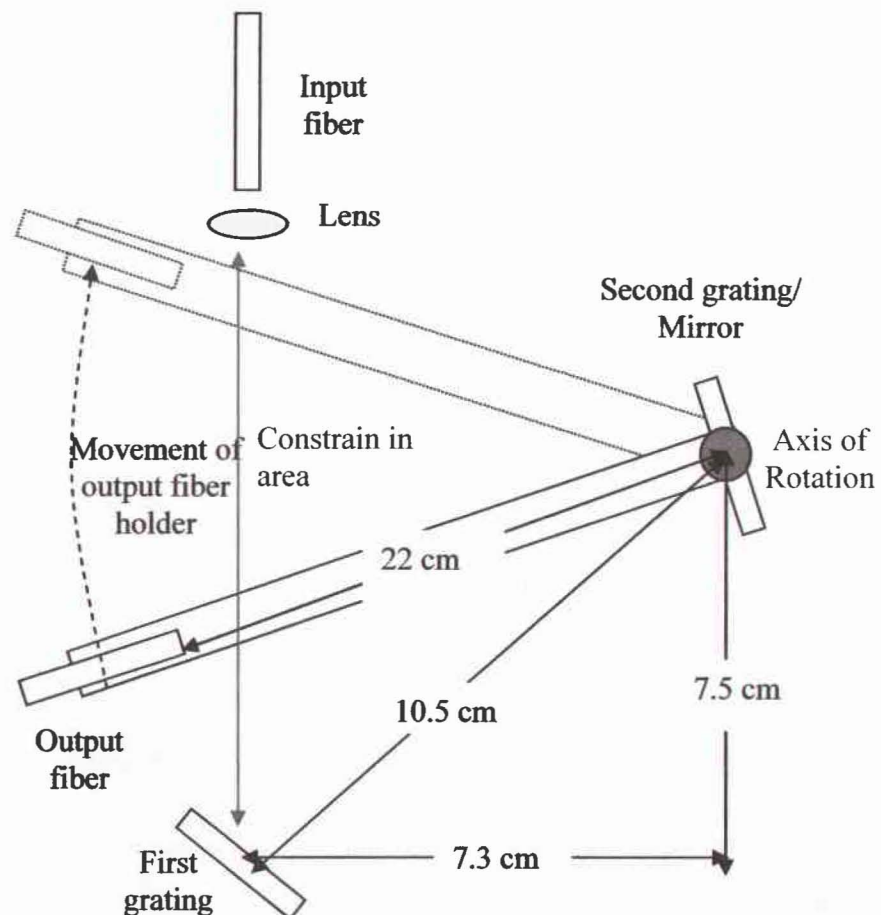


Figure 31: The dimensions for final setup

previous measurements, for consistency.

In the final setup, reference measurements in steps of 1 nm could not be done accurately due to the small angular changes between the wavelengths. Thus measurements were taken at the two end wavelengths, 1545 nm and 1555 nm, and the result was  $\Delta\theta \approx 0.8$  degrees separated the wavelengths.

Due to lack of fine control over the angular movement of the output fiber, actual power measurement of each could not be measured accurately, therefore the actual power measurement done in this testing stage was not conducted. Only the peak powers and the positions of the peak power were measured.

#### 4.3.1.1 Actual Setup

##### Dimensions for Final Setup

For the same reason given in the previous setup, only one lens in front of the input fiber was used to focus the light into output fiber. As many of the dimensions as

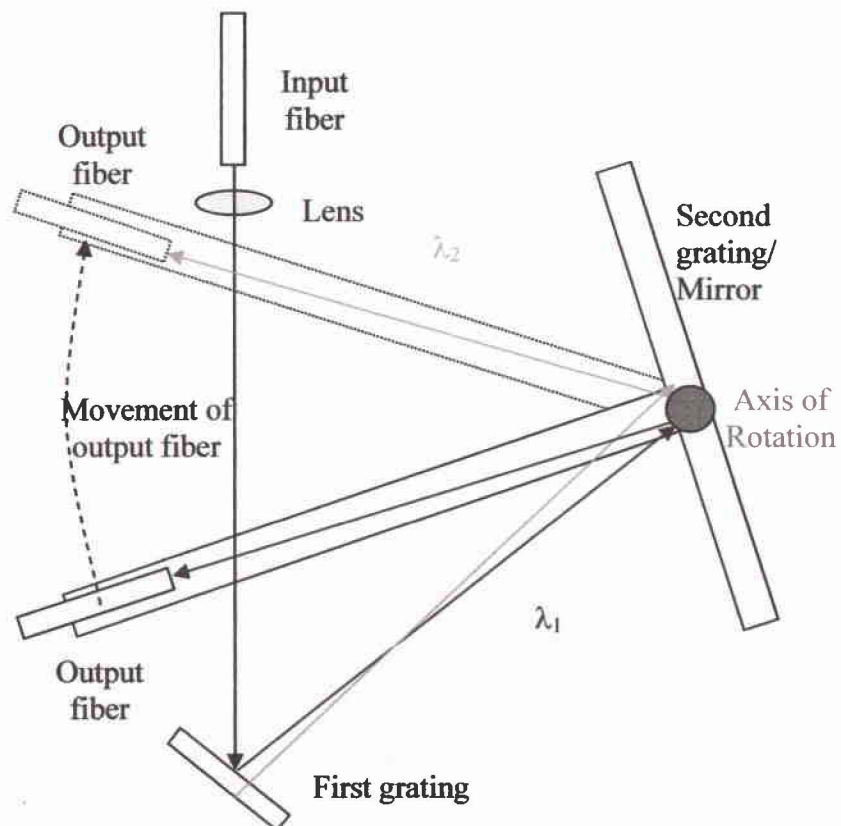


Figure 32: Final setup measurement technique



possible in this final setup were kept the same as before. The difference between the previous setup and this final setup was that the output fiber was placed on the rotation stage and the distance between center of the second grating and the output fiber was increased from 13.5 cm to 22 cm from the axis of rotation. The increase in the distance between the center of the second grating and output fiber in the final setup was due to the additional space introduced by the rotational stage. Also, there was a change in the position of the output fiber holder (now in y-axis position instead of x-axis as it was in previous setup), which did not allow the bulky output fiber holder to be placed closer to the output fiber due to area constraints induced by the first grating and the input fiber holders, shown in Figure 31. However, because angular measurements were determined for both systems, dimensional differences could be removed from the experimental results. This left only the coupling efficiencies as the primary difference.

#### **4.3.1.2 Measurement Technique Final Setup**

Again in the final setup, using a tunable laser in series with EDFA, a single wavelength channel, starting with the lowest wavelength (1545 nm), was transmitted through the multi-grating system. However, in the final setup, precise control over the rotation stage, where the output fiber was placed, was not achievable since the available equipment only allowed unidirectional movement of the rotator (the rotator was only able to be pushed by the micro-meter in one direction). For this reason only the position of the peak power was measured using the wavemeter, unlike the previous measurement, where the whole beam profiles were collected. The peak power for the given wavelength was detected by moving the output fiber in one direction. Since the movement of the rotator

on which the output fiber was placed moved in circular path the position for each wavelength's peak power was recorded in degrees. The wavelength was increased by 1 nm and the rotator was rotated from the position where the previous wavelength was measured to determine the shift in the position. This procedure was repeated until the wavelength reached 1555 nm.

#### **4.3.2 Dual Grating Setup**

For the first dual grating measurement, the mirror was replaced with a second gold-coated 600-grooves/mm ruled grating. Then for the second dual grating measurement, the mirror was replaced with a first chirped ruled grating (groove spacing varying from 300 to 600 grooves/mm). Finally, the mirror was again replaced with a second chirped ruled grating (groove spacing varying from 100 to 600 grooves/mm).

The measurements were taken by rotating on a single fiber from Position I, located at the shortest wavelength to Position II, located at the longest wavelength. All measurements were conducted in same manner to minimize the measurement variation and the first-order diffraction mode was chosen to separate the signals.

Physical wavelength position, starting from the shortest to longest wavelength, is shown in Figures 33 and 35 for both the dual standard grating setup and the standard-chirped grating configurations, respectively. The position of shortest wavelength measured using the single grating with mirror configuration was set as a reference point for all other measurements. In this measurements, the channel wavelength separations were kept at  $\Delta\lambda = 1$  nm, which is larger than the previous measurement ( $\Delta\lambda = 0.5$  nm) for the single grating and dual grating setups due to the limitations with the fine control



of the rotator used to translated the collection fiber. For the chirped grating configuration, the channel separation was 1545 nm at the low end and 1555 nm at the high end. This large wavelength separation was selected in order to avoid the defects that occur at the edges of the gratings, as well as to control groove density encountered by each of the wavelengths.

#### 4.3.2.1 Results for

the Two 600

grooves/mm

Gratings in Series

The normalized

position of each

channel for the

series of two 600

grooves/mm is

shown in Figure 33.

The average angular

separation between

each channel's peak

power position was

$\Delta\theta/\Delta\lambda \approx 0.12 \text{ deg/nm}$ .

The result of the

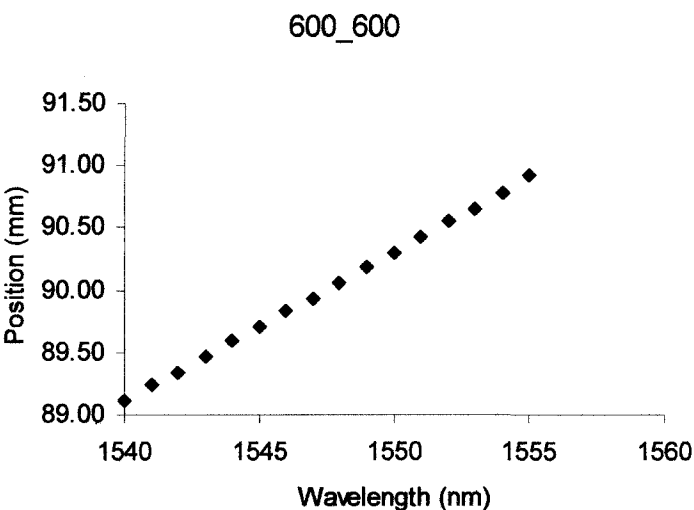


Figure 33: Peak power positions of each wavelength for the two 600 grooves/mm grating in series for the final setup measurement.

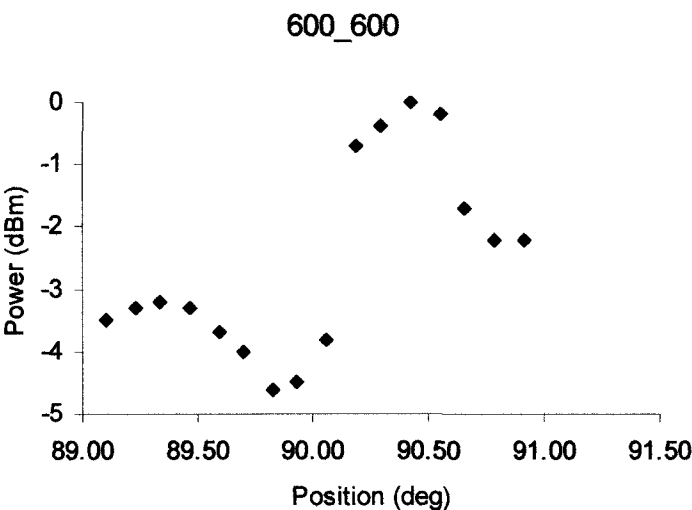


Figure 34: Peak power measurement for each wavelength for the two 600 grooves/mm grating in series for the final setup measurement.

two 600 grooves/mm grating in series is shown in Figure 34. As before, the power fluctuated for each wavelength; however, the fluctuations between the each wavelength were not as severe compared to the previous measurements. On average, the peak power of each channel fluctuated  $\Delta P/\Delta \lambda \approx 0.57$  dBm/nm from the neighboring channels. The power difference

between the highest power channel and the lowest power channel was 4.6 dBm.

#### 4.3.3 Results for the 600 grooves/mm Grating and the 1<sup>st</sup> Chirped Grating in Series

The measurements from 600 grooves/mm grating series with first chirped grating, having groove density varying from 300 grooves/mm to 600 grooves/mm, are shown in

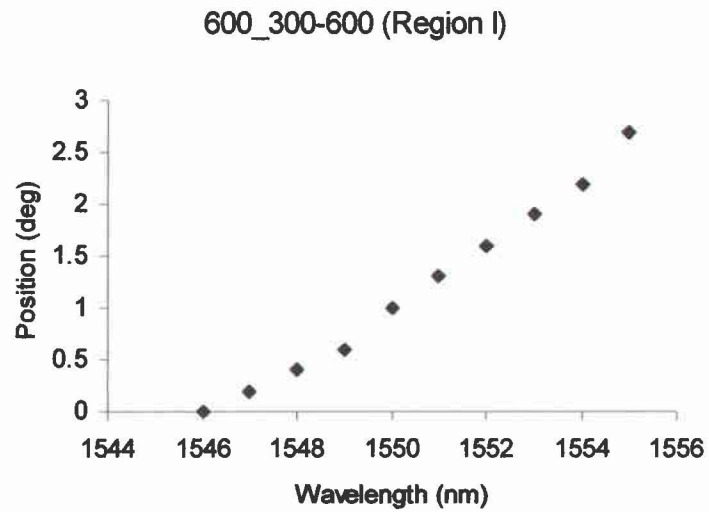


Figure 35: Peak power position of each wavelength for dual grating. 600 grooves/mm and 1<sup>st</sup> chirped grating in series for the testing setup measurement. (at region I of chirped grating)

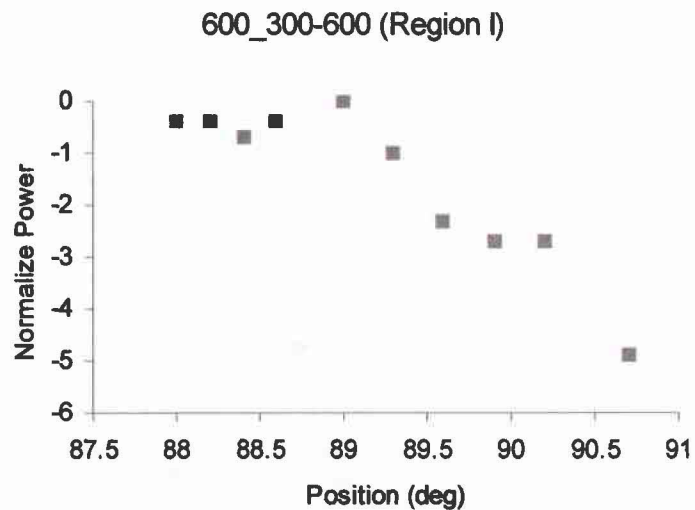


Figure 36: Actual peak power measurement for each wavelength for the 600 grooves/mm and 1<sup>st</sup> chirped grating in series for the testing setup measurement. (at region I of chirped grating).

Figures 35, 36, 37 38, 39, and 40.

#### 4.3.3.1 Results at Region I of the 1st Chirped Grating

The normalized position of each channel for the 600 grooves/mm grating in series with region I of the first chirped grating is shown in Figure 35. The average spatial angular separation between each channel's peak power position was  $\Delta\theta/\Delta\lambda \approx 0.3$  deg/nm.

The actual power measurements from the 600 grooves/mm grating and region I of the 1st chirped grating are shown in Figure 36. On average, the peak power of each channel fluctuated  $\Delta P/\Delta\lambda \approx 0.66$  dBm/nm from the

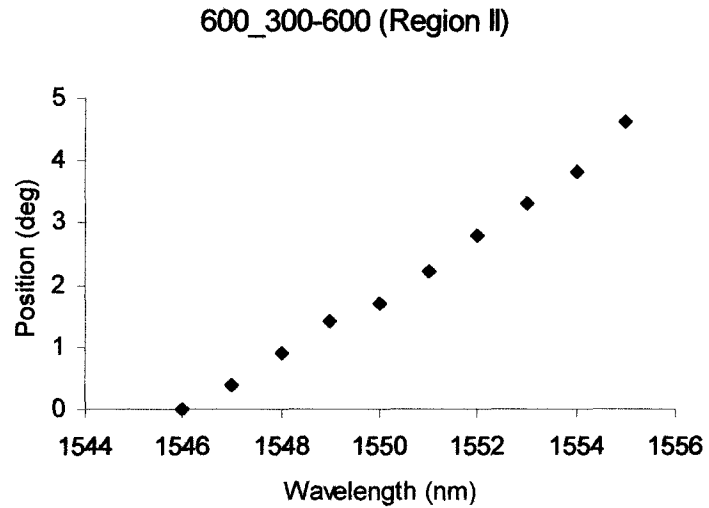


Figure 37: Peak power position of each wavelength for dual grating. 600 grooves/mm and 1<sup>st</sup> chirped grating in series for the testing setup measurement. (at region II of chirped grating)

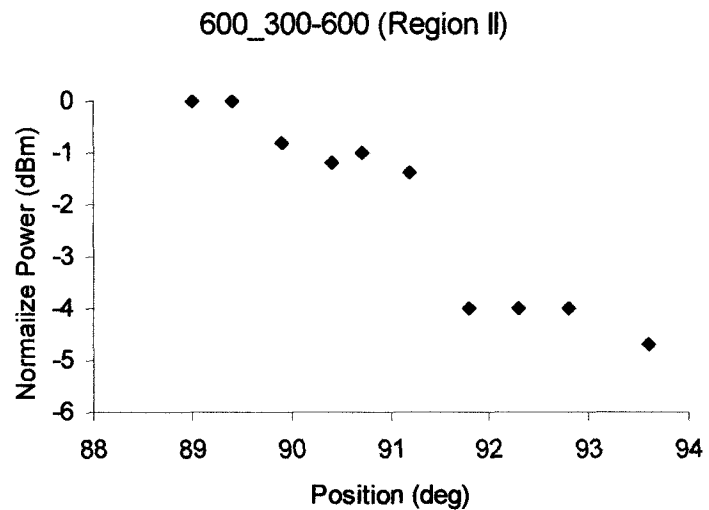


Figure 38: Actual peak power measurement for each wavelength for the 600 grooves/mm and 1<sup>st</sup> chirped grating in series for the testing setup measurement. (at region II of chirped grating).

neighboring channels. The power difference between the highest power channel and the lowest power channel was 4.9 dBm.

#### 4.3.3.2 Results at Region II of the 1st Chirped Grating

The normalized position of each channel for the 600 grooves/mm grating in series with region II of the first chirped grating is shown in Figure 37. The average angular separation between each channel's peak power position was  $\Delta\theta/\Delta\lambda \approx 0.51$  deg/nm.

The actual power measurements of the 600 grooves/mm grating and region II of the 1st chirped grating

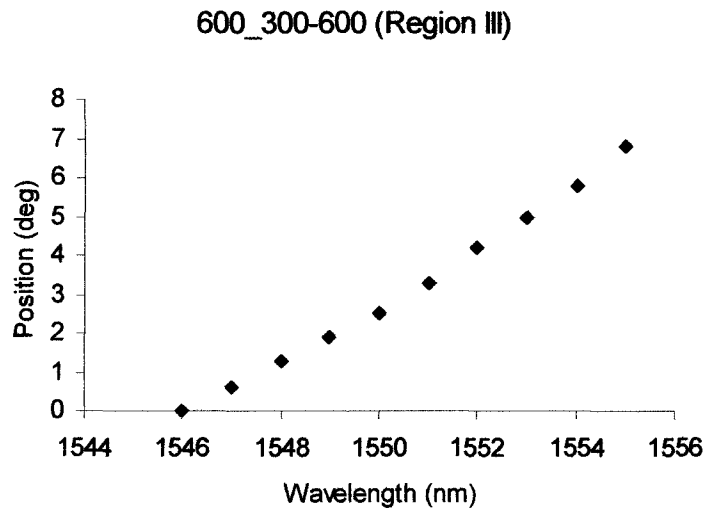


Figure 39: Peak power position of each wavelength for dual grating. 600 grooves/mm and 1<sup>st</sup> chirped grating in series for the testing setup measurement. (at region III area of chirped grating)

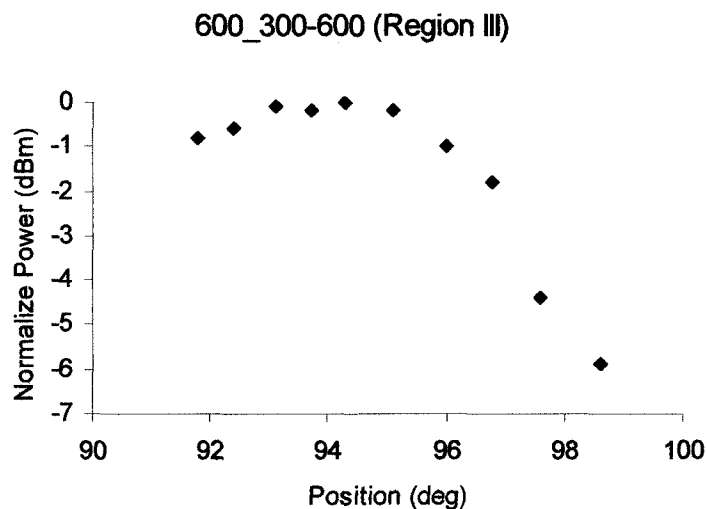


Figure 40: Actual peak power measurement for each wavelength for the 600 grooves/mm and 1<sup>st</sup> chirped grating in series for the testing setup measurement. (at region III area of chirped grating).

are shown in Figure 38. On average, the peak power of each channel fluctuated  $\Delta P/\Delta\lambda \approx 0.56$  dBm/nm from the neighboring channels. The power difference between the highest power channel and the lowest power channels was 4.7 dBm.

#### **4.3.3.3 Results at the Region III of 1st Chirped Grating**

The normalized position of each channel for the 600 grooves/mm grating in series with region III of the 1st chirped grating, grooves density varying from 500 grooves/mm to 600 grooves/mm, is shown in Figure 39. The average angular separation between each channel's peak power position was  $\Delta\theta/\Delta\lambda \approx 0.76$  deg/nm.

The actual power measurements from the 600 grooves/mm grating and region III of 1st chirped grating are shown in Figure 40. On average, the peak power of each channel fluctuated  $\Delta P/\Delta\lambda \approx 0.77$  dBm/nm from the neighboring channels. The power difference between the highest power channels and the lowest power channel was 5.9 dBm.

#### **4.3.4 Results for the 600 grooves/mm Grating and the 2nd Chirped Grating in Series**

The measurements from 600 grooves/mm grating in series with 2nd chirped grating, having groove density varying from 100 grooves/mm to 600 grooves/mm, are shown in Figure 41, 42, 43, 44, 45, and 46.

##### **4.3.4.1 Results at the Region I of 2nd Chirped Grating**

The normalized position of each channel for the 600 grooves/mm grating series with region I area of the 2nd chirped grating is shown in Figure 41. The average angular separation between each channel's peak power position was  $\Delta\theta/\Delta\lambda \approx 0.48$  deg/nm.

The actual power measurements from the 600 grooves/mm grating and region I of the 2nd chirped grating are shown in Figure 42. On average, the peak power of each channel fluctuated  $\Delta P/\Delta \lambda \approx 1.16$  dBm/nm from the neighboring channels. The power difference between the highest power channel and the lowest power channel was 6.1 dBm.

#### 4.3.4.2 Results at

#### Region II Area of the 2nd Chirped Grating

The normalized position of each channel for the for 600 grooves/mm grating in series with region II of the 2nd chirped grating, having groove density varying from 250 grooves/mm to 400 grooves/mm, is shown in Figure 43. The average angular separation between each channel's peak power position was

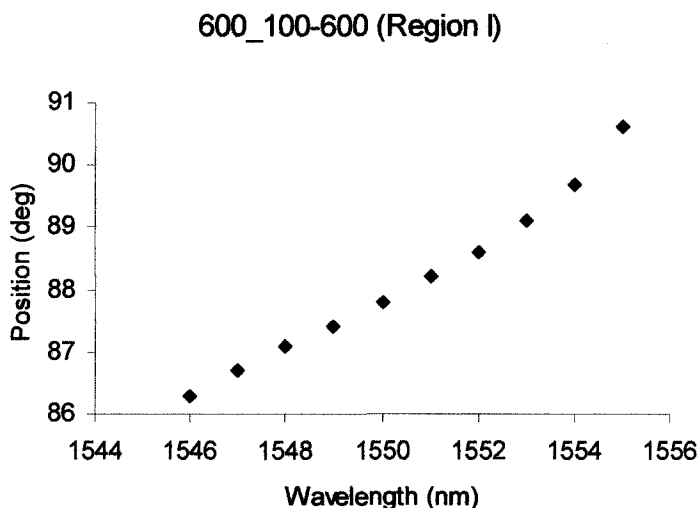


Figure 41: Peak power position of each wavelength for dual grating. 600 grooves/mm and 2<sup>nd</sup> chirped grating in series for the testing setup measurement. (at region I area of chirped grating)

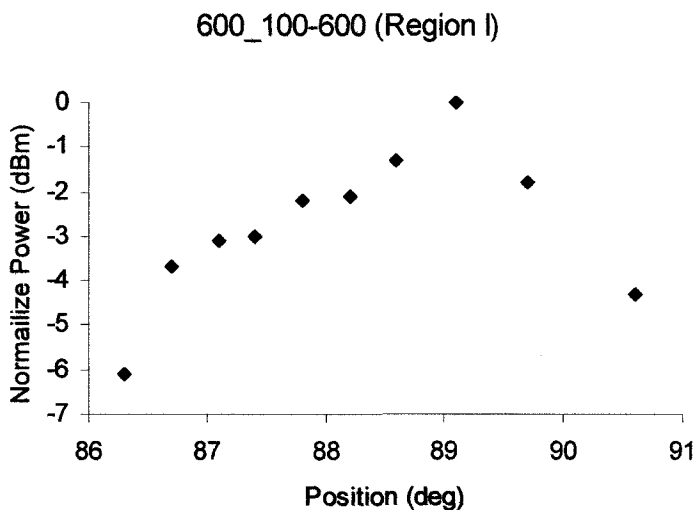


Figure 42: Actual peak power measurement for each wavelength for the 600 grooves/mm and 2<sup>nd</sup> chirped grating in series for the testing setup measurement. (at region I area of chirped grating).

$\Delta\theta/\Delta\lambda \approx 0.84$  deg/nm.

The actual power measurements from the 600 grooves/mm grating and region II of the 2nd chirped grating are shown in Figure 44. On average, the peak power of each channel fluctuated  $\Delta P/\Delta\lambda \approx 0.84$

dBm/nm from the

neighboring channels.

The power difference

between the highest

power channel and the

lowest power channel

was 3.9 dBm.

600\_100-600 (Region II)

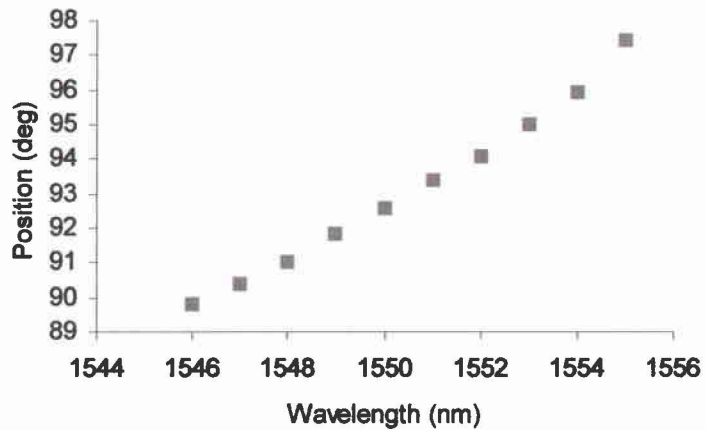


Figure 43: Peak power position of each wavelength for dual grating. 600 grooves/mm and 2<sup>nd</sup> chirped grating in series for the testing setup measurement. (at region II of chirped grating)

#### 4.3.4.3 Results at

#### Region III of the 2nd

#### Chirped Grating

The normalized position of each channel for the 600 grooves/mm grating in series with region III of the 2nd chirped grating is shown in Figure 45. The

600\_100-600 (Region II)

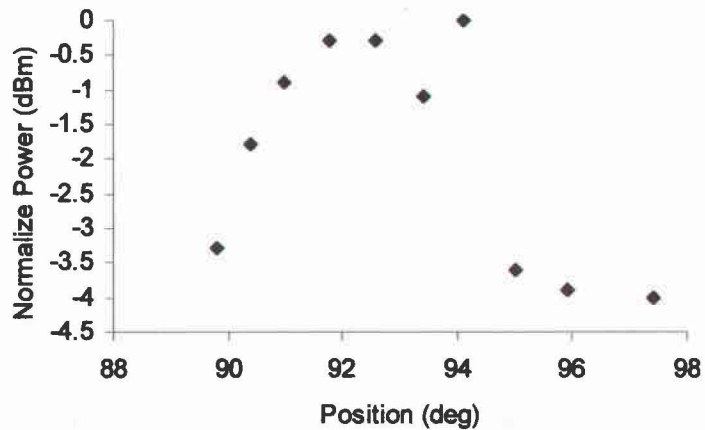


Figure 44: Actual peak power measurement for each wavelength for the 600 grooves/mm and 2<sup>nd</sup> chirped grating in series for the testing setup measurement. (at region II area of chirped grating).

average angular separation between each channel's peak power position was  $\Delta\theta/\Delta\lambda \approx$

1.07 deg/nm.

The actual power measurements from the 600 grooves/mm grating and region III of the 2nd chirped grating are shown in Figure 46. On average, the peak power of each channel fluctuated  $\Delta P/\Delta\lambda \approx$

0.47 dBm/nm from the

neighboring channels.

The power difference between the highest power channel and the lowest power channel

was 2.3 dBm.

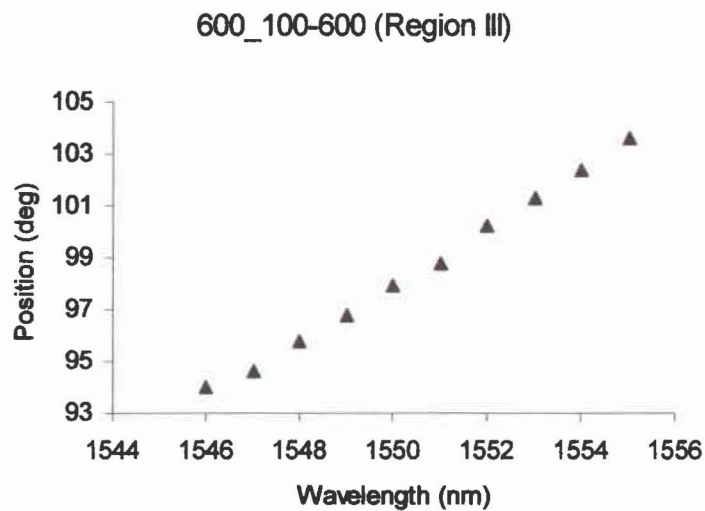


Figure 45: Peak power position of each wavelength for dual grating. 600 grooves/mm and 2<sup>nd</sup> chirped grating in series for the testing setup measurement. (at region III area of chirped grating)

#### 4.4 Wavelength

##### Routing Properties of the Dual Grating System

These results also show how each channel's peak power position shifted depending on the

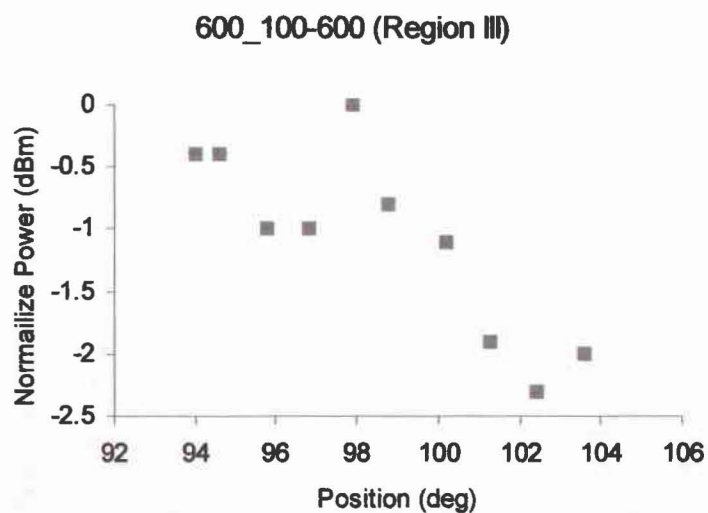


Figure 46: Actual peak power measurement for each wavelength for the 600 grooves/mm and 2<sup>nd</sup> chirped grating in series for the testing setup measurement. (at region III area of chirped grating).



grooves density of the second grating. This shows ability to shift (or move) channel's peak power position just by varying the groove density of second grating, which for the chirped grating can be accomplished by lateral translation.

#### 4.4.1 Results from Lateral Setup Results

The shifting of the channel's peak power positions for the different groove densities of second grating in the first setup is shown in Figure 47 and 48.

Due to the large power fluctuation in chirped grating measurements, the full range of test wavelengths could not be measured. However, even with the limited wavelengths analyzed it

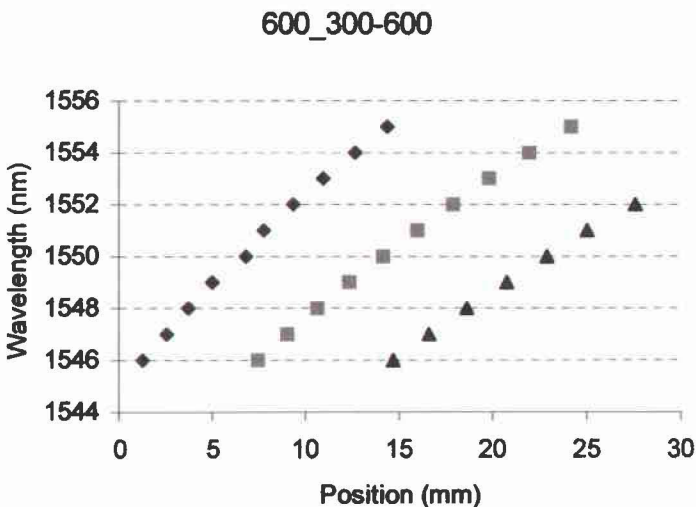


Figure 47: Channel's peak power position shifting as the groove density of 1<sup>st</sup> chirped grating varies from region I to region II and region II to region III.

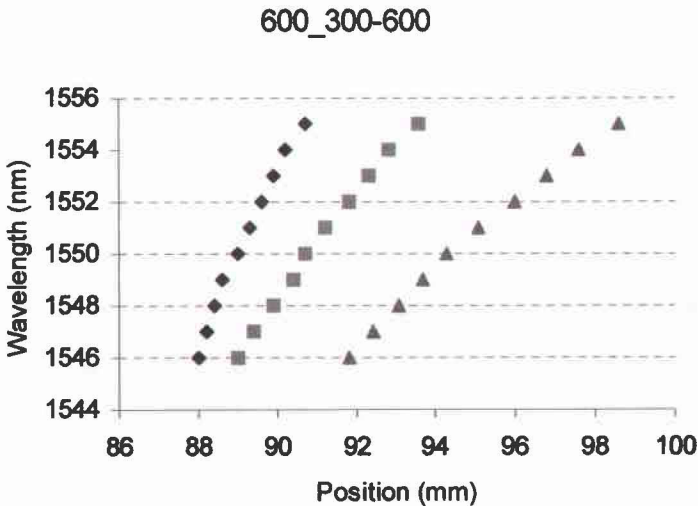


Figure 48: Channel's peak power position shifting as the groove density of 1<sup>st</sup> chirped grating varies from region I to region II and region II to region III.

is clearly shown that each channel's peak power position shifts from one place to another based on the groove density.

#### 4.4.1.1 Position Shifting of 1st Grating

The position shifting of each channel's peak power for the 1st chirped grating, having groove densities varying from 300 grooves/mm to 600 grooves/mm, is shown in Figure 49.

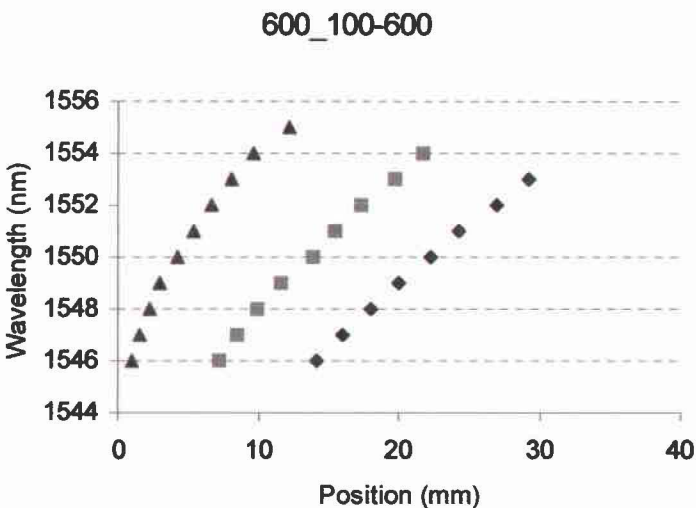


Figure 49: Channel's peak power position shifting as the groove density of 2<sup>nd</sup> chirped grating varies from region I to region II and region II to region III.

#### 4.4.1.2 Position Shifting of 2nd Grating

The position shifting of each channel's peak power for the 2nd chirped grating, having groove density varying from 100 grooves/mm to 600 grooves/mm, is

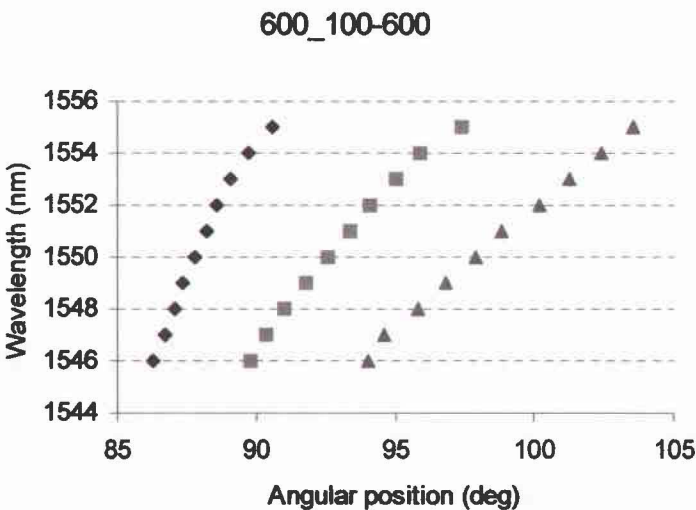


Figure 50: Channel's peak power position shifting as the groove density of 2<sup>nd</sup> chirped grating varies from region I to region II and region II to region III.

shown in Figure 50.

#### **4.4.2 Final Setup Results**

The angular shifting of the channel's peak power positions for different groove densities on the second grating for final setup is shown in Figures 49 and 50.

Unlike previous measurements, where the power fluctuations became larger as the separation between the wavelengths increased, measurements for the full range of wavelengths were collected because power fluctuations were small.

##### **4.4.2.1 Position Shifting of 1st Grating**

The position shifting of each channel's peak power for the 1st chirped grating, having groove density varying from 300 grooves/mm to 600 grooves/mm, is shown in Figure 49.

##### **4.4.2.2 Position Shifting of 2nd Grating**

The position shifting of each channel's peak power for the 2nd chirped grating, having groove densities varying from 100 grooves/mm to 600 grooves/mm, is shown in Figure 50.

In Chapter 5, all the data given in this chapter will be compared and discuss.

## **Chapter 5**

### **Discussion of Results**

#### **5.1 Wavelength Channel's Peak Power Separations**

A summary of the wavelength channel separation for all experimental setups is given in Table 1.

##### **5.1.1 Single Grating (Reference Measurement)**

Using a single 600 grooves/mm grating, reference measurements were conducted to examine the channel separation property of the diffraction grating and to compare the results with the other setups. Reference measurements were conducted for all the various setups, however, for the final setup, due to limited control over the fine angular movement (angle less than 0.05 degree) and limited precision from the angle measurement equipment, measurements of individual wavelength channel separations were not possible.

In setups where single grating measurements were possible, the results showed an average spatial separation of 0.06 deg/nm for the initial setup and 0.06 deg/nm for the testing setup. Even though the two measurements show slight difference in separation, this difference is within measurement error, which was about 0.01 deg/nm for the setups. In addition, these differences could be the result of slight changes in distance between the grating and collection fiber, since the setup was reconstructed for every measurement.

The measurement results show that the single grating setup is ideally suited for wide channel systems, with spacing of  $\Delta\lambda > 1\text{nm}$ , within a reasonable size because it is simple, robust, and cost effective. However, for DWDM systems, which require wavelength

	Theory testing setup	1 <sup>st</sup> Setup using continuous chirped grating setup	Final setup results
	Average Separation between the wavelength ( $\Delta\theta/\Delta\lambda$ ) ( $\Delta x/\Delta\lambda$ )	Average Separation between the wavelength ( $\Delta\theta/\Delta\lambda$ ) ( $\Delta x/\Delta\lambda$ )	Average Separation between the wavelength ( $\Delta\theta/\Delta\lambda$ ) ( $\Delta\theta/\Delta\lambda$ )
Single grating (600 grooves/mm)	$0.06 \pm 0.01$ deg $0.24 \pm 0.05$ mm	$0.06 \pm 0.01$ deg $0.22 \pm 0.05$ mm	NA
Dual grating (Two 600 grooves/mm)	$0.10 \pm 0.01$ deg $0.44 \pm 0.05$ mm	$0.1 \pm 0.01$ deg $0.44 \pm 0.05$ mm	$0.12 \pm 0.01$ deg $0.49 \pm 0.05$ mm
Dual grating (600 and 1 <sup>st</sup> chirped grating) at region I	NA	$0.32 \pm 0.01$ deg $1.46 \pm 0.05$ mm	$0.3 \pm 0.01$ deg $1.15 \pm 0.05$ mm
Dual grating (600 and 1 <sup>st</sup> chirped grating) at region II	NA	$0.38 \pm 0.01$ deg $1.86 \pm 0.05$ mm	$0.51 \pm 0.01$ deg $1.96 \pm 0.05$ mm
Dual grating (600 and 1 <sup>st</sup> chirped grating) at region III	NA	$0.41 \pm 0.01$ deg $2.15 \pm 0.05$ mm	$0.76 \pm 0.01$ deg $2.91 \pm 0.05$ mm
Dual grating (600 and 2 <sup>nd</sup> chirped grating) at region I	NA	$0.28 \pm 0.01$ deg $1.24 \pm 0.05$ mm	$0.48 \pm 0.01$ deg $1.84 \pm 0.05$ mm
Dual grating (600 and 2 <sup>nd</sup> chirped grating) at region II	NA	$0.37 \pm 0.01$ deg $1.81 \pm 0.05$ mm	$0.84 \pm 0.01$ deg $3.23 \pm 0.05$ mm
Dual grating (600 and 2 <sup>nd</sup> chirped grating) at region III	NA	$0.4 \pm 0.01$ deg $2.14 \pm 0.05$ mm	$1.07 \pm 0.01$ deg $4.11 \pm 0.05$ mm

Table 1: Average separation between the channels' peak power. For the theory and 1<sup>st</sup> setup measurement, both measured separations in metric term and calculated value of separation in angular terms are given. For the final setup measurement, both measured angular separations and calculated value of separation in metric terms are given. The calculations were based on the individual experiment's geometry. The calculations were based on the individual experiment's geometry.

channel spacings of  $\Delta\lambda < 1\text{nm}$ , it would not be suitable. Even though the resolution of the channels can be increased by increasing the distance between the grating and output fiber and/or changing the angle of incidence of the input to the grating, this result illustrates the typical lower limit of channel spacing for a single grating setup with a reasonable distance between the input and output.

### **5.1.2 Dual Grating Measurement Results**

As can be seen from the Table 1, all of the dual grating setups improved the average wavelength channel separation compared to the single grating setup. The improvement of separation ranges from 160% to 1700% depending on the setup, which is shown in Table 2.

#### **5.1.2.1 Two 600 groove/mm Gratings in Series**

For the dual grating configuration the spatial separation between each wavelength channel was larger than the single grating setup, as was expected. In the initial measurement setup, dual gratings resulted in greater than 160% improvement over the single grating. In the testing measurement, improvement between the single grating and the dual grating was about 200 %.

The differences in these results could be due to different factors. One such factor is due to the small difference in the separation between the first and the second grating. This difference will result in a difference in incident angles on the second grating, as the separation between the first and second grating increases, the range of the incident angles into the second grating increases. This will result in larger separation.

Secondly, however small the difference might be, the total distance traveled by the separated light will increase the wavelength separations due to angular spread of the light from the grating. This is unavoidable and results in a larger spread in wavelength.

However, the difference in the wavelength separation is within the measurement error in this experiment. The difference in percentage seems larger since the separation between the wavelengths is small compared to the measurement error range.

#### 5.1.2.2 Dual Grating (1<sup>st</sup> Chirped grating)

	1 <sup>st</sup> Setup using continuous chirped grating setup	Final setup results
	% Improved compared to the reference measurements	% Improved compared to the reference measurements
Dual grating (Two 600 groove/mm)	160	200
Dual grating (600 and 1 <sup>st</sup> chirped grating) at region I	533	500
Dual grating (600 and 1 <sup>st</sup> chirped grating) at region II	633	850
Dual grating (600 and 1 <sup>st</sup> chirped grating) at region III	683	1267
Dual grating (600 and 2 <sup>nd</sup> chirped grating) at region I	466	800
Dual grating (600 and 2 <sup>nd</sup> chirped grating) at region II	616	1400
Dual grating (600 and 2 <sup>nd</sup> chirped grating) at region III	667	1783
Table 2: Wavelength channels separation improvement compared to the average reference measurement in percent		

Use of the 1<sup>st</sup> chirped grating, having groove density varying from 300 grooves/mm to 600 grooves/mm, improved the wavelength channel separations in both the testing setup and final setups.

#### **5.1.2.2.1 Testing Setup**

Using the 600 grooves/mm grating, as a master grating, and the different density areas of the 1<sup>st</sup> chirped grating, having groove density varying from 300 grooves/mm to 600 grooves/mm, as the slave grating, in series results in improved wavelength channel separation. The separation between the wavelength channels improved by 530% to 680% depending on the groove density of the chirped grating compared to the average separations of the wavelength channels for the reference measurements, as shown in Table 2.

#### **5.1.2.2.2 Final Setup**

Using the 600 grooves/mm grating, as a master grating, and the different density area of the 1<sup>st</sup> chirped grating, groove density varying from 300 grooves/mm to 600 grooves/mm, as the slave grating, in series results in improving wavelength channel separations. The separations between the wavelength channels improved by 500% to 1200% depending on the groove density of the chirped grating area compared to the average separations of the wavelength channels for the reference measurements, as shown in Table 2.

The large increase in average wavelength separation in the final setup is partly due to a



larger separation in longer wavelengths ranging from 1553 nm to 1555 nm. In previous measurements from the testing setup, the full range of the wavelength channels could not be measured due to the large power attenuation at the larger wavelength, especially in 1555 nm range. However, in the final setup, it was possible to measure these longer wavelengths. This resulted in an increase of the average separation of the wavelength channels due to the longer wavelength combined with the higher groove density of slave grating. Thus for these wavelengths, the separation between the channels was larger than the other wavelength, which increased the average separation. Still, the final setup performed better overall.

#### **5.1.2.3 Dual Grating Setup (2<sup>nd</sup> Chirped Grating)**

Use of the 2<sup>nd</sup> chirped grating improved the channel separation in both the testing setup and final setups.

##### **5.1.2.3.1 Testing Setup**

Using the 600 grooves/mm grating, as a master grating, and the different density areas of the 2<sup>nd</sup> chirped grating, groove density varying from 100 grooves/mm to 600 grooves/mm, as the slave grating, in series results in improving wavelength channel separations. The separation between the wavelength channels improved by 450% to 660% depending on the groove density of the chirped grating, when compared to the average separations of the channels for the reference measurements, as shown in Table 2.

##### **5.1.2.3.2 Final Setup**

Using the 600 grooves/mm grating, as a master grating, and the different density area

of the 2<sup>nd</sup> chirped grating, having groove density varying from 100 grooves/mm to 600 grooves/mm, as the slave grating, in series results in improving channel space separation as well. The separation between the wavelength channels improved by 800% to 1750% depending on the groove density of the chirped grating, when compared to the average separations of the wavelength channels for the reference measurements, as shown in

	Theory testing setup	1 <sup>st</sup> Setup using continuous chirped grating setup	Final setup results
	Average power fluctuation between the neighboring channels ( $\Delta P/\Delta\lambda$ ) [ dBm/nm]	Average power fluctuation between the neighboring channels ( $\Delta P/\Delta\lambda$ ) [ dBm/nm]	Average power fluctuation between the neighboring channels ( $\Delta P/\Delta\lambda$ ) [ dBm/nm]
Single grating (600 grooves/mm)	$3.26 \pm 0.1$	$0.55 \pm 0.1$	NA
Dual grating (Two 600 grooves/mm)	$0.67 \pm 0.1$	$0.67 \pm 0.1$	$0.57 \pm 0.1$
Dual grating (600 and 1 <sup>st</sup> chirped grating) at region I	NA	$1.13 \pm 0.1$	$0.66 \pm 0.1$
Dual grating (600 and 1 <sup>st</sup> chirped grating) at region II	NA	$1.6 \pm 0.1$	$0.56 \pm 0.1$
Dual grating (600 and 1 <sup>st</sup> chirped grating) at region III	NA	$1.35 \pm 0.1$	$0.77 \pm 0.1$
Dual grating (600 and 2 <sup>nd</sup> chirped grating) at region I	NA	$0.86 \pm 0.1$	$1.16 \pm 0.1$
Dual grating (600 and 2 <sup>nd</sup> chirped grating) at region II	NA	$0.74 \pm 0.1$	$0.84 \pm 0.1$
Dual grating (600 and 2 <sup>nd</sup> chirped grating) at region III	NA	$1.76 \pm 0.1$	$0.47 \pm 0.1$
Table 3: Average power fluctuation between the wavelength channels' peak power.			

Table 2.

### 5.1.3 Dual Grating Measured Results verse Calculated Results

In the calculations, the position of each wavelength channel was predominately controlled by the groove density of second grating.

The relationships between the groove density, the wavelengths, and the position of each wavelength channels are shown in Figure 51 and 52. Figure 51 show, each wavelength channel's

position for the different slave (second) gratings: constant 600 grooves/mm, 1<sup>st</sup> chirped grating, with groove density varying from 600 grooves/mm to 300 grooves/mm, and 2<sup>nd</sup> chirped grating, with

Calculation of Wavelength Channel Position

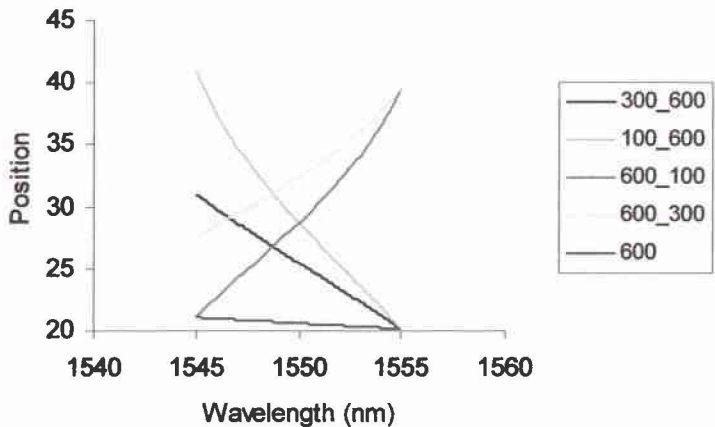


Figure 51: Calculated Position of wavelength channel for 1<sup>st</sup> and 2<sup>nd</sup> chirped grating.

Calculated Wavelength Channel Position

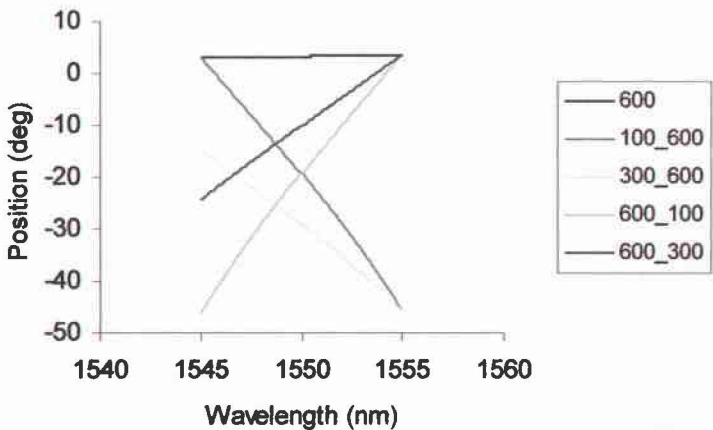


Figure 52: Calculated angular position of wavelength channel for 1<sup>st</sup> and 2<sup>nd</sup> chirped grating.

groove density varying from 600 grooves/mm to 100 grooves/mm. Figure 52 shows each wavelength channel's position for the different slave (second) gratings: constant 600 grooves/mm, 1<sup>st</sup> chirped grating, with groove density varying from 300 grooves/mm to 600 grooves/mm, and 2<sup>nd</sup> chirped grating, with groove density varying from 100 grooves/mm to 600 grooves/mm.

As can be seen from Figures 51 and 52, for a constant groove density on the second (600 grooves/mm) grating, the position of each channel was determined by the wavelength, but the amount of position change between each channel was small. However, for the chirped grating, the position of each wavelength channel was predominately controlled by the groove density of the second (chirped) grating. For example, in the case when the chirped grating density varied from low to high, as the wavelength increases, from 1545 nm to 1555 nm, the position of the each channel was determine by the groove density not by the wavelength. For the case when the groove

density of the chirped grating decreases as the wavelength increases, the calculated results show a mirror image from top to bottom of the case when the groove density of the chirped grating increases as the wavelength

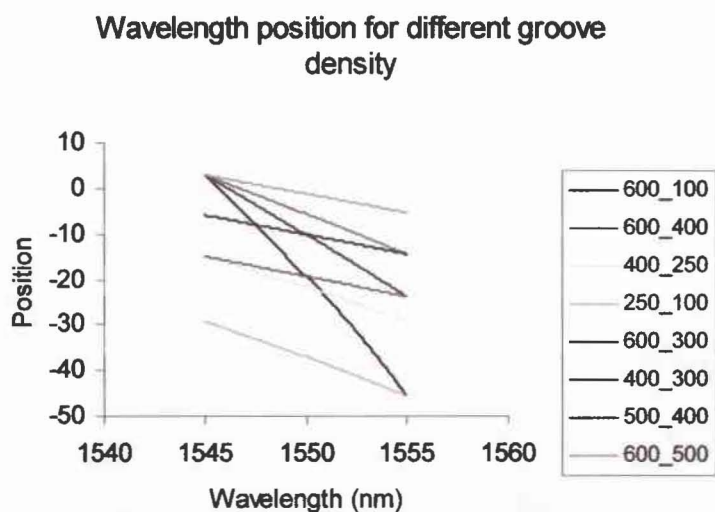


Figure 53: Calculated position of wavelength channel for 1<sup>st</sup> and 2<sup>nd</sup> chirped grating for the different region.

increase, except the position is shift by the effect of 1<sup>st</sup> (master) grating's spectral spreading.

However, in the actual measurement, when the direction of the density gradient was switched, the results did not give mirror images of each other. When the groove density of the chirped grating increased as the wavelength increased, the result could not be obtained due to the wide beam broadening effect. However, in the case when the groove density of the chirped grating decreased as the wavelength increased, there was less broadening. This broadening effect will be discussed later on.

In the measurement, each chirped grating was divided into three sections, each with different groove density. Each groove density period resulted in different wavelength channel separation abilities, some sections showing larger separation abilities than others. However, in the calculations, the three sections seem to show similar abilities, except for the lower end (groove density around 100 grooves/mm) of the grating, which shows slightly better performance, see Figure 53.

## **5.2 Power Fluctuation**

### **5.2.1 Initial Setup**

The power fluctuation in the measurements is partially due to the ineffective coupling into the output single-mode fiber, due to the small numerical aperture. The loss is also attributed to the angle of incidence for the single-mode fiber, which differs for each wavelength. The angle of incidence for light coupling into output fiber was difficult to control due to small angle changes for each wavelength; therefore, the output fiber was

fixed at a single angle relative to the grating, while light came from slightly different angles. Also, the power from the input fiber was not completely uniform over the wavelength range tested, which was a function of the laser source and amplifier.

### **5.2.2 Testing Setup**

The output (collected) power for the testing setup fluctuated due to problems with coupling, as mentioned before. For the first measurement, this power fluctuation was not as severe as the other two measurements, since the separation between the wavelengths was not as large, and thus, the incident angle of light on the fiber did not vary as much. But, for mid and high density areas, the power fluctuation between the wavelengths was severe as the wavelength separation increased. The highest power of the wavelength channel occurs at one wavelength position, where the incident angle of the light on fiber was optimum, and the power decreased as the position shifted away from this optimum angle. For this reason, the measurement of power for longer wavelengths incident on the high density area of grating was not possible, since the power dropped below the detectable limit of the wave-meter.

### **5.2.3 Final Setup**

In the final setup measurements, the power fluctuated as well. However, the power fluctuation in the final setup differed from the other setups. Unlike the other setups, where there were one or two distinctive peak powers and a gradual lowering of the power for the adjacent wavelength channels, the final power fluctuated without a distinctive pattern.

Even though there were power fluctuations within the measurements, the fluctuations were not as severe as in the testing measurements, especially when considering the difference between the highest power and the lowest power received by the collection fiber. The power fluctuations from the final setup could arise for different reasons. It could be due to the differences

in incident angles of the beams

into the fiber, which is caused

by small differences in the

origin of the rotating axis

where the collection fiber is

placed. The difference in the

rotation axis occurs from the

distribution of the wavelength

channels at the second (slave)

grating, since no matter how

small the distribution of the

wavelength channels are, there

can only be one origin of the

rotational axis for collection

fiber. In addition, any power

fluctuations in the input

channel will appear directly on

Position shift as groove density varies

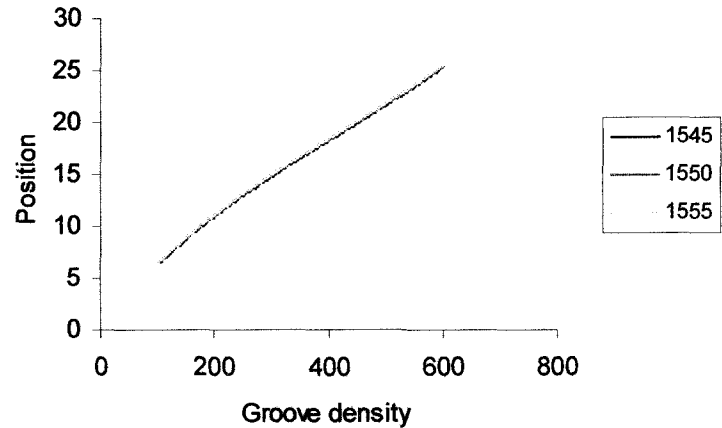


Figure 54: Calculated position of each wavelength channel as the groove density varies for testing setup

Angular position shifting as the groove density varies

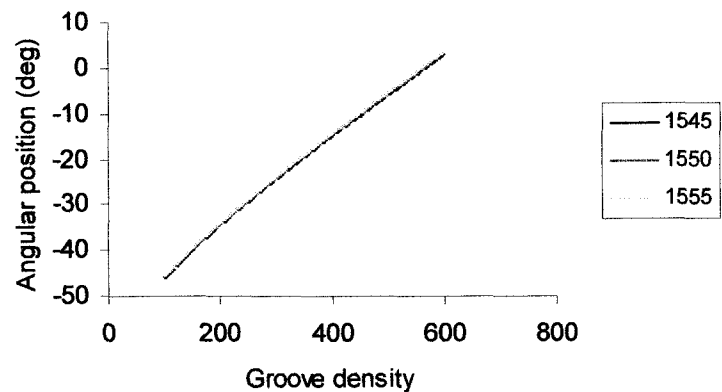


Figure 55: Calculated angular position of each wavelength channel as the groove density varies for the final setup

the output. Furthermore, there was a limit to resolution of the angular movement of the output fiber, which made positioning of the output fiber at the peak power position difficult.

### 5.3 Wavelength Routing Properties

#### 5.3.1 Routing of Wavelength Channels in the Testing Setup

The position shifts for each wavelength channel in the testing setup are shown in Table 3 and 4.

##### 5.3.1.1 1<sup>st</sup> Chirped Grating

The position shift of each wavelength channel for the 1<sup>st</sup> chirped grating is shown in

	Theory testing setup	1 <sup>st</sup> Setup using continuous chirped grating setup	Final setup results
	Amount of position shifted as chirped grating is moved from region I to region II (deg)	Amount of position shifted as chirped grating is moved from region II to region III (deg)	Amount of position shifted as chirped grating is moved from region I to region III (deg)
1546 nm	$1.41 \pm 0.02$	$1.56 \pm 0.02$	$2.97 \pm 0.02$
1547 nm	$1.48 \pm 0.02$	$1.59 \pm 0.02$	$3.07 \pm 0.02$
1548 nm	$1.55 \pm 0.02$	$1.64 \pm 0.02$	$3.18 \pm 0.02$
1549 nm	$1.61 \pm 0.02$	$1.68 \pm 0.02$	$3.29 \pm 0.02$
1550 nm	$1.57 \pm 0.02$	$1.72 \pm 0.02$	$3.29 \pm 0.02$
1551 nm	$1.73 \pm 0.02$	$1.72 \pm 0.02$	$3.46 \pm 0.02$
1552 nm	$1.76 \pm 0.02$	$1.81 \pm 0.02$	$3.57 \pm 0.02$
1553 nm	$1.79 \pm 0.02$	NA	NA
1554 nm	$1.83 \pm 0.02$	NA	NA
1555 nm	$1.88 \pm 0.02$	NA	NA

Table 4: The wavelength channels' peak power position shift as change in the 1<sup>st</sup> chirped grating density for the testing setup.



Table 4. The position shifting of each wavelength channel is not linear, but does monotonically increase as the wavelength increases. The change in the amount of the position shifting for different wavelengths is due to a change in the incident position of the light within the region. This is expected as seen from the calculation result in Figure 54 and Figure 55. This figure shows the position of a wavelength channel as the groove density changes in the 2<sup>nd</sup> (slave) grating.

### 5.3.1.2 2<sup>nd</sup> Chirped Grating

The position shift of each wavelength channel for the 2<sup>nd</sup> chirped grating is shown in Table 5. The position shifting is not linear, but again increases monotonically as the wavelength increases, which is due to the changes in incident position within the region. This is expected as seen from calculations, in Figure 54 and 55. However, for the longer wavelengths, the amount of shift per channel increased progressively more than what the

	Amount of position shifted as chirped grating is moved from region I to 2egion II (deg)	Amount of position shifted as chirped grating is moved from region II to region III (deg)	Amount of position shifted as chirped grating is moved from region I to region III (deg)
1546 nm	1.46± 0.02	1.49 ± 0.02	2.95 ± 0.02
1547 nm	1.60± 0.02	1.57 ± 0.02	3.17 ± 0.02
1548 nm	1.75± 0.02	1.67 ± 0.02	3.42 ± 0.02
1549 nm	1.94± 0.02	1.68 ± 0.02	3.63 ± 0.02
1550 nm	2.11± 0.02	1.66 ± 0.02	3.78 ± 0.02
1551 nm	2.15± 0.02	1.7 ± 0.02	3.86 ± 0.02
1552 nm	2.24± 0.02	1.8 ± 0.02	4.04 ± 0.02
1553 nm	2.39± 0.02	1.75 ± 0.02	4.14 ± 0.02
1554 nm	NA	NA	NA
1555 nm	NA	NA	NA
Table 5: The wavelength channels' peak power position shift as change in the 2 <sup>nd</sup> chirped grating density for the testing setup.			

calculations predicted. This could be due to difference in the incident angle of the shorter wavelength and the longer wavelength on to the second grating since the longer wavelength is diffracted at larger incident angle than the shorter wavelength in the experiment.

### 5.3.2 Routing of Wavelength Channel in Final Setup

The amount of the position shift of each wavelength channel for the final setup is shown in Tables 6 and 7.

#### 5.3.2.1 1<sup>st</sup> Chirped Grating

The position shift of each wavelength channel for the 1<sup>st</sup> chirped grating is shown in Table 6. As with the previous setups, the position shifting of the wavelength channel was not linear and monotonically increased with wavelength, which was predicted by the

	Amount of position shifted as chirped grating is moved from region I to 2egion II (deg)	Amount of position shifted as chirped grating is moved from region II to region III (deg)	Amount of position shifted as chirped grating is moved from region I to region III (deg)
1546 nm	1	2.8	3.8
1547 nm	1.2	3	4.2
1548 nm	1.5	3.2	4.7
1549 nm	1.8	3.3	5.1
1550 nm	1.7	3.6	5.3
1551 nm	1.9	3.9	5.8
1552 nm	2.2	4.2	6.4
1553 nm	2.4	4.5	6.9
1554 nm	2.6	4.8	7.4
1555 nm	2.9	5	7.9

Table 6: The wavelength channels' peak power position shift as change in the 1<sup>st</sup> chirped grating density for the final setup.

calculations in Figure 54 and 55. The figure shows position of a wavelength channel as the groove density changes in the 2<sup>nd</sup> (slave) grating.

### 5.3.2.2 2<sup>nd</sup> Chirped Grating

The position shift of each wavelength channel for the 2<sup>nd</sup> chirped grating is shown in Table 7. The position shifting of the wavelength channel is not linear, but does increase as the wavelength increases. In addition, the amount of the position shifting is different between positions due to change in the region groove density. This is expected as seen from the calculations, shown in Figure 54 and 55. This figure shows the position of a wavelength channel as the groove density changes in the 2<sup>nd</sup> (slave) grating. However, for the higher wavelengths, the amount of shifting of each channel position increased progressively more than what the calculation predicted. As before, this could be due to difference in the incident angle of the shorter wavelength and the longer wavelength.

	Amount of position shifted as chirped grating is moved from region I to region II (deg)	Amount of position shifted as chirped grating is moved from region II to region III (deg)	Amount of position shifted as chirped grating is moved from region I to region III (deg)
1546 nm	3.5	4.2	7.7
1547 nm	3.7	4.2	7.9
1548 nm	3.9	4.8	8.7
1549 nm	4.4	5	9.4
1550 nm	4.8	5.3	10.1
1551 nm	5.2	5.4	10.6
1552 nm	5.5	6.1	11.6
1553 nm	5.9	6.3	12.2
1554 nm	6.2	6.5	12.7
1555 nm	6.8	6.2	13

Table 7: The wavelength channels' peak power position shift as change in the 2<sup>nd</sup> chirped grating density for the final setup.

## 5.4 Beam Broadening

Due to the limitations in controlling the beam waist of the light incident on the chirped grating, a noticeable

increase of beam waist at

the output was observed.

Even though it is possible

to focus or collimate the

light beam into small spot

size, there was a limit to

minimum output spot size

that could be achieved, due

to the wavelength of the

light as well as diffraction

effects from the optics.

Therefore, when the beam

hit the chirped grating in

which the groove density

varies continuously, each

part of the beam is incident

on a slightly different

portion of the grating, and

Beam broadening

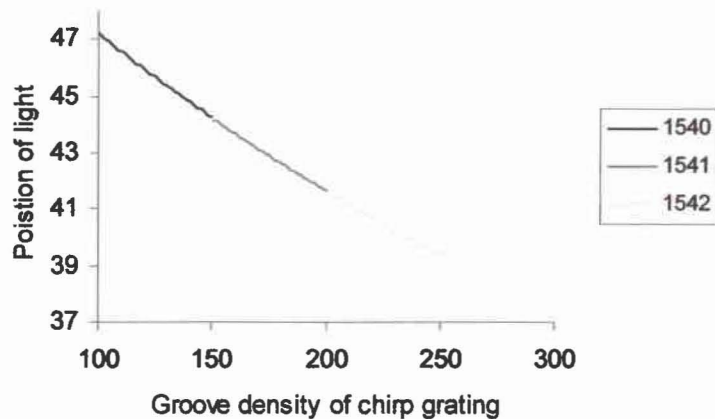


Figure 56: Calculated position of wavelength channel for the case when the wavelength channel interacted over the range of the chirped grating without overlapping the same groove density area.

Overlapping of the wavelength

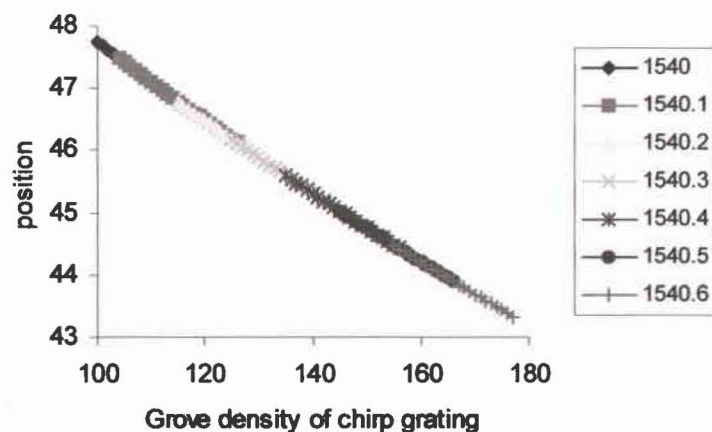


Figure 57: Calculated position of wavelength channel for the case when the wavelength channel interacted over the range of the chirped grating with overlapping the same groove density area.

thus encounters various groove densities. As the beam spot size increased, the area of chirped grating hit by the light increased. For example, if the spot diameter for the light containing only a single wavelength and with evenly distributed power is comparable to the length of the chirp on the grating, then the diffracted angle would be different for each spatial location along the length of the grating. This would result in spreading of light at different angles according to groove density. Figure 56 shows the affect of grove density variation on the final position of an individual wavelength channel.

In the experiment, due to the beams of closely spaced channels physically overlapping following diffraction from the first grating, some of the same area of the chirped grating is shared by the different channels. This results in over lapping of the wavelengths at the final destination (output), as shown in Figure 57. As the area shared by each wavelength channel at the chirped grating increases, the overlapping of each channel at the output increases.

The spatial overlapping of the wavelengths leads to high levels of cross-talk between the channels. In order to minimize the effect of overlapping of the beam on the chirped grating, it would be necessary to focus each channel's beam at the chirped grating to reduce the area shared by each wavelength.

## **Chapter 6**

### **Conclusion**

The fast paced increase in the need for higher bandwidth in current communication systems has led to the development optical networks. However, today's communication technologies do not completely utilize the full potential of optic communication systems, due to limiting constraints from the optical components. Even with the advancement in optical components within optical communication systems, the available wavelength channel ranges are limited. This limitation arises from the optical fiber, which has narrow wavelength ranges with low loss coefficients centered at 0.8  $\mu\text{m}$ , 1.3  $\mu\text{m}$ , and 1.5  $\mu\text{m}$ . In addition to the limitations of the optical fiber, the optical amplifiers currently in used, such as the erbium dope fiber amplifier (EDFA), also limit the maximum channel spacing due to the limited range of wavelengths it can amplify uniformly, typically about 35-40 nm [23]. Therefore, in order to increase the efficiency of optical communication systems, the number of channels within the available wavelength ranges needs to be increased.

One means to accomplish this is wavelength division multiplexing. However, in today's optical communication systems, the demultiplexer is one of the factors which limits the number of channels that can be transmitted through the optical fiber, since it can only demultiplex wavelength channels with certain wavelength separations, typically larger than 0.5 nm. Therefore, to increase the number of the wavelength channels, there is a need for the demultiplexer that is capable of separating closely packed wavelength

channels. To meet this need, this thesis discussed the research and development of a demultiplexer constructed with cascading diffraction gratings to achieve a robust and cost-effective demultiplexer that is capable of separating the closely packed wavelength channels, with separation less than 0.5 nm.

## **6.1 Testing of Grating System**

In the initial stage of the research, a single 600 grooves/mm grating was used for reference measurements. These measurements were conducted to examine the wavelength channel separation property of diffraction gratings and to compare the results with other demultiplexer setups published in the literature. Reference measurements were conducted with this configuration for all the different experimental setups examined in this thesis.

The initial reference measurement results showed that the single grating setup, within reasonable size, is ideally suited for wide channel systems, with spacing of  $\Delta\lambda > 1\text{nm}$  because it is simple, robust, and cost effective. However, for DWDM systems, which require wavelength channel spacings of  $\Delta\lambda < 1\text{nm}$ , it would not be suitable. Even though the resolution of the channels can be increased by increasing the distance between the grating and collection fiber and/or changing the angle of incidence of the input to the grating, this results in achieving only the typical lower limit of channel density for a setup with a reasonable distance between input and output.

## **6.2 Testing of Dual Grating System**

### **6.2.1 First Stage**

In the beginning of this research, the feasibility of a demultiplexer using dual grating

in series was tested [25]. Once the feasibility was proven, two proto-type chirped gratings were fabricated, by Oceanic Inc., one chirped grating with groove density varying from 300 grooves/ mm to 600 grooves/mm and another chirped grating with groove density varying from 100 grooves/mm to 600 grooves/mm.

With these two proto-type chirped gratings, testing of two different setups were conducted; the testing setup and then final setup. In this research, two different measurement setups were conducted due to the power fluctuation problems in the first setup, called the testing setup.

### **6.2.2 Testing Setup**

Using the 600 grooves/mm grating, as a master grating, and the different groove density areas of the chirped grating that had groove density varying from 300 grooves/mm to 600 grooves/mm, as the slave grating, in series resulted in improved wavelength channel separations. Following this test, the 1<sup>st</sup> chirped grating was replaced by the 2<sup>nd</sup> chirped grating, having groove density varying from 100 grooves/mm to 600 groove/mm. In both case, the separations between the wavelength channels improved by 450% to 850% depending on the groove density, when compared to the average separations of the wavelength channels for the reference measurements.

However, even though this testing setup showed improvement of the physical separation between the wavelengths, the power of each channel fluctuated depending on the position of receiving fiber. This power fluctuation in the measurements was partially due to the ineffective coupling into the output single-mode fiber, which has small numerical aperture. The loss is also due to the angle of incidence for the single-mode



fiber, which differs for each wavelength. The angle of incidence for light coupling into the collection fiber was difficult to control due to small angle changes for each wavelength; therefore, the output fiber was fix at a single angle, while light came from slightly different angles.

### **6.3 Final Setup**

To reduce the power fluctuations in the testing stage of this research, a different setup was used. Identical to the configuration of the testing setup, the 600 grooves/mm grating was used as a master grating, and 1<sup>st</sup> chirped grating, having groove density varying from 300 grooves/mm to 600 grooves/mm, was used as the slave grating. The two gratings in series resulted in improved wavelength channel separation. Then, as it was done with testing setup, the 1<sup>st</sup> chirped grating was replaced by the 2<sup>nd</sup> chirped grating, having groove density varying from 100 grooves/mm to 600 grooves/mm. In this setup, the separations between the wavelength channels improved by 370% to 1700% for the 1<sup>st</sup> chirped grating and 800% to 1780% for the second chirped grating, depending on the groove density, when compared to the average separations of the wavelength channels for the reference measurements.

Compared to the first setup, which had more than 10 dB difference between the highest power and the lowest power, the second setup reduced the power fluctuation between the highest and the lowest power to less than 10 dB. However, the improvement in received power came at the cost of additional measurement error due to a larger limitation on movement control. In the design of an actual demultiplexer device, this could be compensated for by precise control of the arrangement of the output fiber.

#### **6.4 Dual Grating Measured Results verse Calculated Results**

From the calculations, it was evident that the position of the each wavelength channel was predominately controlled by the groove density of second grating. This is attributed to the difficulty encountered in controlling the accuracy of the light from the first grating to hit the area of the desired groove density of the second grating. Through the experiment using the chirped grating as a routing element, the relationship of wavelength and the groove density was partly verified.

#### **6.5 Routing Property**

In addition to the demultiplexing capability of the chirped grating, it was tested for the routing property.

The position shifting of the wavelength channel was found to be non-linear, but monotonically increasing as was expected. The position of the selected wavelength changed as the groove density increased and decreased. These position changes were different between the 1<sup>st</sup> and 2<sup>nd</sup> chirped gratings, where 2<sup>nd</sup> chirped grating had a larger groove density change. This routing of the wavelength also verified that position shifting of the given wavelength is depended on groove density.

#### **6.7 Unwanted Effects of Chirped Grating**

Due to the limitation in controlling the beam waist of the light going into the chirped grating, an increase of beam waist was observed. Even though it is possible to focus or collimate the light beam into small spot size, there was a limit to minimum size, achieved in this experiment. Therefore, when the beam hit the continuously chirped grating, the

light interacted with various groove densities, and as the beam spot size increased, the area illuminated on the chirped grating increased. This resulted in spreading of light in different direction according to groove density. This effect is more severe for the setup where the chirped grating was used compared to the uniform groove density grating.

The beam broadening effect caused large cross talk between the neighboring wavelength channels, since the each wavelength coming out of the master grating could not be easily separated before the chirped grating (slave grating).

Other than the beam broadening, the typical loss due to the coupling the light into the output fiber was large, typically about 20 dB. This can be significantly reduced by inserting collection optics in front of each fiber, which is common technique employed in fiber optic systems.

## **Closing**

This research shows that all of the dual grating setup improved the average wavelength channel separation compare to the single grating systems. The improvements of the wavelength separation ranges from 50% to 1700% depending on the setup, which clearly shows capability of the system of separating the wavelength channel spacing of less than 0.5 nm for reasonably sized demultiplexer.

## Reference

- [1] D. R. Wisely, *Electron. Lett.* **27**, 520 (1991).
- [2] Jean-Pierre Lande, “DWDM Fundamentals, Components, and Applications”, Artech House, 2002,
- [3] Rajiv Ramaswan, Kumar N. Sivarajar, “Optical Networks, A Practical Perspective 2<sup>nd</sup>”, Academic Press, 2002
- [4] Takada, K., Abe, M., Shibata, T., Ishii, T., Inoue, H., Yamada, Y., Hibino, Y., and Okamoto, K., “10-GHz-spaced 1010-channel AWG filter achieved by tandem connection of primary and secondary AWGs”, ECOC 200, Munich, 2000, Postdeadline Paper PD3-8
- [5] Takada, K., Abe, M., Shibata, T., Okamoto, K., “Low-loss 10-GHz-spaced tandem multi/demultiplexer with more than 1000 channels using a  $1 \times 5$  interference multi/demultiplexer as a primary filter”, *IEEE Photonics Technology Letters* , Volume: 14 Issue: 1 , Jan 2002 Page(s): 59 –61
- [6] Takada, K., Abe, M., Shibata, T., Okamoto, K., “Three-stage ultra-high-density multi/demultiplexer covering low-loss fibre transmission window 1.26-1.63  $\mu\text{m}$ ”, *Electronic Letters* , Volume: 39 No. 9, April 2002, Page(s): 405-406
- [7] Sun, Z.J., McGreer, K.A., Broughten, J.N., “Demultiplexer with 90 channels and 0.3 nm channel spacing Vertical-Cavity Lasers, Technologies for a Global Information Infrastructure, WDM Components Technology, Advanced Semiconductor Lasers, Gallium Nitride Materials, Processing”, 1997 Digest of the IEEE/LEOS Summer Topical Meetings , 11-15 Aug 1997, Page(s): 52 -53
- [8] Stavdas, A., “A single WDM multi/demultiplexer for all SMF transmission windows in 1280-1680 nm”, *IEEE Photonics Technology Letters* , Volume: 14 Issue: 11 , Nov 2002, Page(s): 1542 –1544
- [9] William B. Jones Jr., “Introduction to Optical Fiber Communication System”, Holt, Rinehart and Winston, Inc., 1988
- [10] Robert J. Hoss, Edward A. Lacy, “Fiber Optics”, PTR Prentice-Hall Inc., NJ, 1993
- [11] Josep Prat, Pere E Balaguer, Joan M. Gene, Oscar Diaz, Sergi Figurola, “Fiber to the Home Technologies”, Academic Publishers, 2002
- [12] Katsunari Okamoto, “Fundamentals of Optical Waveguides”, Academic Press, 2000

- [13] Robert J. Hoss, "Fiber Optic Communications: Design Handbook", Prentice Hall Inc., 1990
- [14] John P. Powers, "Introduction to Fiber Optic Systems", Aksen Association Inc., 1993
- [15] Andreas Othonos, Kyriacos Kalli, "Fiber Bragg Grating: Fundamentals and Applications in Telecommunications and Sensing", Artech House Publishers, 1999
- [16] William O. Grant, "Understanding Lightwave Transmission: Applications of Fiber Optics", Harcourt Brace Jovanovich, 1988
- [17] Thomas E. Stern, Krishna Bala, "Multiwavelength Optical Network: A Layered Approach", Addison Wesley Longman, Inc., 1999
- [18] Dr. Martin Amersfoort, "Arrayed Waveguide Grating", Concept to Volume b.v., 15 June 1998
- [19] P.D. Rinh, S. Yegnanarayanan, F. Coppinger, B. Jalali, "Silicon-on-insulator Phased-Array waveguide grating WDM filter", OFC '97 Technical Digest, p301-302, 1997
- [20] Tsunetoshi Saito, Toshihiko Ota, Tomoaki Toratani, Yoshimi Ono, "16-ch Arrayed Waveguide Grating Module with 100-GHz Spacing", Furukawa Review, No. 19. 2000
- [21] C. Dragone, "Planar 1 N Optical Multiplexer With Nearly Ideal Response", IEEE Photonics Technology Letters, VOL. 14, NO. 11, pp.1545-1547, NOVEMBER 2002
- [22] Alexandros Stavdas, "A Single WDM Multi/Demultiplexer for All SMF Transmission Windows in 1280–1680 nm", IEEE Photonics Technology Letters, VOL. 14, NO. 11, pp1542-1542, NOVEMBER 2002
- [23] Tizhi Huang, Jeff Huang, Yueai Liu, Ming Xu, Yatao Yang, Minchun Li, Chongchang Mao and Jung-Chih Chiao, "Performance of a Liquid-Crystal Optical Harmonic Equalizer", 2001 Optical Fiber Communications Conference, TX, March 2001
- [24] Stamatis V. Kartalopoulos, "DWDM Networks, Devices, and Technology", IEEE Press, NJ., 2003

- [25] Ray Park, Audra Bullock, Multigrating Demultiplexer, Optical Devices for Fiber Communication IV; Michel J. Digonnet; Ed Proc. SPIE Vol. 4989, p 168-173, June 2003.

**RECEIVED**  
**AS**  
**FOLLOWS**

## **Acknowledgement**

I would like to thank Dr. Bullock for her support throughout the project.

I would also like to thank Dr. Malhotra and Dr. Lubecke for being on thesis member.



## **Acknowledgement**

I would like to thank Dr. Bullock for her support throughout the project.

I would also like to thank Dr. Malhotra and Dr. Lubecke for being on thesis member.